# Development of a HVAC System for Moderating Humidity Removal Efficiency

**Sheida Rezaei**

Department of Bioresource Engineering

McGill University, Montreal, Quebec, Canada

April 2025

A dissertation submitted to the Faculty of Graduate Studies and Research,

McGill University, in partial fulfillment of the requirements of the degree of

Doctor of Philosophy

© Sheida Rezaei, 2025

# Dedication

This thesis is dedicated to

My Parents (Mohsen and Parvin),

Sisters (Mehrnoosh, Mina & Fariba), and

other family members.

**Table of Contents**

**List of Figures**

## List of Tables

**Nomenclature and Abbreviations**

$cp$: specific heat capacity of air, J $kg^{-1}$ $^{o}C^{-1}$ (approximately 1005 J $kg^{-1}$ $K^{-1}$)

h: enthalpy, kJ $kg^{-1}$

l: latent heat of evaporation, kJ $kg^{-1}$ $K^{-1}$

L$f$: latent heat of fusion (approximately 334 kJ $kg^{-1}$ = 334,000 J $kg^{-1}$)

M: mass transfer, kg $s^{-1}$

$\dot{m}$: air flow rate, kg $s^{-1}$

$m_{air}$: mass flow rate of dry air, kg $s^{-1}$

$p$: atmospheric air pressure, kPa (typically 101.33 kPa)

$pi$: partial pressure of water vapor in air at any RH, kPa

$ps$: partial pressure of water vapor in air at saturation, kPa

$e_s$: saturation vapor pressure, Pa

Q_sensible: sensible heat

Q_latent_vaporization: latent heat of vaporization (approximately 2260 kJ $kg^{-1}$ = 2,260,000 J $kg^{-1}$ at 0°C)

Q_latent_fusion: latent heat of fusion (approximately 334 kJ $kg^{-1}$ = 334,000 J $kg^{-1}$)

Q_total: total heat transfer

$R^2$: coefficient of determination

RH: relative humidity, %

$RH_{in}$: inlet relative humidity, %

$RH_{out}$: outlet relative humidity, %

SHR: sensible heat ratio

STD: standard deviation

T: temperature, $^{o}C$

$T_{in}$: inlet temperature, ºC

$T_{out}$: outlet temperature, ºC

w: humidity ratio, g $kg^{-1}$

$w_{out}$, $w_{in}$: humidity ratio at outlet and inlet, g $kg^{-1}$

W: evaporation rate, g $s^{-1}$

Δ: value difference

ΔH: change in enthalpy ($H_{out}$ - $H_{in}$)

$ABH_{in}$: inlet absolute humidity, g $m^{-3}$

$ABH_{out}$: outlet absolute humidity, g $m^{-3}$

ΔABH: difference in absolute humidity ($ABH_{in}$ - $ABH_{out}$)

$H_{in}$: inlet enthalpy, kJ $kg^{-1}$

$H_{out}$: outlet enthalpy, kJ $kg^{-1}$

η_dehum: dehumidification efficiency

μ: mean of data

ρ: density, kg $m^{-3}$

σ: standard deviation

ΔT: temperature difference between the inlet and outlet air, K

MRR: moisture removal rate, g $s^{-1}$

**Abstract**

Global warming significantly impacts the energy sector, which intensifies the consumption of cooling power further contributing to environmental stressors. The major functions of heating, ventilating, and air-conditioning (HVAC) systems have historically been to offer thermal comfort for buildings and to assist in maintaining consistent indoor air quality. The HVAC system's operation throughout the summer is often adequate to meet both the sensible and latent cooling demands of the building and its occupants. However, the moisture load can be substantially larger than the air conditioner's capacity to remove water at times of the year when sensible loads are lower. This results in uncomfortable indoor conditions and high indoor relative humidity (RH) levels. In order to condense moisture, conventional HVAC systems first cool the air below the dew point, to remove the water vapor. The system then reheats the air to a comfortable temperature before sending it to the building spaces. In this study, a new way of dehumidification method is outlined, inspired by what happens in nature when ice crystals fall from the clouds. The aim of this research was to absorb moisture from the saturated vapor and facilitate condensation and freezing to generate fog or ice particles, and return condensed-phase water to the system. Temperature, RH and pressure are defined as the main variables to manage the production of fog or ice crystals.

This investigation explored the thermodynamic performance of a novel dehumidification system, which integrates a vortex cooling gun with a cold plate, aiming to optimize moisture extraction efficiency. The experimental analysis focused on the system's impact on thermodynamic properties such as temperature, RH, absolute humidity, moisture removal rate (MRR), and enthalpy. The initial observations reveal a rapid decrease in temperature from approximately 15 °C to just below 5 °C within the first 1000 seconds for an air volume of 0.05 $m^3$,. Concurrently, RH levels demonstrated a significant reduction, with the inlet RH decreasing from around 90 % and the outlet RH stabilizing at approximately 30 %, thereby illustrating the system's efficacy in reducing the moisture content. Absolute humidity measurements further

validated the dehumidification efficiency of the system, showing a substantial decrease in moisture content from an initial 14 g $m^{-3}$ to 4 g $m^{-3}$. The analysis of the relationship between the MRR and inlet absolute humidity indicated that higher initial humidity levels enhance the dehumidification process. This finding aligns with phase transition phenomena observed in cloud physics, where adjustments in relative humidity are critical for cloud formation dynamics. This study offers critical insights into advanced dehumidification methodologies that leverage direct contact cooling mechanisms and constant condensation nuclei, with potential implications for their broader application across various climatic and industrial contexts.

**Développement d'un système de chauffage, ventilation et climatisation (CVC) pour modérer l'efficacité de l'élimination de l'humidité**

**Résumé**

Le fonctionnement des systèmes de chauffage, ventilation et climatisation (CVC) pendant l'été est souvent suffisant pour répondre aux besoins de refroidissement sensible et latent d'un bâtiment et de ses occupants. Cependant, la charge d'humidité peut être considérablement plus importante que la capacité du climatiseur à l'éliminer pendant les périodes de l'année où les charges sensibles sont plus faibles. Cela entraîne des conditions intérieures inconfortables et des niveaux élevés d'humidité relative intérieure (HR). Pour condenser l'humidité, les systèmes CVC conventionnels refroidissent d'abord l'air en dessous du point de rosée, pour éliminer la vapeur d'eau. Le système réchauffe ensuite l'air à une température confortable avant de l'envoyer dans les espaces du bâtiment. Dans cette étude, une nouvelle méthode de déshumidification est décrite, inspirée de ce qui se passe dans la nature lorsque des cristaux de glace tombent des nuages. L'objectif de cette recherche était d'absorber l'humidité de la vapeur saturée et de la transformer en brouillard ou en particules de glace, puis de la renvoyer sous forme d'eau dans le système. La température, l'humidité relative et la pression sont définies comme les principales variables pour gérer la production de brouillard ou de cristaux de glace.

Cette enquête a exploré les performances thermodynamiques d'un système de déshumidification novateur, qui intègre un pistolet de refroidissement à vortex avec une plaque froide, dans le but d'optimiser l'efficacité de l'extraction de l'humidité. L'analyse expérimentale s'est concentrée sur l'impact du système sur les propriétés thermodynamiques telles que la température, l'humidité relative (HR), l'humidité absolue, le taux d'élimination de l'humidité (MRR) et l'enthalpie. Les observations initiales révèlent une diminution rapide de la

température d'environ 15 °C à un peu moins de 5 °C dans les 1000 premières secondes pour un volume d'air de 0,05 $m^3$, ce qui signifie une extraction efficace de l'énergie thermique. Parallèlement, les niveaux d'humidité relative (HR) ont montré une réduction significative, avec l'HR d'entrée diminuant d'environ 90 % et l'HR de sortie se stabilisant à environ 30 %, illustrant ainsi l'efficacité du système à réduire la teneur en humidité. Les mesures d'humidité absolue ont en outre validé l'efficacité de déshumidification du système, montrant une diminution substantielle de la teneur en humidité initiale de 14 g $m^{-3}$ à 4 g $m^{-3}$. L'analyse de la relation entre le taux d'élimination de l'humidité (MRR) et l'humidité absolue d'entrée a indiqué que des niveaux d'humidité initiaux plus élevés améliorent considérablement le processus de déshumidification. Cette découverte s'aligne sur les phénomènes de transition de phase observés en physique des nuages, où les ajustements de l'humidité relative sont essentiels pour la dynamique de formation des nuages. Cette étude offre des informations essentielles sur les méthodologies de déshumidification avancées qui exploitent les mécanismes de refroidissement par contact direct, avec des implications potentielles pour leur application plus large dans divers contextes climatiques et industriels.

**Acknowledgements**

I want to express my deepest gratitude to my supervisor, Dr. Mark Lefsrud, for his guidance and support throughout my research. This work would not have been possible without his invaluable encouragement and advice. I also extend my sincere thanks to Dr. Valerie Orsat, a member of my graduate advisory committee, for her excellent advice during my Ph.D. studies. I am especially grateful to Dr. Sarah MacPherson for her assistance.

I would like to acknowledge Mr. William Boyd Dumais and all the members of the Biomass Production Lab for their help in setting up and conducting the experiments. I am also thankful for the financial support provided by Graduate and Postdoctoral Studies at McGill University, including the Schulich Graduate Fellowship and the Graduate Excellence Award from the Department of Bioresource Engineering. Additionally, I appreciate the financial support from Mitacs and Upculture Inc., Canada, which enabled me to complete this research.

Lastly, I am deeply grateful to my parents, Mohsen and Parvin, for their sacrifices, love, and prayers. I also wish to thank my sisters, Mehrnoosh, Mina, and Fariba, as well as my other family members, teachers, and friends, for their unwavering support and encouragement throughout every step of my journey.

**Declaration of AI and AI-assisted technologies in the writing process**

During the preparation of this thesis, ChatGPT was used to find grammatical error of some sentences. After using this tool/service, the text was extensively reviewed and edited with all modifications and changes accepted by the author(s).

**Contributions to original knowledge**

This thesis introduces a novel HVAC system designed to enhance humidity removal efficiency, addressing challenges posed by global warming and increasing energy demands. The research explores advanced dehumidification techniques inspired by natural processes, significantly deviating from traditional HVAC methods by utilizing innovative components such as a vortex cooling gun and cold plate. The contributions to original knowledge from this research are as follows:

1. This thesis provides a detailed analysis of the limitations of conventional HVAC systems in managing moisture under varying thermal loads, highlighting the need for more efficient dehumidification strategies.
2. It presents a comprehensive study on the development and application of a vortex cooling gun combined with a cold plate, offering new insights into direct contact cooling mechanisms for optimizing moisture extraction.
3. The research investigates the thermodynamic performance of the proposed dehumidification system, focusing on key parameters such as temperature, relative humidity, absolute humidity, moisture removal rate, and enthalpy, thereby demonstrating its effectiveness in rapidly reducing indoor humidity levels.
4. It examines the relationship between initial humidity levels and moisture removal rates, revealing how higher inlet absolute humidity enhances the dehumidification process, which aligns with natural phase transition phenomena observed in cloud physics.
5. The study explores the potential of this innovative system to efficiently convert moisture from saturated vapor into fog or ice particles, and subsequently return it as water, showcasing a unique approach to humidity control in HVAC systems.
6. By integrating direct contact cooling and natural dehumidification principles, this work offers a novel solution for managing indoor air quality with greater energy efficiency,

reduced operational costs, and lower environmental impact, providing valuable insights for future HVAC system designs in diverse climatic and industrial contexts.

## Contribution of authors

In accordance with the McGill Guidelines for a Manuscript Based Thesis, the contributions made by the candidate and the co-authors to the completion of this work are described as follows;

Sheida Rezaei is the main author of this work, supervised by Dr. Mark Lefsrud from the Department of Bioresource Engineering, McGill University, Quebec, Canada.

Dr. Mark Lefsrud is Sheida Rezaei's supervisor and Director of the Biomass Production Lab at McGill University. He co-authored, co-edited and reviewed all manuscripts, in addition to providing scientific guidance in the planning and execution of the work.

Dr. Valerie Orsat is a committee member and co-author/co-editor of two manuscripts.

**Journal Papers**

1. **Rezaei, S.,** Lefsrud, M., Orsat, V., & Rahman, M. S. (2024). Novel Dehumidification Technique Using Vortex Cooling and Cold Plate Ice Formation. Science and Technology for the Built Environment. Manuscript ID: STBE-0197-2024. Submitted on August 4, 2024.
2. **Rezaei, S.,** Lefsrud, M., & Orsat, V. (2024). Ice Formation for Enhanced Dehumidification: An Innovative Approach to Moisture Control. Journal of Building Performance Simulation. Submission ID: 248802876. Submitted on August 29, 2024.

# CHAPTER 1

## General Introduction

### 1.1 Background

Heating, ventilation, and air-conditioning (HVAC) systems are extensively utilized in buildings worldwide and typically account for the largest portion of total energy consumption. These systems are crucial in maintaining comfortable indoor temperatures for occupants, regardless of external weather conditions (Selamat et al., 2020). Enhancing the performance of conventional HVAC systems presents a promising opportunity to substantially reduce energy usage. Approximately half of the energy demand in commercial buildings is dedicated to maintaining indoor thermal comfort (Enteria & Mizutani, 2011).

Figure 1.1 illustrates the energy consumption percentages attributed to HVAC and related systems across various regions, highlighting their significant impact on overall energy use (Balaras et al., 2007; CO_GEN, 2007; Desideri et al., 2009; El-Dessouky et al., 2004; Fong et al., 2010; Ma et al., 2006; Pérez-Lombard et al., 2008; Vakiloroaya et al., 2014; Yao & Chen, 2010).

Various strategies are needed to enhance HVAC energy efficiency and lower environmental impact. Recent optimization methods often prove costly, complex, and require continuous monitoring. A promising approach is combining HVAC components for an efficient setup that adjusts with varying cooling loads. Though initial costs may be higher, optimizing traditional HVAC designs can lead to significant long-term savings by reducing maintenance expenses (Vakiloroaya et al., 2014).

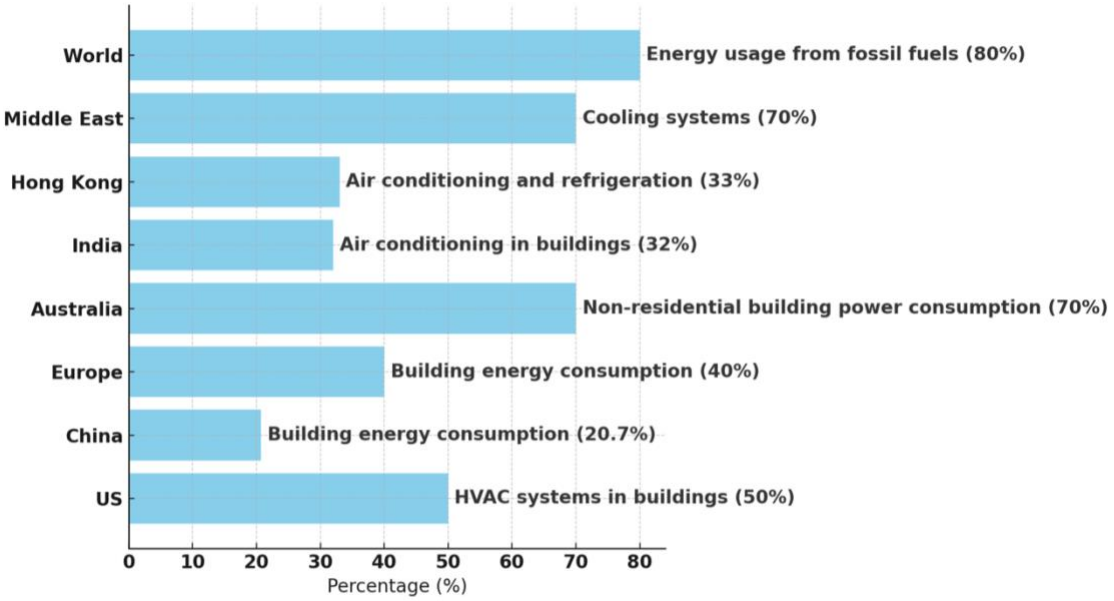


**Figure 1.1.** Regional comparison of energy consumption by HVAC and related systems, showcasing their contribution to total building energy use worldwide.

Humidity issues arise in various settings such as offices, museums, libraries, manufacturing, and commercial facilities (Huh & Brandemuehl, 2008). HVAC coils often struggle to handle high latent loads caused by internal moisture or humid outdoor air, leading to discomfort, mold, damage, and increased energy costs (Huh & Brandemuehl, 2008). These challenges are intensified by the need for more outdoor air to improve indoor air quality (Huh & Brandemuehl, 2008).

In most commercial and residential applications, humidity control is indirect. A traditional air-conditioning (AC) system handles both sensible and latent cooling (Nawaz & Gluesenkamp, 2018). Sensible cooling occurs as the evaporator lowers supply air temperature. When the refrigerant is below the air's dew point, moisture condenses on the evaporator, reducing humidity and removing latent heat.(Nawaz & Gluesenkamp, 2018). In commercial buildings, humidity is typically controlled by cooling air to the dew point and reheating, which is energy-intensive. However, maintaining humidity below 50% allows for raising the dry bulb temperature to 25–26 °C while ensuring comfort, resulting in significant energy savings. Each

degree increase in set point reduces energy use by 5% (Daou et al., 2006). This causes relative humidity to fluctuate based on equipment capacities versus building loads. Depending on whether temperature or humidity dictates operation, energy penalties arise from overcooling and reheating. Addressing dehumidification requires proper HVAC system design to handle both sensible and latent loads, with adjustments made for varying load conditions. The balance between sensible and latent loads is described by the sensible heat ratio (SHR) (Huh & Brandemuehl, 2008).

In HVAC systems, the optimal range for relative humidity (RH) is 40-60%. Studies suggest this range reduces the survival of viruses like SARS-CoV-2 and minimizes microbial growth risks, as recommended by ANSI/ASHRAE and EPA standards. (Murphy, 2002; Sugarman, 2022; Thornton et al., 2022). A typical commercial air conditioning system includes a cooling coil, heating coil, and supply/extract fans (Li et al., 2012).

Table 1.1 provides an overview of studies on air conditioning and desalination systems, summarizing methods and key findings. It covers hybrid systems, integrative units, and renewable energy applications, focusing on performance, energy use, and water production efficiency (Lawal et al., 2018).

**Table 1.1.** Summary of studies on air conditioning and desalination systems, highlighting methods and key findings on performance, energy use, and water production (Lawal et al., 2018).

| Study | Method | Key Findings and Observations |
|---|---|---|
| (Nada et al., 2015b) | Hybrid humidification-dehumidification using vapor compression refrigeration. | Produces fresh water; uses steam boiler for humidification; high energy consumption. |
| (Yuan et al., 2005) | Integrative air-conditioning and desalination unit with condenser heating seawater. | Condenser heats seawater; evaporator cools humid air for water production. |

| | | |
|---|---|---|
| (Gao et al., 2008) | Heat pump desalination unit with air-heated humidification and dehumidification. | Air heated by heat pump and solar; seawater pre-heated via condenser. |
| (Habeebullah, 2010) | Combined heat pump-dehumidification system for water extraction and conditioning. | Heat pump extracts water; used for office conditioning; waste heat not utilized. |
| (S. A. Nada et al., 2015) | Hybrid air conditioning and humidification-dehumidification system (HDH) for hot/dry regions. | Six cases analyzed; steam generator used; rejected heat not utilized. |
| (Zubair et al., 2017) | Humidification-dehumidification desalination with solar evacuated tubes. | Solar evacuated tubes used; assessed in six locations in Saudi Arabia. |
| (Rajaseenivasan & Srithar, 2017b) | Dual-purpose solar collector for HDH desalination. | Solar collector heats both water and air simultaneously for HDH. |
| (Srithar & Rajaseenivasan, 2017) | Solar bubble column HDH desalination system with turbulators. | Investigated effect of turbulators, humidifier water depth, and air flowrate. |
| (Rajaseenivasan & Srithar, 2017a) | Biomass energy for bubble column HDH desalination. | Biomass used to power HDH system with bubble column. |

### 1.2 Thesis hypothesis

In this experiment, a vortex cooling gun and a cold plate are utilized to maintain cooling and dehumidification, while an ultrasonic humidifier keeps the humidity stable. The hypothesis is that the hot and humid inlet air can be transformed by reducing temperature and RH, with the released latent heat driving condensation and forming ice crystals on the cold plate. More ice crystals are expected to result in increased moisture absorption. The effectiveness of the moisture removal rate, depending on the inlet RH, is assessed to determine the system's efficiency.

The process begins by introducing hot and humid air into the system, which is then subjected to rapid cooling by the vortex cooling gun. As the cooled air passes over the cold plate, its temperature drops below the dew point, leading to condensation of the moisture in the air. This condensed moisture is expected to freeze on the cold plate surface, forming ice

crystals. These ice crystals not only indicate the effectiveness of the condensation process but also act as a means to absorb additional moisture from the incoming air.

The ultrasonic humidifier ensures that the inlet air maintains a consistent humidity level, allowing for controlled testing conditions and enabling a more accurate evaluation of the dehumidification performance. By maintaining a stable RH, it is possible to study the precise impact of cooling and condensation processes on moisture removal under various conditions.

The hypothesis underlying this experiment is that by managing the latent heat release and promoting the freezing of condensed moisture, a more efficient dehumidification process can be achieved. By evaluating the moisture removal rate across different inlet RH levels, we aim to understand the relationship between the initial humidity and the efficiency of the system. This understanding could help optimize dehumidification strategies for HVAC systems, providing improved energy efficiency and enhanced indoor comfort in buildings with high latent cooling demands.

### 1.3 Statement of research objective

This research combines the knowledge of dehumidification in HVAC systems with cloud physics. The main and specific objectives of this whole work are as follows.

#### 1.3.1 Main objectives

a) Study if latent and sensible heat loads can be separated when using water as a HVAC working fluid
b) Produce heavy and cold fog to act as a simulated cloud in the experimental unit.
c) Control and decrease the RH and absolute humidity by creating ice particles.
d) Measure how much moisture can be absorbed from the system as the air stream changes phase from saturated vapor to solid ice crystals.

### 1.3.2 Specific objectives

a) Produce heavy fog inside the chamber

b) Produce ice crystals and direct them with an ice scrapper system

c) Measure the temperature reduction when using a vortex cooling gun and a cold plate.

d) Analyze how the system can modify the relative humidity and absolute humidity.

## 1.4 Organization of thesis

This dissertation is structured into six chapters, along with references and appendices. Chapter 1 introduces the background, objectives, and structure. Chapter 2 reviews relevant literature. Chapters 3, 4, and 5 cover the research and experiments conducted to meet the objectives. Chapter 6 presents the overall discussion and conclusions. Transitional texts between chapters clarify the flow and rationale of the research. The International System of Units (SI) is used throughout, with imperial units provided in parentheses where applicable.

# CHAPTER 2

## Literature Review

### 2.1 Background

Heating, cooling, and ventilation systems account for a notable share, approximately 35%, of energy consumption in the United States (Khalilnejad et al., 2020). Currently, the prevailing approach in modern constructions remains focused on conditioning indoor spaces for peak occupancy rather than considering the actual utilization patterns (Ding et al., 2015). The demand for advanced heating, ventilating, and air conditioning (HVAC) systems capable of achieving effective dehumidification and cooling has grown exponentially in recent years (Ding et al., 2015).

HVAC systems play a crucial role in energy consumption, constituting a substantial and increasing portion of overall energy usage. In tropical regions, the energy used for HVAC can account for more than half of a building's total energy consumption (Chua et al., 2013). In developed countries, the building sector accounts for 20-40% of final energy consumption, often surpassing other major sectors like industry and transport (Pérez-Lombard et al., 2008). Among the building-related energy consumption, HVAC systems are the most significant contributors, accounting for approximately 50% of the total energy usage, equating to 10-20% of the final energy consumption (Enteria & Mizutani, 2011).

Figure 2.1 illustrates the energy consumption in American buildings. The major contributors to this consumption, accounting for more than 50%, are space conditioning, water heating, lighting which encompasses outdoor lighting, and the cooling of the majority of data centers (U.S. Energy Information Administration – EIA – Independent Statistics and Analysis, n.d.).

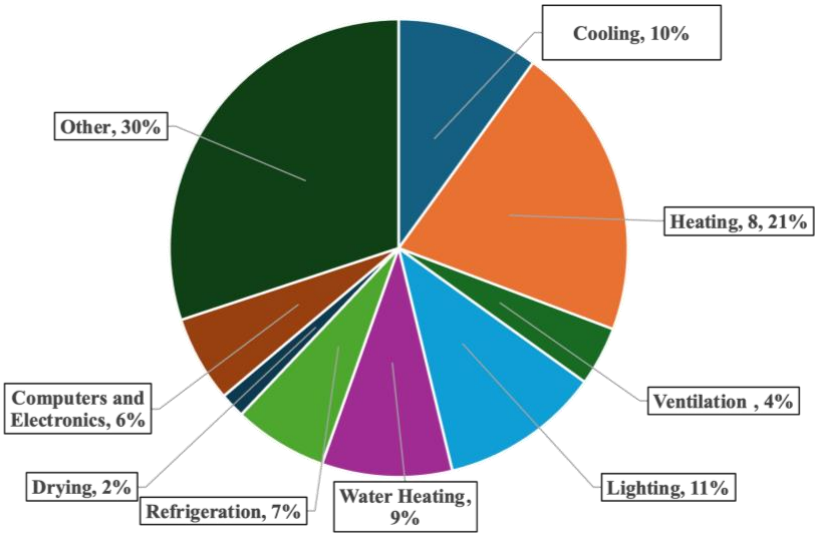


**Figure 2.1.** Primary Energy Consumption in Residential and Commercial Buildings (Quadrillion BTUs)

Diverse techniques need to be implemented to enhance energy efficiency and minimize the environmental impact of HVAC systems. In recent years, a range of control and optimization strategies have been adopted to effectively reduce the energy consumption rates of these systems (Li et al., 2008). Nonetheless, these approaches come with either high expenses or intricate implementation, necessitating continuous monitoring. To attain the objective, an alternative option is to integrate different HVAC components, creating an energy-efficient configuration (Vakiloroaya et al., 2014). Given the variability of any building's cooling demands, the HVAC system should be designed with an optimized scheme, maintaining process variables at the required set points to ensure comfort under varying load conditions. Despite incurring extra upfront costs when enhancing the mechanical design of traditional HVAC systems, such modifications can yield significant long-term savings by reducing ongoing maintenance expenses associated with control and optimization strategies (Vakiloroaya et al., 2014).

## 2.2 Environmental concerns and global warming potentials

The heart of the vapour-compression system lies in the refrigerant, whose chemistry has evolved in response to policy and environmental concerns (Corberan, 2016).

HFC-134a ($CH_2FCF_3$) is a fluorinated greenhouse gas that is used widely in a range of applications: principally refrigeration and air conditioning and in blowing plastic matrix foams and propelling medical and technical aerosols (Kamal, 1994). The use of aerosols and system leakage has impacted the greenhouse effect with climate change events that have an impact on the ecosystem (Chen et al., 2021). The size of this impact will depend on both the volume of emissions and the global warming potential (GWP) of HFC-134a. The latter parameter's value compares the greenhouse effect of releasing 1 kg of HFC-134a to that of releasing 1300 kg of carbon dioxide ($CO_2$) over the first 100 years after both releases (Ramaswamy et al., 2001).

The GWP of the refrigerants used in vapor compression systems, like HFCs, is relatively high (Henderson & Rengarajan, 1996). Hydrofluorocarbons (HFCs), like R-134a with 1430 times higher global warming potential than of carbon dioxide (Benedick, 1996) is against the Montreal Protocol in 1987. The United States, Canada and Mexico announced to restrict their use of HFCs by more than 80% between 2016-2033 (Velders et al., 2012). The possibility of these refrigerants being accidently released will impact global warming (Andersen et al., 2021). The traditional vapor compression method is often powered by electricity, which requires the use of primary energy (fossil fuel, coal, etc.), endangering the growing global energy deficit (Sanaye & Taheri, 2018).

In order to attain the aforementioned objectives, it is imperative to substantially enhance the energy efficiency of both newly constructed and pre-existing residential structures. It is noteworthy that buildings sector contribute significantly to the United Kingdom's carbon dioxide emissions, accounting for approximately 50% of the total emissions, with residential housing alone responsible for over 27% of this sector's emissions (Karmacharya et al., 2012).

In Canada, residential buildings accounted for 17.1% of the nation's energy consumption in 2015, while commercial and institutional buildings contributed an additional 11.2% (Berardi & Jafarpur, 2020). Together, greenhouse gas emissions from these residential, commercial, and institutional buildings made up 22.6% of the total GHG emissions associated with secondary energy use across the country (Berardi & Jafarpur, 2020).

### 2.3 ASHRAE standard for HVAC system

The American Society of Heating, Refrigerating and Air Conditioning Engineers (ASHRAE) has standards for the desired range of temperature, humidity and air movement for ensuring a comfort zone for humans. In the comfort zone, the temperature is between 20 - 24 °C for winter and 23 - 25 °C for summer with a relative humidity of 50 % and air velocity of 9 meter per minute or less. The HVAC system works in a cycle to absorb or remove the heat in a conditioned area (Olesen, 2020).

The required volume of air to heat, cool, ventilate and supply desired air quality is monitored based on the heating, cooling and ventilation loads. The unit of air volume is typically defined as cubic feet per minute (cfm) (Becker et al., 2007).

The HVAC system is composed of three primary units: a heating unit with a boiler, a ventilation unit with fans, and a cooling unit with a chiller. The heating function is commonly used in colder climates, while the cooling function is frequently employed in warmer and hot climates. Air conditioning involves the removal of indoor air humidity (Mendes et al., 2008).

The HVAC system commonly encounters several issues, including insufficient indoor air exchange, inadequate control over indoor thermal conditions, and unfavorable space ergonomics that impact the ventilation system's efficiency (Teke & Timur, 2014). Additionally, poor maintenance of technical installations and understaffed technical departments contribute to the problems. International regulations and standards typically recommend maintaining

indoor air temperatures between 20–24°C and indoor relative humidity levels between 30% and 60%. Most standards advise achieving 20 air changes per hour (ACH) to achieve a suitable level of less than 50–150 colony forming units (CFU) $m^{-3}$ of air (Dharan & Pittet, 2002).

## 2.4 Different types of HVAC systems

Figure 2.2 illustrates the various approaches employed to enhance HVAC energy efficiency (Vakiloroaya et al., 2014).

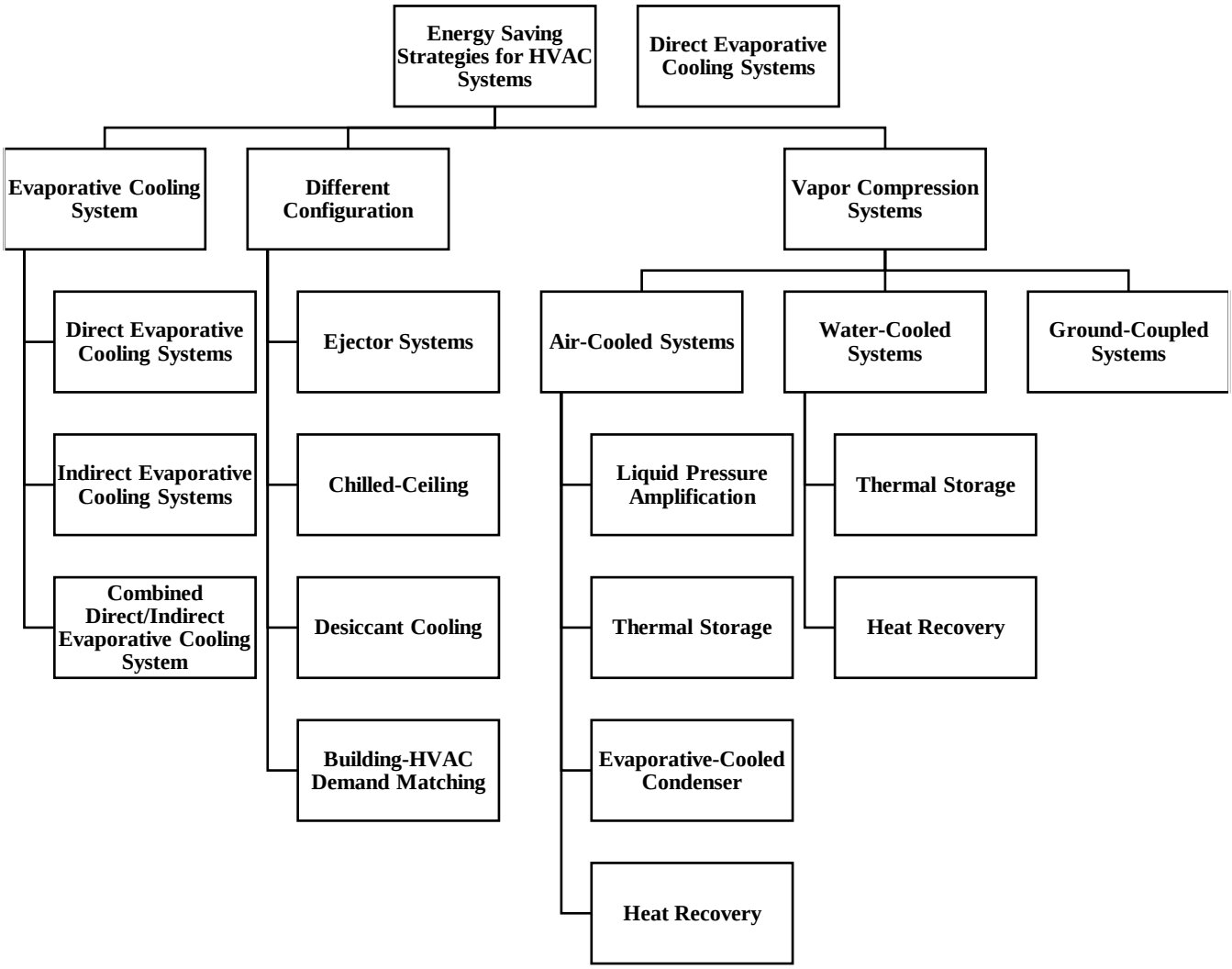


**Figure 2.2.** Enhancing HVAC Energy Efficiency: Illustrated Approaches (Vakiloroaya et al., 2014)

**Figure 2.2.**

### 2.4.1 Evaporative cooling

Evaporative cooling is the process of transferring heat and mass to cool the air by water evaporation, resulting in a reduction of the temperature of the air. This process can be done in two ways: (1) Direct evaporative cooling, in which there is direct contact between air and water; (2) Indirect evaporative cooling, where the working fluids are separated by a surface; (3) Combined system of direct and indirect evaporative coolers (Duan et al., 2012).

Evaporative cooling systems are well-known because of having low running costs and easy installation. The thermal comfort zone is achieved by converting sensible heat to latent heat in evaporative cooling systems, however, the temperature reduction is limited to the wet-bulb temperature of the outside air. As a result, evaporative cooling systems combined with different hybrid pre-cooled technologies improve the cooling system's efficiency (Vakiloroaya et al., 2014).

However, the main issue of the evaporative cooling systems is their performance which is highly linked to the ambient air conditions. The difference between dry-bulb and wet-bulb temperature is significant in mild and humid climates and can negatively affect the cooling capacity of evaporative cooling systems (Amer et al., 2015). Hybrid systems have been developed to enhance performance.

In one study, vertical ground heat, exchanger, and cooling coil unit were combined with an indirect evaporative cooler to cool the entering air (Khalajzadeh et al., 2012).

A combination of an air-to-air sensible heat exchanger and a cooling coil was used to obtain the dry-bulb temperature lower than the wet-bulb temperature of the outside air. The results show that the energy-saving potential was up to 52%, compared with the conventional chilled water central cooling plant (Vakiloroaya et al., 2011)

A hybrid system of nocturnal radiative cooling, cooling coil and direct evaporative cooling was applied by means of a flat-plate radiator to circulate water through the night. The ambient air was pre-cooled by the cold water over the next day which results in a higher effectiveness of the system than a normal evaporative cooling system (Heidarinejad et al., 2010).

### 2.4.2 Evaporative-cooled air conditioning system

The coefficient of performance (COP) of the air conditioning systems with air-cooled condensers can remove higher heat by pre-cooling the air before entering the condenser. Consequently, condensing temperature and energy usage decrease, allowing the compressor to work less frequently (Vakiloroaya et al., 2014). Spraying mist directly into the ambient air before the air-cooled condenser can reduce the energy consumption by up to 20% and results in higher COP by 50% in a split air-conditioner (Hajidavalloo & Eghtedari, 2010). Table 2.1 compares the efficiency of different dehumidification methods based on their moisture removal capacity.

**Table 2.1.** Summary of Key Studies Addressing HVAC System Challenges and Energy Efficiency Improvements in Buildings

| Dehumidification Methods | Dehumidification performance | References |
|---|---|---|
| Condensation on a cold surface | 198.3 kWh $L^{-1}$ | (Gao et al., 2011) |
| Natural convection condensation | 1 m length of the finned tube could remove 50–65 ml $h^{-1}$ of water vapor<br><br>40 (g $hm^{-2}$) moisture removal from the moist air with 80% RH and a temperature of 20°C | (Campen & Bot, 2001) |
| Mechanical refrigeration with controlled condensation | 1.3 L $h^{-1}$ under room conditions | (Han et al., 2015) |

| | | |
|---|---|---|
| Air-to-air heat exchanger | 1.506 kW-h $L^{-1}$ | (Gao et al., 2011) |
| Del-Air RA400 heat exchanger | 200-400 L $day^{-1}$ | (Han et al., 2015) |
| Desiccant-based hybrid air-conditioning technologies | 10.2 g at 0.6 kW cooling capacity | (Park & Lee, 2020) |
| Adsorption by hygroscopic materials (liquid desiccant) | dehumidifier can reduce cooling energy usage by up to 30–50%. | (Liang et al., 2020) |

### 2.4.3 Desiccant dehumidification

In regions with high humidity, where direct evaporative cooling underperforms due to the minimal disparity between outdoor dry and wet bulb temperatures, one might explore the use of a desiccant evaporative cooling system as an alternative for cooling (Jamil et al., 2023). In condensing dehumidification, moisture is removed from the air after it has been cooled below its dew point. The differential in vapor pressure between the air and the desiccant is what drives moisture during desiccant dehumidification. Desiccant comes in two different forms: liquid and solid (Lowenstein, 2008).

Since the liquid desiccant's vapor pressure is lower than that of the air during the dehumidification process, moisture will move from the air to the desiccant and vice versa throughout the regeneration process (Zhang et al., 2012). Liquid desiccant dehumidification systems (LDDS) are a type of air-conditioning system that uses a liquid desiccant to dehumidify the air. The regeneration process is one of the most critical processes in LDDS system as the whole system's performance depends on the effectiveness of this process. The liquid desiccant solution, after absorbing the water vapor from the air, it should be regenerated. The concentration of the liquid desiccant solution reduces after absorbing the water vapor. Therefore, it needs to be processed back to the original concentration. This process is called the regeneration process (Chen et al., 2020). To re-use the desiccant, it needs to be reactivated through a process in which moisture is driven off by heat from an energy source such as electricity, waste heat, natural gas, or solar energy (Pesaran et al., 1992).

### 2.4.4 Different cooling tower models

Cooling towers are extensively employed for heat removal in both industrial processes and HVAC systems. The heat rejection process in cooling towers involves heat and mass transfer occurring between hot water droplets and the surrounding ambient air (Bhatia, 2014).

#### 2.4.3.1 Mechanical cooling towers

Mechanical draft cooling towers are more widely utilized compared to natural draft cooling towers (Ehsan et al., 2020). These mechanical towers utilize large fans to propel air through the circulated water. As the water descends over the surfaces, it prolongs the contact time between water and air, resulting in enhanced heat transfer efficiency. The two main types of mechanical draft cooling towers are counterflow and cross-flow. In counterflow, water flows downward while fans force air upwards, ensuring that fresher, cooler, and less saturated air comes into contact with the water, thereby improving cooling efficiency. In crossflow, warm water descends through a cooling unit and is cooled by air drawn upwards by a fan, leading to a rapid decrease in temperature due to evaporation and direct heat exchange (Kloppers & Kro¨ ger, 2005).

## 2.5 Measuring the performance of HVAC systems

Various models for heat exchangers are currently available, and they can be classified based on their complexity and empirical nature into theoretical or design models, empirical or engineering models, and hybrid models (Sarfraz et al., 2018). Theoretical or design models are detailed and rely on fundamental heat and mass transfer principles, relying on extensive information about the heat exchanger's structure and fluid properties, which may not be readily obtainable from manufacturers' catalogs. These models are commonly used as the theoretical foundation for coil or heat exchanger design. An example of such a model can be found in the ASHRAE HVAC 1 and 2 Toolkit, which requires input parameters like fin dimensions, tube thickness, diameter, and spacing to calculate heat transfer coefficients. Empirical or engineering models offer the advantage of requiring minimal geometric specifications, unlike theoretical models (Wang et al., 2004).

Stoecker proposed a model that the total heat transfer rate is calculated based on the cooling coil's base rating, wetted surface factor, and log mean temperature difference (Stoecker, 1975). These equations do not incorporate transport properties, resulting in consistent predicted performance for a coil regardless of the fluid type in the tubes (Zhou & Braun, 2007). As a result, different sets of empirical constants are necessary for different fluids (Rabehl et al., 1999).

Hybrid modelling combines model structures derived from physical or thermodynamic principles with parameters evaluated using catalogue, commissioning, or operating data. Braun et al. (1989) introduced the concept of air saturation specific heat to create an effective model. By utilizing catalogue data from an operating condition, the number of transfer units is determined and applied to predict performance at other operating conditions (Braun et al., 1989). Rabehl et al. have presented a model based on Braun's model and thermodynamic theory. This new model requires the determination of heat transfer parameters, eliminating the need for detailed geometric specifications while still capturing the impact of geometry on performance. This model requires the knowledge of dynamic viscosity, Prandtl number, Reynolds number, etc., for the two fluids, which may limit its real-time applications (Rabehl et al., 1999).

Another cooling coil model in the ASHRAE HVAC 1 and 2 Toolkit uses the effectiveness-number of transfer units (Ntu), derived from calculating the overall heat transfer coefficient area product (UA) at a rated condition. When evaluating coil performance at other operating points, UA is assumed to remain constant, as at the rated condition (Brandemuehl & Gabel, 1994). Wang et al. (1998) proposed a nonlinear dynamic model based on energy conservation and developed a control method for such a nonlinear system. However, this model overlooks several crucial heat transfer properties and presents challenges for its application in system optimization (Wang et al., 1998).

Merkel's model is founded on several critical assumptions (Merkel, 1925). It assumes that the Lewis factor, governing the relationship between heat and mass transfer, is set to a value of 1. Second, the model assumes that the air leaving the tower is saturated with water vapor and characterized solely by its enthalpy. Last, the model neglects to consider the reduction in water flow rate caused by evaporation when analyzing the energy balance (Jin et al., 2007). Researchers suggest that by employing advanced design techniques and tools with an integrated system design approach, substantial savings of around 70 % can be attained. This approach involves optimizing the interaction between different factors and their constraints. Nevertheless, existing software lacks the required continuity and integration, limiting its effectiveness in supporting optimal design practices (Donnelly et al., 1994).

### 2.6 Energy balance in HVAC systems

Reliable energy consumption data serves as the cornerstone for assessing a building's energy performance. The energy balance load, a metric derived from the principles of the first law of thermodynamics through comprehensive whole-building energy analysis, has been theoretically validated as a valuable instrument for validating the accuracy of whole-building energy consumption data (Shao, 2006). The impact of the dynamic performance of an HVAC system on both energy consumption and indoor air quality is widely recognized (Moghadam et al., 2023). The condensation-based approach to dehumidification is widely favored in dynamic modeling of HVAC systems for its ability to accurately predict the transient behavior of cooling and dehumidifying coils (Zhou & Braun, 2007). It entails chilling indoor air to a temperature below its dew point, which causes water vapor in the air to condense. This results in the cooling of the entire air mass, encompassing both the moisture and dry air components (Mumtaz et al., 2023).

In a study on the condensation of humid air used in a typical adsorption dehumidifier, the results show that the maximum level of condensation occurs when there is a significant

increase in heat transfer, brought about by a sufficiently high flow rate on the cold side (Amer et al., 2019).

An investigation into the mechanical compression refrigeration system and evaporative cooling system established that as the minimum temperature rises, the efficacy of the condensation process decreases, leading to a decline in the gain-output-ratio. Similarly, an increase in minimum temperature results in reduced effectiveness of the condensation process, leading to a decrease in the recovery ratio. The findings in Figure 2.3 demonstrate that a higher maximum temperature leads to an increased optimal mass-flow-rate ratio, as air can carry a greater amount of water vapour (Sharqawy et al., 2014).

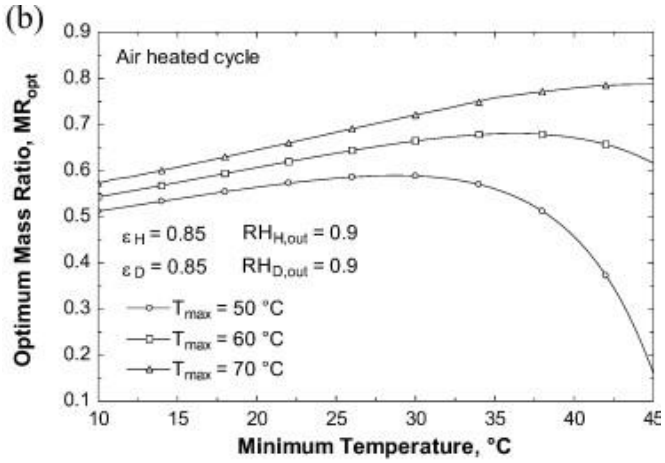


**Figure 2.3.** Effect of minimum temperature and inlet air conditions on the Optimum Mass Ratio in an air-heated cycle (Sharqawy et al., 2014)

Hasani Balyani et al. (2015) conducted a study to determine the most effective cooling systems for small-scale residential buildings. The findings revealed that using the desiccant enhanced-evaporative system in temperate and wet, temperate and humid and hot and semi-humid areas led to increased annual cooling costs of $195, $194, and $267, respectively, compared to the vapor compression system. Conversely, in arid regions, replacing direct evaporative cooling with the vapor compression system resulted in a reduction of 3750, 4875,

and 3964 kWh in annual primary energy consumption for temperate and dry, hot and semi-dry, and hot and very dry areas, respectively (Hasani Balyani et al., 2015). Karmacharya et al. (2012) developed a Matlab/Simulink model to predict building temperatures and assess energy needs for comfort. Heating demand is influenced by factors like building characteristics, weather, heating system efficiency, user preferences, and internal heat gain (Henn et al., 2022). Their model comprehensively considers these elements for energy analysis in the building-HVAC system (Karmacharya et al., 2012). The fundamental goal in the design of energy-efficient HVAC configurations is the reduction of heating and cooling requirements by minimizing (1) the external air load, (2) the load within individual zones, and (3) the energy losses incurred during the air-conditioning process. In moderate seasons, free cooling effectively expels surplus heat from a building when the enthalpy of the outside air is lower than the indoor air. However, during winter and summer, fresh air supply contributes significantly to the system load, which is determined by the enthalpy contrast between ambient and zone air, multiplied by the mass flow rate (Zhang et al., 2006). Hence, minimizing the outside air load entails reducing outside airflow, lowering the enthalpy disparity, or employing a combination of both strategies. An effective strategy for reducing the outside air load involves minimizing the enthalpy difference between the external air and exhaust air. In Figure 2, which depicts two zones characterized by distinct design indoor air conditions (T1 and T2), the calculation of the sensible load for outside air intake ($Q^{\cdot}{}_{s}^{O/A}$) is articulated in Equation 2.1 (Wang et al., 2004):

$$Q^{\cdot}{}_{s}^{O/A} = m^{\cdot}{}^{O/A} Cp(T_{db}{}^{O/A} - T_2) \quad (2.1)$$

where $m^{\cdot}{}^{O/A}$ and $T_{db}{}^{O/A}$ signify the mass flow rate and dry-bulb temperature of the outside air. It is imperative to arrange the two zones in a manner that aligns the design temperature of zone 2 closely with the ambient temperature thereby to curtail the external air load on the system. Where $C_p$= specific heat of air, 1.0061 kJ $kg^{-1}$ $K^{-1}$ at 20 °C, $m^{\cdot}{}^{O/A}$ = mass

flow rate of outside air (kg/s) , $T_{db}^{O/A}$ = dry-bulb temperature of outside air (°C) ,$Q\cdot_s^{O/A}$ sensible outside air load (kW) (Zhang et al., 2006) Figure 2.4.

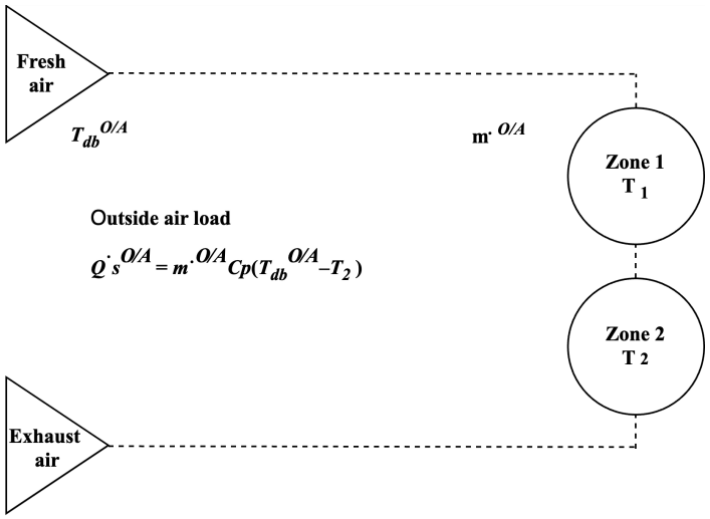


**Figure 2.4.** Minimizing enthalpy fresh between fresh and exhaust air (Zhang et al., 2006)

Wang et al. (2004) have introduced a simplified hybrid model for the prediction of the operational efficiency of chilled water-cooling coils or exchangers under steady-state conditions. This model, which is grounded in heat transfer principles and the energy balance concept, employs a minimal set of three characteristic parameters to encapsulate the collective geometric properties. It facilitates the calculation of the cooling load by employing the overarching heat resistance derived from established heat transfer theory while adhering to the principles of energy balance. Consequently, the heat transfer equation governing the cooling coil is expressed as follows in Equation 2.2 (Wang et al., 2004):

$$Q = \frac{c_1 \dot{m}_a^e}{1 + c_2 \left(\frac{\dot{m}_a}{\dot{m}_{chw}}\right)^e} (T_a - T_{chw}) \qquad (2.2)$$

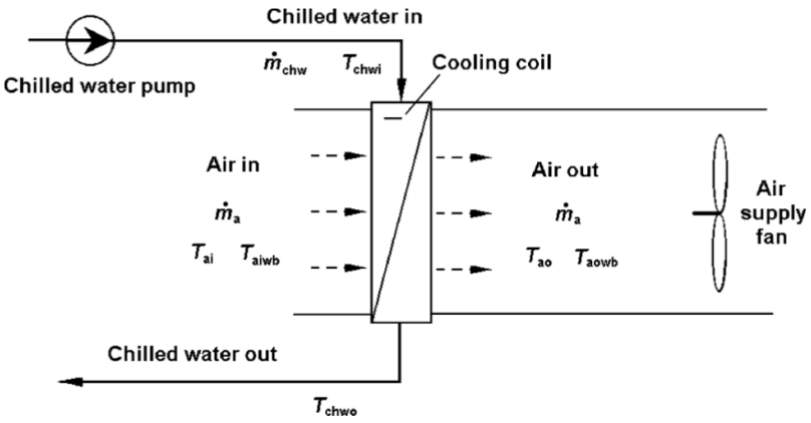

Fig. 1. Schematic drawing of AHU.

**Figure 2.5**. schematic drawing of AHU (Wang et al., 2004)

In Figure 2.5 (Wang et al., 2004), the air handling unit (AHU) comprises two distinct circuits: the chilled water loop and the air loop. The chilled water is compelled from the inlet of the chilled water coil unit (CCU) to its outlet, driven by a chilled water pump, featuring an initial temperature denoted as $T_{chwi}$ and a flow rate indicated as $m_{chw}$ (Wang et al., 2004). During the thermal exchange process with the air external to the cooling coil pipes, the temperature of the chilled water ascends to $T_{chwo}$. Concurrently, the supply air moves from its inlet to the outlet of the cooling coil, under the influence of a supply air fan. The characteristics of the air within the coil include its dry bulb temperature ($T_{ai}$), wet bulb temperature ($T_{aiwb}$), and air flow rate ($m_a$). In a similar fashion, the air external to the coil experiences a reduction in its dry bulb and wet bulb temperatures, ultimately reaching $T_{ao}$ and $T_{aowb}$ due to the thermal interaction with the chilled water circulating within the cooling coil pipes (Wang et al., 2004). A comprehensive investigation into a dynamic model designed for the regulation of an HVAC system is conducted. This system is comprised of several integral elements, including a zone, heating coil, cooling and dehumidifying coil, humidifier, ductwork, fan, and mixing box. According to this model (Equation 2.3), the alteration rate in the moisture content within the

zone is contingent upon the distinction between the moisture vapor introduced into and removed from the zone (Tashtoush et al., 2005).

$$V_z \frac{dW_z}{dt} = f_s(W_s - W_z) + \frac{P(t)}{\rho_a} \quad (2.3)$$

Where $W_{si}$ humidity ratio of the supply air (to the humidifier) in kg/kg (dry air), P(t) is evaporation rate of the occupants = 0.08 kg $h^{-1}$, $p_a$ is density of air=1.25 kg $m^{-3}$, $V_Z$ is volume of the zoneZ36 $m^3$, $W_Z$ is humidity ratio of the zone in kg/kg (dry air), $f_{sw}$ water flow rate 8.0 $\times 10^{-5}$ $m^3$ $s^{-1}$ (Tashtoush et al., 2005).

Humidification is a mass transfer phenomenon involving the addition of water vapor to atmospheric air, leading to an augmentation of the water vapor content within the mixture. Inadequate moisture levels can have adverse consequences on human well-being. Monitoring and regulating air moisture levels are pivotal aspects of air conditioning. The equations governing energy and mass balances for the humidifier model established by Kasahara et al. (2001) can be described as follows in equations 2.4 and 2.5 (Tashtoush et al., 2005):

$$C_h \frac{dT_h}{dt} = f_{sa} C_{pa}(T_{si} - T_h) + \alpha_h(T_o - T_h) \quad (2.4)$$

$$V_h \frac{dW_h}{dt} = f_{sa}(W_{si} - W_h) + \frac{h(t)}{\rho_a} \quad (2.5)$$

h(t) is the rate of humid air that the humidifier can produce and it is a function of the humidity ratio. Where $C_h$ overall thermal capacitance of the humidifier=0.63 kJ $°C^{-1}$, $T_h$ supply air temperature (in humidifier) in (°C), $f_{sa}$ volume flow rate of the supply air=0.192 $m^3$ $s^{-1}$ , $C_{pa}$ specific heat of air=1.005 kJ $kg^{-1}$ $°C^{-1}$, $T_{si}$ temperature of supply air (to the humidifier)

(°C) , $T_h$ supply air temperature (in humidifier) in (°C), $a_h$ $(UA)_h$ overall transmittance area factor of the humidifier=0.0183 kJ $s^{-1}$ $°C^{-1}$ , $T_o$ temperature outside,=32 °C (Summer)= 5 °C (Winter), $T_h$ supply air temperature (in humidifier) in (°C), $V_h$ volume of humidifier=1.44 $m^3$, $W_h$ supply air humidity ratio (in humidifier) in kg $kg^{-1}$ (dry air), h(t) rate of moisture air produced in the humidifier (Tashtoush et al., 2005).

The energy equilibrium of a building based on the second law of thermodynamics is described by a non-geometric model, employing a single air node per zone to represent the thermal capacity of the air within that zone. In this non-geometric model, all air points within the zone share identical characteristics such as temperature and humidity. Equation (2.6) illustrates the building energy balance for a zone, and it corresponds to the TRNSYS output within the multi-zone building component labeled 'NTYPE 904 (Biserni & Garai, 2016).

$$\frac{DQ_{air}}{dt} = \dot{Q}_{heating} - \dot{Q}_{cooling} + \dot{Q}_{\inf} + \dot{Q}_{vent} + \dot{Q}_{tran} + \dot{Q}_{gain} + \dot{Q}_{sol} \qquad (2.6)$$

$DQ_{air}/dt$ represents the alteration in the thermal energy of the air within the zone over the time period (dt). $Q_{heating}$ and $Q_{cooling}$ denote the thermal energy supplied by heating and cooling equipment per unit of time, respectively. $Q_{inf}$ and $Q_{vent}$ represent the thermal gains resulting from infiltration and ventilation. $Q_{tran}$ signifies the thermal gain due to heat transmission between the inner surface nodes and the environment through the walls, encompassing both the total transmitted portion and the thermally accumulated portion in the wall. $Q_{gain}$ is the internal thermal energy gain, involving both convective and radiant components, generated by occupants and appliances per unit time. Finally, $Q_{sol}$ represents the solar gains, encompassing both direct and diffuse components, absorbed by the boundary

surfaces of the zone (Biserni & Garai, 2016). Ji et al. (2008) introduced an enthalpy-based model to examine the influence of latent load on the energy balance load, aiming to improve data screening accuracy for buildings located in hot and humid climates. The underlying principles of the energy balance load screening methodology are rooted in the fundamentals of the first law of thermodynamics. In a comprehensive whole-building thermodynamic model, the heat and enthalpy flow rates across the control volume's boundaries, along with work rates applied to the building, can be disaggregated into their primary components. This results in a simplified form of the energy balance equation (Equation 2.7) for a building, as follows (Biserni & Garai, 2016):

$$\frac{d}{dt}\overline{E} = \overline{Q}vent + \overline{Q}solar + \overline{Q}cond + \overline{Q}occ + \overline{W}bheat - \overline{W}bcool + f\overline{W}bele \quad (2.7)$$

The variables are defined as follows: E stands for energy storage, $W_{bele}$ represents non-HVAC electrical use for lighting and equipment, $W_{bcool}$ indicates chilled water for cooling, and $W_{bheat}$ signifies heating hot water for heating. $Q_{solar}$ is solar radiation through the envelope, $Q_{vent}$ covers ventilation and infiltration, $Q_{cond}$ relates to heat transmission through the structure, and $Q_{occ}$ accounts for heat generated by occupants. The factor "f" quantifies the portion of electricity converted to heat within the building. Based on the results, when the variance in the dry-bulb model increases with temperature, the enthalpy model exhibits superior fitting and more constrained control limits in areas characterized by high temperatures and humidity levels (Ji et al., 2008).

## 2.7 Impact of improved dehumidification on HVAC energy performance

Examining how buildings store heat, it was found that the storage of latent heat, especially through moisture, increases the workload on air conditioning, leading to higher

electrical energy consumption (Bailey et al., 1996). Homes with highly efficient cooling systems but low cooling load struggle to maintain indoor humidity below 60% for much of the year. Despite improved thermal distribution within these homes, there may be compromised comfort with moisture issues due to inadequate humidity control. Air conditioning alone faces challenges, with reduced runtime on both cooler days and hot nights. To achieve precise humidity control, the inclusion of a supplemental dehumidification system becomes imperative (Withers & Center, 2018). In hot and humid climates, dehumidifier energy consumption, in mechanically ventilated homes, can reach 10 kWh $day^{-1}$, accounting for nearly half of the cooling and dehumidification energy use (Rudd et al., 2005). The cooling load consists of two components: sensible (controlled by dry air temperature) and latent (related to moisture content in the air) (Daou et al., 2006). The sensible heat ratio (SHR) represents the ratio of sensible load to the total cooling load (Khattar, 1997). Air conditioners have specific rated SHRs, but actual SHRs vary based on incoming air conditions. Manufacturer data indicates that air conditioners that have higher SHRs with cooler, drier air, and lowering coil temperature, can improve moisture removal (Liang et al., 2022).

In a reported study, reducing the RH setpoint from 60% to 50% led to a notable rise in dehumidifier energy consumption, even dropping to 40% RH. At 40% RH, the dehumidifier surpassed cooling energy usage, accounting for 44% of annual space conditioning energy (Fang et al., 2011; Withers & Center, 2018). A 50% RH setpoint resulted in a contribution of the dehumidifier to around 35% of total annual space conditioning energy. Lowering the RH setpoint increased air conditioning load and annual cooling energy use. Notably, lower-rated SEER air conditioning systems, while enhancing dehumidification, could reduce total space conditioning energy (heating, cooling, and dehumidification) compared to higher-efficiency units (Withers & Center, 2018) as illustrated in Figure 2.6.

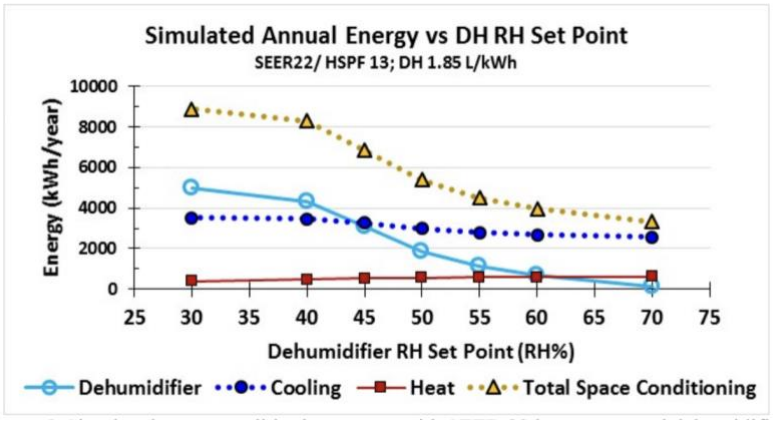


**Figure 2.6.** Simulated space conditioning energy with SEER 22 heat pump and dehumidifier (Withers & Center, 2018).

Research investigated the performance of modified large-scale hybrid HVAC and humidification-dehumidification desalination (HDD) systems tailored for hot, arid climates using water-cooled chiller units (S. A. Nada et al., 2015). The modifications notably reduce the cooling coil capacity by pre-cooling air in an evaporative cooler, lowering enthalpy at the cooling coil inlet (Catrini et al., 2018). Elevated supply air temperature (Ts) amplifies the cooling load across all systems, necessitating increased airflows and higher cooling coil loads. Moreover, power savings improve with higher Ts and lower outdoor air wet bulb temperatures, highlighting the potential for energy-efficient operation in hot, arid environments (S. A. Nada et al., 2015). Analyzing heat pumps in hot and humid climates, particularly for summer dehumidification, highlights the critical importance of efficiency. A study combined validated thermodynamic heat transfer models for heat pumps and structural buildings and focused on three climate zones in China: Guangzhou, Wuhan, and Jiuquan (Jin et al., 2023). Using thermodynamics, the air enthalpy is determined from dry bulb temperature and absolute humidity, aiding accurate AC load calculations. Hourly outdoor air state points in the cities throughout the year depict enthalpy distribution tied to temperature and humidity. Guangzhou experiences high temperatures and humidity, while Jiuquan records lower outdoor air enthalpy,

reflecting high temperatures and lower humidity during cooling seasons. Increased absolute humidity elevates latent heat load, impacting AC efficiency. While enhancing heat pump COP is vital, improving the dehumidification efficiency significantly influences energy performance, especially in humid areas like Wuhan and Guangzhou. In extremely dry and hot cities like Jiuquan, dehumidification improvements may have limited impact (Jin et al., 2023).

To enhance energy efficiency, researchers have explored various methods to control indoor temperature and humidity. Traditionally, to improve the ability of buildings to absorb and desorb heat, materials like stone, brick, and concrete have been used for thermal control in buildings for thousands of years. Nevertheless, these materials stored thermal energy as sensible heat, requiring massive amounts of these materials. In recent developments, there is a growing interest in innovative materials like phase change materials (PCM), which can efficiently store both sensible and latent heat. This has the potential to reduce the dependence on traditional heating and cooling methods, significantly improving energy conservation in buildings (Cui & Wei, 2017; Lee et al., 2000).

### 2.8 Ice nucleation

The main steps of the frosting process on the surface of a cold plate start with droplet condensation and developing droplet nucleation. Then, it follows with the assimilation of small droplets which have less resistance, compared with bigger droplets. Over the solidification step, ice crystals are created at the critical time and the crystallization starts vertically from the tip of the droplet. The tip extends by absorbing vapor from the surrounding air to form a partly uniform porous layer of frost. Numerous tiny ice branches emerge from the tip of the vertical growth, and the layer of porous frost is created by hollow frost. Due to water vapor permeation and frost layer surface melting, the density of the frost layer will rise during the fourth phase, known as the full growth period of the frost layer as seen in Figure 2.7 (b) (Song & Dang, 2018; Song, Dang, Higashi, & Hihara, 2020).

In terms of temperature reduction, the temperature variation of a water droplet during the cycle of droplet freezing can be divided into four distinct stages, Figure 2.7 (c). The temperature of the droplet falls at the pre-cooling or supercooling step from the beginning freezing temperature ($T_i$) to the nucleation temperature ($T_N$). Figure 2.7 shows the recalescence stage's starting temperature. The temperature of the upside-down liquid water then quickly rises to the phase change temperature, or the solidification temperature, due to the latent heat released from the ice (Song et al., 2020; X. Zhang, Wu, Min, & Liu, 2017).

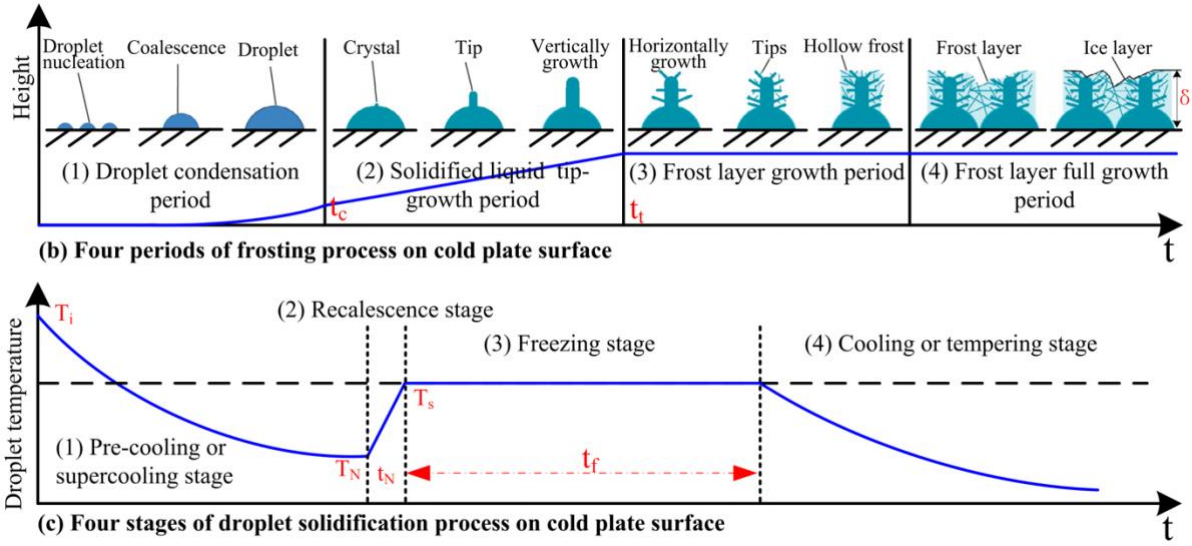


**Figure 2.7**. Temperature reduction, cycle over droplet freezing (Song et al., 2020; X. Zhang, Wu, Min, & Liu, 2017)

In a water droplet, homogeneous nucleation and heterogeneous nucleation are both potential types of ice nucleation. Volume-induced nucleation has a nucleation rate that is proportional to the volume of the droplet, whereas the other has a nucleation rate that is proportional to the length of the three-phase line or the surface area of the interfaces (Schutzius et al., 2015).

Throughout the process of cloud formation, homogenous nucleation can be found. While in laboratory investigations, basic ice nucleation phenomena are frequently studied by

purposefully exploiting micro-scale surfaces. This is due to how much more accurate and stable the controls are in micro-scale experiments. However, it was unable to properly translate the repeatable homogeneous ice nucleating activity on the relevant macro-scale interfaces (Inada, Koyama, Goto, & Seto, 2011; Li et al., 2012; Murray, O'sullivan, Atkinson, & Webb, 2012; Peter et al., 2006).

### 2.8.1 Latent heat in clouds

The energy needed to keep a convective cloud floating in a stable environment comes from the latent heat released when cloud particles change phases. This heat helps the cloud stay warmer than its surroundings at different pressure levels, compensating for entrainment—a mixing process that dilutes cloudy air with drier, colder air. Entrainment is the main factor slowing down the growth of cumulus clouds (Lamb et al., 1981).

Generating more latent heat occurs when larger volumes of ice phases are formed, necessitating lower cooling temperatures to sustain a consistent draw temperature (Drewett & Hartel, 2007).

In an experimental investigation into the development of ice crystals, it is documented that three principal factors contribute to their growth: supercooled fog, fall velocity, and the characteristics of shape, size, and mass (Tan et al., 2021). The cooling process was accomplished through the evaporation of fog droplets where the most substantial growth of ice crystals was observed, signifying an accelerated mass growth rate facilitated by swift vapor diffusion towards ice crystals with a larger surface area, coupled with the rapid dissipation of the released latent heat from the crystal (Bayer-Giraldi et al., 2018). Another facet of the mass growth rate involves the shift of the highest peak towards colder regions as crystals expand, associated with the nucleation and growth of round crystals or their radiating assemblages. Within the temperature zone exhibiting the swiftest growth, the rapid release of latent heat

serves to warm both the local system surrounding the ice crystal and the overall system (Fukuta, 1969).

### 2.8.2 Cloud formation and latent heat over the phase change

Latent heat is a crucial factor in the dynamics of a storm, influenced by changes in water phase (Allan et al., 2020). According to Li et al. (2013) the absorption of latent heat during processes like melting, evaporation, and sublimation strengthens downdrafts, while the release of latent heat during condensation, freezing, and deposition enhances updrafts (Li et al., 2013). These effects are more pronounced in continental clouds than in maritime clouds, primarily due to the increased occurrence of cold rain processes in continental environments, involving significant latent heat changes (Fernández-González et al., 2016).

Water vapor turning into water droplets in the air occurs on small particles known as condensation nuclei (McMurry, 2000). Clouds composed of water droplets can persist at temperatures as low as -40°C, but ice can form at higher temperatures due to ice condensation nuclei (ICN). While homogeneous nucleation can occur, it requires an RH of ~500%, making it unlikely in the atmosphere. Instead, cloud condensation nuclei (CCN) aid liquid droplet formation, while ICN facilitate ice crystallization. Notably, CCN are generally poor ICN and vice versa, and biological particles often act as ICN, enabling ice formation at higher temperatures (Bigg, 1953).

In the troposphere, liquid water often exists at temperatures below ice's melting point due to energy barriers in phase transitions. Ice formation in the atmosphere is a result of nucleation, primarily through homogeneous processes without catalysis. According to classical nucleation theory, the energy barrier between supercooled liquid and crystalline ice can be calculated. When the contribution from the bulk surpasses the surface term at a critical size, determined by how far below the melting point the liquid is cooled, it marks the magnitude of the energy

barrier to nucleation. Ice forms homogeneously in the upper troposphere, where temperatures stay below -33°C. Freezing at higher temperatures in the atmosphere happens through heterogeneous nucleation, involving catalysis by a foreign body (Cantrell & Heymsfield, 2005). Contact nucleation, a challenging aspect of ice formation in the atmosphere, occurs when a droplet freezes upon touching an aerosol particle. Various substances exhibit distinct freezing thresholds as contact nuclei compared to other roles like deposition, condensation, or immersion nuclei. This suggests that the freezing mechanism differs across these different modes (Cantrell & Heymsfield, 2005).

In an experiment, water droplets (millimeters in size) containing a single ash particle (~100 μm diameter) were repeatedly frozen and thawed by cycling through various freezing events while immersed in silicon oil which is a type of synthetic fluid that is composed of polymerized siloxanes. The freezing temperature in each cycle was identified by monitoring the temperature rise caused by the release of latent heat during the phase transition. The findings indicate a consistently stable freezing temperature for a specific setup of the ash-droplet system. The temperature doesn't change, just by the ash particle touching the water droplet, rather it remains stable as long as the ash particle intersects with the droplet's surface (Mi et al., 2004).

Ice crystals help reduce cloud droplets by sticking to them, which slows down the formation of larger drops and the drizzle process. Since ice crystals are good at collecting bigger droplets, their growth can delay drizzle formation. Additionally, ice crystals can collide with and freeze drizzle drops, stopping the freezing drizzle. Studies have found that how we describe ice crystals influences how freezing drizzle forms in stable clouds (Geresdi et al., 2005).

A study on heavy rain development revealed that cold clouds with ice due to convection play a key role, especially in the southern area like low-latitude, warm, and tropical regions. These areas tend to have a deeper boundary layer, leading to higher and colder cloud tops that promote more cloud ice formation and intensify precipitation processes. Warm clouds with water instead of ice cause widespread but weak precipitation. Rainstorm growth and the evaporation of cloud and rainwater significantly boost precipitation. The condensation of water vapor into cloud water contributes the most to latent heat during heavy rain. Positive latent heat processes, like condensation of water vapor and rainwater, promote precipitation, while negative processes, such as rainwater evaporation and graupel melting, weaken it. Rainwater condensation is crucial for sustaining atmospheric heating and convection during heavy rain, influencing precipitation intensity. Without rainwater droplet formation, overall latent heating weakens, causing a significant drop in moisture and precipitation. This reduction in latent heat can result in a decrease in moisture content in the atmosphere and lead to lower precipitation levels. Latent heat is released when water vapor condenses into liquid droplets, driving cloud formation and precipitation. Without this phase change, the system loses a key source of energy and moisture, thereby reducing overall rainfall (Jiang-nan et al., 2016).

Clouds in Earth's atmosphere vary, composed of liquid droplets, ice crystals, or a combination. While temperature primarily dictates cloud phases, other factors come into play. Aerosols, small particles in the atmosphere, influence clouds differently based on their phase. These aerosols act as cloud condensation nuclei (CCN) or ice nuclei (IN), known as indirect aerosol effects. Cloud droplets typically require hygroscopic aerosols for formation in Earth's atmosphere. In a hypothetical aerosol-free environment, clouds could form through homogeneous nucleation, but in reality, aerosols, both natural and human-made, are always present and seldom limit liquid cloud formation, which initiates when humidity exceeds 100% (Storelvmo, 2017). CCN play a vital role in the formation of cloud droplets, driven by the

Kelvin effect, which describes the alteration in saturation vapor pressure due to surface curvature (McGouldrick & Barth, 2023). This concept parallels the dehumidification process in HVAC systems where humidity control is crucial for preventing condensation and maintaining indoor air quality.

Figure 2.8 illustrates the fundamental mechanisms of cloud and rain formation, including the corresponding phase change processes and the associated release of latent heat. In deep convective and stratiform rains, latent heat-related phase changes include condensation-evaporation (gas-liquid), freezing-melting (liquid-solid), and deposition-sublimation (gas-solid). Current remote sensing and in situ instruments can't directly measure these processes, as they mainly focus on atmospheric water states like vapor, cloud water, and precipitation. Retrieving latent heat relies on physical parameterization or cloud-resolving models (CRMs). Additionally, the formation of convective, stratiform, and warm rain involves various phase change processes depending on different dynamic and thermodynamic conditions (Li et al., 2013). After fog forms, processes like water vapor condensation, collision–coalescence, and droplet evaporation or sedimentation influence its microphysics. Parameterizations of activation and condensation processes significantly impact fog characteristics and life cycle.

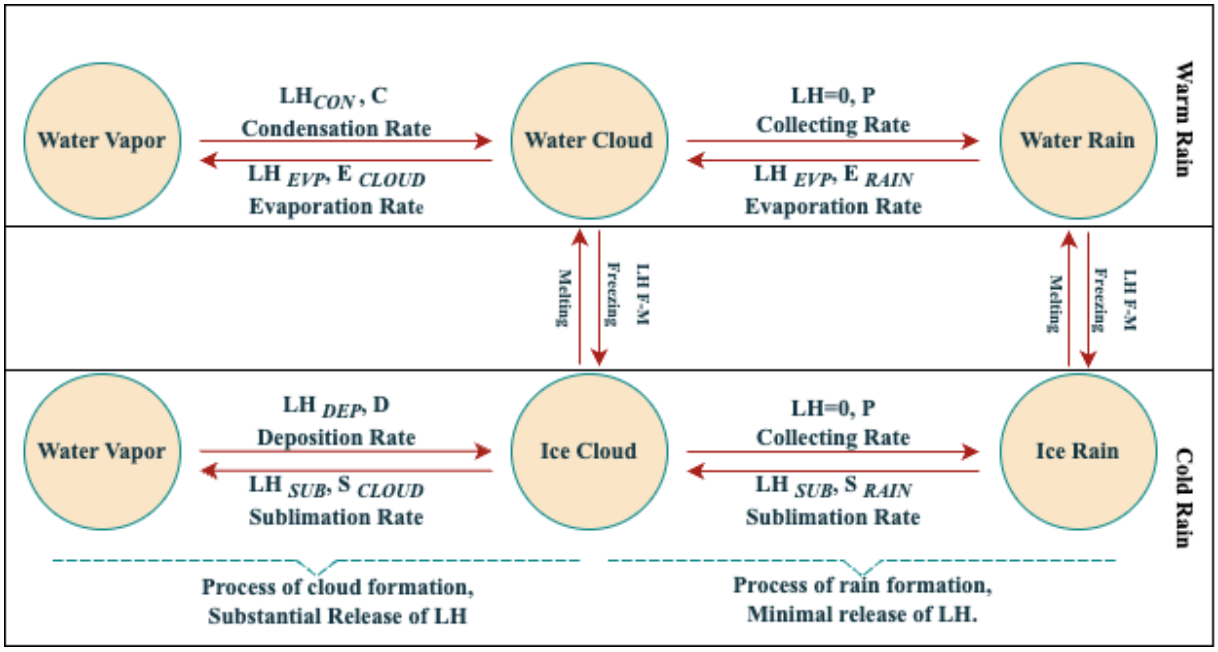


**Figure 2.8.** The diagram illustrating the processes of cloud formation, rain generation, and the associated release of latent heat in warm and cold rain events (Li et al., 2013).

Latent heat, released or absorbed during transitions between water phases, plays a crucial role in fortifying storms. Warm rain processes involve solely evaporation-condensation, while cold, deep convective clouds encompass melting-freezing and sublimation-deposition (Li et al., 2013). As warm air rises and water vapor condenses, the released latent heat heightens instability, strengthening updrafts. Likewise, the freezing of liquid droplets releases latent heat, contributing to the same effect. Latent cooling, absorbed during sublimation, evaporation, and melting, amplifies negative buoyancy, reinforcing downdrafts, intensifying updrafts, and enhancing the overall instability (Szeto & Stewart, 1997). This underscores the significance of latent heat as the primary driving force behind vertical currents within a storm. In cold clouds, which consist of ice, the particles have complex microstructures due to the rigid nature of ice crystals. Unlike warm clouds, the particles in cold clouds are not spherical, as they do not respond to surface tension. This introduces particle shape as a new variable in describing cloud properties, adding complexity beyond just particle sizes (Lamb & Verlinde, 2011).

## 2.9 Thermodynamics of fog formation

In balanced air conditions, the air can only hold a certain amount of water vapor at a given temperature. This capacity decreases as the temperature decreases. Relative humidity measures the actual water vapor in the air compared to its holding capacity. When two air streams with different humidity levels mix, the resulting air mixture may have more water vapor than it can hold, causing the extra vapor to turn into tiny water droplets, Figure 2.9. These droplets form fog, reducing visibility in the air to less than 1 m close to the surface (Mazoyer et al., 2022; Wadnerkar et al., 2018).

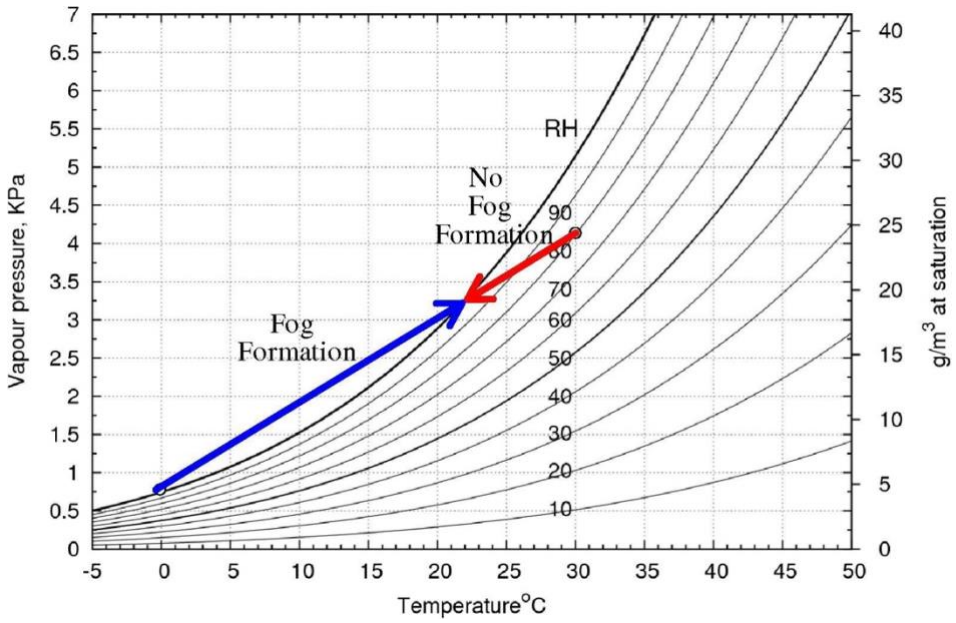


**Figure 2.9.** Mixing hot and cold air streams is depicted on psychometric charts, illustrating how the formation of fog depends on the degree of mixing (Wadnerkar et al., 2018)

Accurate fog modeling requires precise identification of microphysical parameters, including liquid water content (LWC), droplet number concentration ($N_d$), and effective diameters ($D_{eff}$). The initial values for $N_d$ and $D_{eff}$ are influenced by both ambient supersaturation and the aerosol population, which functions as cloud condensation nuclei (CCN) (Mazoyer et al., 2019; Stolaki et al., 2015). Once fog is formed, various physical processes impact its microphysical characteristics. Droplets can increase in size through water

vapor condensation, collision–coalescence, or Ostwald ripening, a process in which smaller droplets deactivate and evaporate, favoring vapor diffusion onto larger droplets. Conversely, droplets can settle due to gravity or turbulent motions, or evaporate if there's a decrease in supersaturation, for instance, through heating or drying of the air mass, like when mixing with residual dry air (Mazoyer et al., 2019; Wærsted et al., 2019). When supersaturation is low, droplet growth through condensation might be limited, allowing extra water vapor to activate more aerosols into cloud droplets. As fog progresses, turbulent motions can boost supersaturation and trigger new aerosol activation (Boutle et al., 2018).

### 2.9.1 Ice fog

Ice particles in the atmosphere have diverse sizes, ranging from a few micrometers to over 10 cm. Clouds display a size distribution, with more small particles (frozen fog or cloud droplets) than large ones (like snow aggregates or hail) in a given cloud volume. The concentration of ice particles varies naturally, with smaller particles at higher altitudes (lower temperatures) and larger particles at lower altitudes (higher temperatures). This pattern is opposite to warm clouds. Some ice particles are challenging to classify and are termed "irregular," making the study of cold clouds complex (Lamb & Verlinde, 2011).

Ice fog, known by various names like frozen fog or arctic mist, occurs in extremely cold arctic winters when temperatures drop below −30°C and relative humidity exceeds 80%. It consists of suspended ice crystals and is operationally defined by visibility less than 1 km. This distinguishes it from "diamond dust," another surface cloud type formed in similar conditions but with higher visibility. The upper size limit (d) and number concentration ($N_i$) criteria for ice fog are $d < 30$ μm and $Ni > 1000\ L^{-1}$. Many studies report that the sizes and concentrations of ice fog crystals frequently vary outside these limits, causing a somewhat blurred differentiation between diamond dust and ice fog (Girard & Blanchet, 2001a). Table 2.2 shows the average temperature, size and water content of ice fog based on other studies.

**Table 2.2.** Average temperature, size and water content of ice fog

| Temperature (°C) | Size | Water Content | Reference |
|---|---|---|---|
| less than − 40 °C | | Less than 100% | (Gotaas & Benson, 1965) |
| -5 to -10 °C | 1–50 $\mu$m | water amount of 0.12 g $m^{-3}$ ice water amount of 0.10 g $m^{-3}$ | (Pu et al., 2023) |
| -5 to -37 °C | average of 1.3 mm (20 $\mu$m to 3.5 mm) | | (Kuhn & Gultepe, 2016) |
| -15 to -34 °C | below 30 μm | concentration exceeds 1000 $L^{-1}$ | (Girard & Blanchet, 2001b) |

Ice crystals in fog form through either homogeneous or heterogeneous nucleation. In homogeneous nucleation, water droplets freeze uniformly when the temperature drops below -38°C. Heterogeneous nucleation involves pathways like immersion freezing, contact freezing, or deposition ice nucleation. Immersion and contact freezing occur at temperatures above -38 °C, where the droplet freezes due to nuclei composition or contact with an ice nucleation (IN) particle. Deposition nucleation activates an ice crystal by directly transferring water vapor to an IN particle without liquid water (Ismail Gultepe et al., 2017). Identifying the phase status of cold fog, whether it's liquid, ice, or a mix, poses a challenge due to its high variability in both space and time (Pu et al., 2023). Ice fog and clouds with low optical densities disperse after exposure to dry air, light precipitation, or solar heating. Their formation depends on temperature and moisture content in the atmospheric boundary layer, influenced by factors like ocean vapor and wet surfaces. Turbulent heat and moisture fluxes over these surfaces play a crucial role (I Gultepe et al., 2017; Gultepe et al., 2015; Vihma et al., 2014). Global change

processes, including regional air pollution, impact fog due to a limited understanding of ice nucleation (IN) processes, especially homogeneous ice nucleation, occurring at very cold temperatures (~−40 °C). Exploration is needed, particularly for high ice crystal concentrations during Arctic ice fog events (Gultepe & Heymsfield, 2016; Heymsfield et al., 2005; Heymsfield & Sabin, 1989).

Observations during the cold fog amongst complex terrain (CFACT) field campaign in Utah's Heber Valley reveal notable variations in meteorological conditions around fog events. Moisture near the surface declines in the early morning, likely due to fog formation and subsequent moisture deposition. While persistent deep fog events were absent, the campaign provides valuable data for studying spatially heterogeneous and ephemeral fog occurrences (Pu et al., 2023).

### 2.10 Hydrological cycle in atmosphere

The hydrological cycle encompasses processes across the hydrosphere, driven by solar radiation and gravity. It involves interactions among oceans, atmosphere, and land, facilitating water and energy exchange (Kleidon & Renner, 2013). Water plays a vital role in the atmosphere, existing in its three forms: solid, liquid, and gas. Phase changes involve substantial energy exchange, influencing the local energy balance and atmospheric dynamics. The average global latent heat flux is approximately 80 W $m^{-2}$, considering a mean insulation of 342 W $m^{-2}$ (Kiehl & Trenberth, 1997).

Water vapor serves as the origin for clouds and fog, influencing radiative transfer and evaporation/condensation processes. Cloud formation is regulated by relative humidity, atmospheric dynamics, and the presence of condensation nuclei. The altitude at which

saturation occurs is influenced by temperature and specific humidity vertical profiles (Vihma et al., 2016).

Water balances with evaporation matching precipitation, but regional variations exist. The northern hemisphere (10-40°N) loses substantial water to higher latitudes, gaining around 3,000 $km^3$ from the southern hemisphere. Between the equator and 30°S, there's a net loss of 32,700 $km^3$, mainly moving to higher latitudes. The westerlies transport about 56,000 $km^3$ of water vapor toward polar fronts, significantly influencing Earth's heat transfer (Fairbridge et al., 1998).

The dominant phase change in dehumidification systems has traditionally been condensation, where water vapor is absorbed. However, in this study, we explored a different approach. Deposition nucleation happens when vapor adheres to a solid surface and transforms directly into ice without passing through a liquid phase (Dymarska et al., 2006). This phenomenon is evident in nature, such as the formation of frost when atmospheric water vapor deposits as ice crystals. The energy required for vapor to condense (latent heat of vaporization) is about 540 calories per gram (2,260 kJ $kg^{-1}$), which is significantly higher than the energy needed to freeze water into ice (latent heat of fusion), which is 80 calories per gram (Richards & Mathews, 1911).

In this study, the reverse process of sublimation is examined, where vapor transitions directly into ice, releasing substantial latent heat. This release of energy facilitates greater moisture absorption from the air, enhancing the drying process through the latent heat released during the phase change from water vapour to ice through sublimation and condensation, Figure 2.10 (Giorgini, 2016).

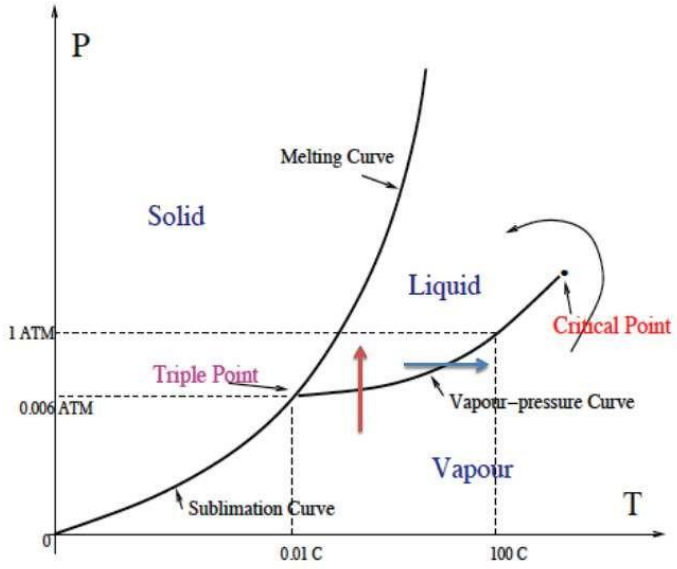


**Figure 2.10.** Phase Transition Diagram by Latent Heat Release during Sublimation and Condensation (Giorgini, 2016)

Negative pressure systems, combined with latent heat mechanisms, may offer an efficient approach to thermal management in extreme environments. In such systems, negative pressure lowers the boiling or sublimation point of water, facilitating phase change processes such as sublimation (solid to vapor) or evaporation (liquid to vapor). Water sublimators use porous plates where ice sublimates under low-pressure conditions, absorbing the latent heat of sublimation to remove waste heat effectively. The role of negative pressure in such a system would be to create an environment where water vapor transitions directly to the solid phase (ice) without passing through the liquid phase (Chang et al., 2023).

**Connecting text**

Chapter 2 lays the groundwork for this research by presenting an in-depth review of existing dehumidification and HVAC systems, highlighting current challenges and innovations in energy-efficient climate control. This chapter provides a comprehensive overview of various dehumidification methods and the physical principles governing them, which form the theoretical basis for the novel approach proposed in this study.

# CHAPTER 3

## Novel dehumidification system using vortex cooling and Cold Plate Ice Formation cold plate ice formation

Sheida Rezaei[1], William Boyd Dumais[1], Md Sazan Rahman[2], Sarah MacPherson[1], Valerie Orsat[1], Mark Lefsrud[1]*

[1]Department of Bioresource Engineering, Macdonald Campus, McGill University, 21111 Lakeshore Road, Ste-Anne-de-Bellevue, QC, H9X3V9

[2] Agriculture, Nutrition and Food Systems, University of New Hampshire, Durham, NH 03824

*Corresponding author: mark.lefsrud@mcgill.ca

### 3.1 Abstract

Dehumidification systems are crucial for maintaining comfort and energy efficiency in buildings, especially in hot and humid climates. Traditional dehumidification technologies often struggle with energy consumption and efficiency. This investigation examines the thermodynamic performance of a novel, proof-of-concept dehumidification system that combines a vortex cooling gun with a cold plate to optimize moisture extraction efficiency. In this method, the hot and humid air comes into contact with the cold plate and vortex cooling gun, releasing heat and forming ice crystals on the surface of the cold plate. The new system's effect on relative humidity (RH), absolute humidity, temperature, moisture removal rate, and enthalpy was quantified. Data indicate that RH levels dropped significantly, with inlet RH decreasing up to 80% and outlet RH stabilizing at 30%, demonstrating effective moisture reduction ($p < 0.05$). Absolute humidity measurements further validated the system's dehumidification capability, with a notable decrease in moisture content from an initial 14 g $m^{-3}$ to 2 g $m^{-3}$. A rapid temperature drop from 15°C to below 5°C within 1000 seconds in an air volume of 0.05 $m^3$ indicates efficient thermal energy extraction. The system achieved a substantial reduction in air enthalpy by 20 kJ $kg^{-1}$, highlighting its utility in cooling and moisture control scenarios. The relationship between moisture removal rate and inlet absolute humidity showed that higher initial humidity levels enhance dehumidification. This research provides critical insights into advanced dehumidification methodologies leveraging direct contact cooling mechanisms, potentially offering an alter approach to lower energy consumption cooling in climatic and industrial applications.



**Keywords:** building cooling; dehumidification, energy savings; environmental control; heating, ventilation and air conditioning (HVAC), moisture control, supercooling

## 3.2 Introduction

Approximately 40% of total energy consumption in the United States is attributed to building operations, with heating and cooling comprising the predominant share (Ghoniem, 2011). In geographic regions characterized by hot and humid climates, cooling systems play a pivotal role. However, surpassing humidity thresholds can pose challenges in the design and operation of building heating, ventilation and air conditioning (HVAC) systems by exacerbating issues like poor air quality because of dust accumulation, mite proliferation, and disease transmission. Consequently, devising effective and tailored dehumidification strategies tailored to the climatic conditions of each region, particularly those grappling with elevated humidity levels, becomes imperative. Enhancing existing HVAC systems by optimizing dehumidification processes stands out as a viable, accessible solution to address this need effectively and affordably in diverse climatic conditions.

HVAC systems are vital across various building types, aiming to maintain occupants' thermal comfort by adjusting outdoor air conditions. Selection depends on climate, building age, owner preferences, budget, and architectural design (ASHRAE, 1996). HVAC systems vary based on design and functionality. Centralized systems serve large buildings with a single unit distributing heating and cooling via ducts. Decentralized systems, like window units, cater to individual areas without ductwork. Split and mini-split systems, ideal for residential and small commercial spaces, separate condenser and evaporator units for flexibility and efficiency. Heat pumps provide both heating and cooling by transferring heat between indoors and outdoors, suitable for diverse climates. Hybrid systems combine fossil fuel heating with electric heat pump technology, enhancing energy efficiency. Each type is tailored to specific applications and building needs (Teke & Timur, 2014).

Present dehumidification options primarily consist of traditional condensation dehumidifiers and desiccant dehumidifiers (Gurubalan & Simonson, 2021). The initial investigation into the transfer of heat and moisture involving phase change and condensation

dates back to the 1980s. Ogniewicz and Tien (1981) were pioneers in analyzing the interconnected processes of heat and moisture transfer with condensation. Their work focused on the assumption that heat moves through conduction and convection, while the condensate exists in a pendular state (Fan et al., 2000; Ogniewicz & Tien, 1981).

Traditional condensation dehumidifiers are typically part of a vapor compression refrigeration system. Cold water cools the air to remove moisture, but this process often requires overcooling and subsequent reheating to achieve the desired moisture levels, resulting in greater energy consumption (Yao, 2010). Additionally, these systems only provide comfort when the sensible heat ratio (SHR) exceeds 0.75, making it challenging to achieve thermal comfort in warm, humid regions where the sensible heat ratio is often lower (Ding et al., 2022; Rafique et al., 2015). The SHR measures the proportion of an HVAC system's capacity used for sensible cooling versus latent cooling. A lower SHR indicates higher dehumidification capability, crucial for humid climates, aiding in system design and selection (Pillai et al., 2018).

Cloud condensation nuclei (CCN) play a vital role in the formation of cloud droplets, driven by the Kelvin effect, which describes the alteration in saturation vapor pressure due to surface curvature (McGouldrick & Barth, 2023),. This concept parallels the dehumidification process in HVAC systems where humidity control is crucial for preventing condensation and maintaining indoor air quality. Clouds forming just above freezing levels primarily consist of supercooled liquid droplets, whereas those at higher altitudes, where temperatures are colder, tend to form as ice crystals (Murray et al., 2012). Insufficient condensation particles at or above the condensation level can lead to air becoming supersaturated, hindering cloud formation (Pidwirny, 2006). As air rises, atmospheric pressure decreases, causing expansion that expends energy and cools the air, promoting water vapor condensation into clouds (Makarieva et al., 2013). Experimental findings indicate that elevating air pressure enhances the dehumidification efficacy of moist air. As pressure rises, the temperature disparity between air and cooling

sources diminishes while maintaining consistent dehumidification requirements. When the temperature difference between air and cooling source remains constant, heightened pressure correlates with increased heat and mass transfer coefficients (Zhang et al., 2024).

Natural occurrences exhibit these concepts. When the upper ocean reaches freezing temperatures, further heat loss causes slight supercooling, leading to ice formation. The minimal degree of supercooling required for ice growth is typically on the order of a few hundredths of a degree Celsius. However, observations in certain Antarctic polynyas and areas near Greenland have shown supercooling of 0.2 to 0.4°C down to depths of tens of meters. Initial ice formation usually occurs at or near the water surface in the form of small platelets and needles called frazil ice, with crystals generally not exceeding 3 to 4 mm in diameter. Subsequently, ice crystals absorb and freeze additional water vapor from the surrounding air (Maykut, 2018). In the presence of air exhibiting supersaturation above the freezing threshold, moisture within the atmosphere can undergo condensation into minuscule liquid droplets, resulting in the recognizable meteorological phenomenon, fog. Conversely, under comparable conditions with air temperature below freezing, , "ice fog" formation is anticipated. Airborne ice crystals, typically constituents of fog, display a notable propensity to adhere to cold surfaces, thereby predisposing them to deposition on surfaces encountered within a freezer environment (Mago & Sherif, 2005). Snow-like formations, as elucidated by Sherif et al. (2001) and the studies by Mago and Sherif (Mago & Sherif, 2005), share resemblances with snow in both visual attributes and crystal morphology, contrasting with the typical frost formation observed under subsaturated conditions. These formations manifest promptly, within a timeframe spanning from 15 min to 2 h, and are notable for their elevated intensity, which contributes to a rapid deterioration in heat transfer effectiveness and cooling efficiency of freezer coils (Sherif et al., 2002).

Drawing parallels between these natural processes and HVAC systems, the present investigation explores proof-of-concept dehumidification of hot and humid air using vortex cooling gun and a cold plate to induce a phase transition in cooled air from a gaseous to a solid state, consequently releasing latent heat. The primary aim was to quantify the latent heat released during this transition and evaluate the efficacy of ice crystal formation in augmenting air dehumidification with lower energy requirement potential. When humid air encounters a cold surface with temperatures below both the dew point of the water vapor and the freezing point, ice crystals are likely to form. This process presents a promising method to improve dehumidification, particularly under saturated conditions, and holds significant potential for developing energy-efficient cooling strategies in HVAC systems.

## 3.3 Materials and methods

### 3.3.1 Chamber structure

A combined vortex gun and cold plate system was designed and constructed to effectively monitor the behavior of hot and humid air as it interacts with cooled devices. Two PVC pieces (0.10 m diameter) were arranged on opposite sides of a circular hard-plastic chamber measuring 0.33 m in diameter to facilitate the connection of a booster fan (GLFANXBOOSTER6 model, iPower US, Los Angeles, CA, US) with a diameter of 0.152 m. The output area of the pipes was insulated using Fibreglass Pipe Wrap measuring 0.03 × 0.01 × 0.25 m. A large model ultrasonic mist humidifier, Lacidoll ultrasonic mist humidifier (27 × 27 × 63 cm; Lacidoll, Cerritos, CA, US) with adjustable moisture settings continuously supplied moisture. Cold airflow within the chamber was generated using a small Vortex cooling gun (3404 model, EXAIR LLC., Cincinnati, OH, US). Cooling of the system was achieved using an ATS-CP-1003-DIY aluminium cold plate (0.202×0.13×0.02 cm) with a flow

rate of 4 L $min^{-1}$, capable of transferring 1000 W of heat with a temperature difference of 6.8℃ between the cold plate base and inlet fluid temperature. The cold plate was positioned in the center of the circular hard-plastic chamber, with its input and output connected to a circulator bath. Heated Immersion Circulators (4100 R20, Fisher Scientific Isotemp®, Saint-Laurent, Qc, Canada) were employed, utilizing both heated and chilled baths.

### 3.3.2 Experimental setup

The overall design of the vortex cold gun-ice plate dehumidification system and experimental setup is schematically presented in Figure 3.1 with a photograph in Figure 3.2 The body of the dehumidifier camper consists of the ultrasonic humidifier with the output of 2000 ml $h^{-1}$ was used for humidity supply to the chamber and the output air velocity of hot and saturated air was 0.74 m $s^{-1}$. A 10.16 cm duct was used to connect the exit of the humidifier to the inside area of the chamber. A circulator bath was set up to circulate the cold mixture of water and coolant into the cold plate. Every circulator bath can pump to an external system to meet the temperature control needs. The maximum flow rate of the circulator bath was 0.033 $m^3$ $h^{-1}$ with temperature stability between -10 and 100 °C. The air ducts were connected with reducers (10.16 cm-to-15.24 cm) to the duct booster fan to improve the ventilation (240 CFM). Temperature, humidity, and pressure sensors (Raspberry pi: BME280, Adafruit Industries, New York, NY, US) were placed before and after the chamber to check inlet and outlet conditions of air, and in-room area (S1, S2, S3 and S4). A digital hot wire anemometer was used to record the flow velocity of air inside the chamber and air temperature readings. The air flow and pressure rate were kept constant at 1.03 m $s^{-1}$ and 1013.3 Pa respectively. The total calculated air volume of this setup was approximately 0.05 $m^3$.

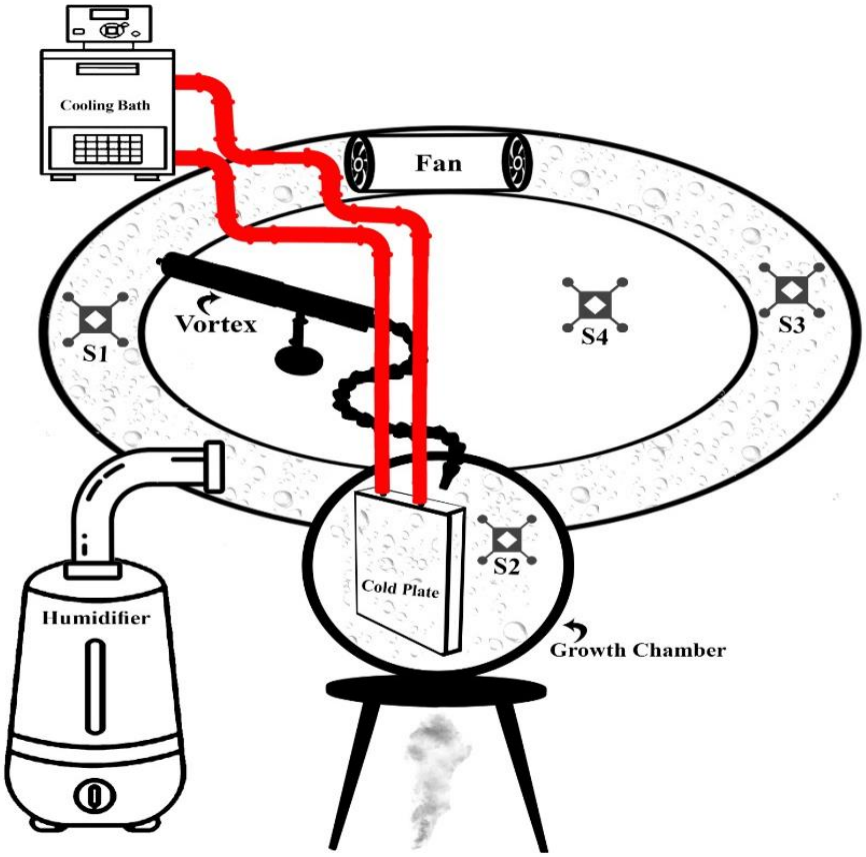


**Figure 3.1.** Schematic view of the vortex cold gun-ice plate dehumidification system (top) and experimental setup (bottom) presenting sensors and data logger positions. S1:S4, measuring RH, temperature and air pressure.

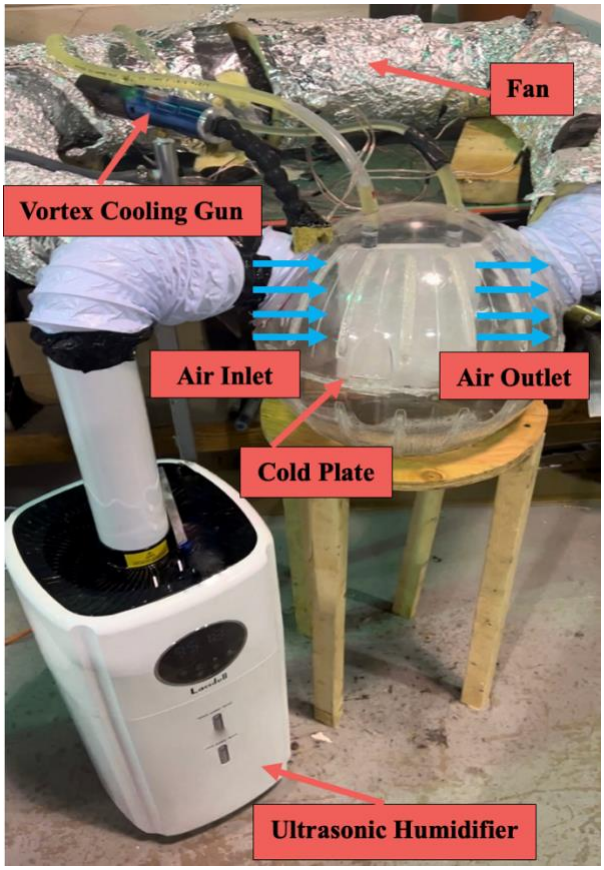


**Figure 3.2.** Photograph of the overall experimental setup to show instrumentation and data logging positioning. Blue arrows indicate the airflow rate.

### 3.3.3 Data collection

A Python-coded automatic data logger Pi (4B, Raspberry Pi, Wales, UK) was used to record temperature, pressure, and RH data every 2 s with BME 280 environment sensors (Adafruit: BME 280, Adafruit Industries, New York, NY, US). The automatic sensors' error levels for recording temperature data are 0.5°C and RH data are 3%, respectively, according to the manufacturer's specifications (Adafruit, 2020). During the test, the temperature of the circulator bath varied from -9 °C to -16 °C. For dehumidification testing, the RH and absolute humidity were measured by comparing the initial and final relative humidity and temperature.

### 3.3.4 Cooling Capacity

#### 3.3.4.1 Energy balance with ice formation

When ice forms, the energy balance must consider the heat removed to lower the air temperature (sensible heat), the heat removed to condense water vapor into liquid (latent heat of vaporization), and the heat removed to freeze water (latent heat of fusion). The energy balance equation (3.1 incorporates) incorporating these factors in SI units (where heat quantities are in Watts (W) is as follows:

$$Q_{\ total} = Q_{sensible} + Q_{latent\ vaporization} + Q_{latent\ fusion} \quad (3.1)$$

### 3.3.5 Sensible and latent heat calculation

Sensible and latent heat were calculated with equation 3.2 and 3.3 respectively.

*Sensible Heat ($Q_{\ sensible}$):*

$$Q_{\text{sensible}} = \text{m}_{\text{air}} \times \text{c}_{\text{p}} \times \Delta\text{T} \quad (3.2)$$

Where $m_{\ air}$ is the mass flow rate of dry air kg $s^{-1}$, $c_p$ is the specific heat capacity of air (approximately 1005 j $kg^{-1}$ $k^{-1}$), ΔT is the temperature difference between the inlet and outlet air (K). Latent heat of vaporization ($Q_{\ latent\ vaporization}$):

$$Q_{\text{latent vaporization}} = \text{m}_{\text{water vapor}} \times \text{L}_{\text{v}} \quad (3.3)$$

Where $m_{\ water\ vapor}$ is the mass flow rate of water vapor removed before freezing (kg $s^{-1}$), $L_{\ v}$ is the latent heat of vaporization (approximately 2260 kj $kg^{-1}$= 2,260,000 j $kg^{-1}$ at 0°C).

Latent heat of fusion ($Q_{\ latent\ Fusion}$):

$$Q_{\text{Latent Fusion}} = \text{m}_{\text{ice}} \times \text{L}_{f} \quad (3.4)$$

Where $m_{ice}$ is the mass flow rate of water that freezes (kg $s^{-1}$), $L_{\ f}$ is the latent heat of fusion (approximately 334 kj $kg^{-1}$ = 334,000 j $kg^{-1}$).

### 3.3.6 Enthalpy

#### 3.3.6.1 Mass transfer

The RH change in the air at the entrance and outflow was used to compute the mass transfer rate. To measure the rate of moisture transfer, the humid air was continued through the chamber. These steps were used to calculate the moisture transfer rate in Equation 3.5:

$$\Delta w = m \times w_{out} - w_{in} \tag{3.5}$$

Where, m is the mass flow rate of air (kg $s^{-1}$), and $w_{out}$, and $w_{in}$ is the humidity ratio (g $kg^{-1}$) inside and outside the chamber (assuming dry air density is 1approximately kg $m^{-3}$ in lower atmosphere), $w_{out}$ and $w_{in}$ are the humidity ratios (g $kg^{-1}$) inside and outside the chamber, respectively, and m is the air mass flow rate (kg $s^{-1}$) inside and outside the chamber, the temperature and RH were monitored. Using the psychometric relationship, the humidity ratio was derived from the temperature and RH readings as follows (ASHRAE, 2017).

$$p_s = 0.611 \times \text{Exp}\left(\frac{17.27 \times \text{T}}{273 + T}\right) \tag{3.6}$$

$$p_i = RH \times p_s \tag{3.7}$$

$$\text{w}_i = 0.62198 + \left(\frac{p_i}{p - p_i}\right) \tag{3.8}$$

Where T is the air temperature (°C), pi is the partial pressure of water vapor in the air at any RH, $p_s$ is the partial pressure of water vapor at saturation (kPa), and p is the atmospheric air pressure (101.33 kPa). The enthalpy of moist air, expressed in kj $kg^{-1}$ of dry air, is calculated using equation 3.9:

$$h = (1.005 \times T + \left(w \times (1.86 \times T + 2501)\right) \tag{3.9}$$

In this p, T represents the dry bulb temperature of the air (°C), and 1.005 kj $kg^{-1}$ $°C^{-1}$ is the specific heat capacity of dry air, accounting for the sensible heat component. The term w is the humidity ratio (g $kg^{-1}$). The specific heat capacity of water vapor is 1.86 kj $kg^{-1}$ $°C^{-1}$ and

2501 kj $kg^{-1}$ is the latent heat of vaporization of water. Thus, the equation incorporates both the sensible heat of the dry air and the total enthalpy (sensible and latent heat) of the water vapor.

### 3.3.7 The relation between humidity and liquid water content in fog

The Magnus formulation was used to determine the saturation vapor pressure $e_s$ (Pa) is used to calculate RH from temperature data. A formulation, Equation 3.10, from a review study by Alduchov and Eskridge (1996) is used.

$$e_s = exp(-6096.94T^{-1} + 16.64 - 2.71 \times 10^{-2}T + 1.67 \times 10^{-5}T^2 + 2.43\ ln\ T) \quad (3.10)$$

where T (K) is the outside temperature recorded by the temperature recorder TR-1050.

Equation 3.11 shows the ideal gas equation was used to calculate the actual vapor pressure, e (Pa).

$$e = \frac{m_v}{V} R_v T \quad (3.11)$$

where $\frac{m_v}{V}$ is the mass of vapor per air volume and Rv is the gas constant for water vapor 461 (j $k^{-1}$ $kg^{-1}$).

The key parameters used to evaluate the effectiveness of dehumidification are the moisture removal rate, (MRR) expressed in grams per second, and the dehumidification efficiency, determined through Equations (3.12) and (3.13) respectively (Kumar et al., 2023):

$$MRR = \mathrm{m_{air}} \times (W_{in} - W_{out}) \quad (3.12)$$

$$\eta_{dehum} = \frac{W_{in} - W_{out}}{W_{in}} \quad (3.13)$$

In this equation, MRR is measured in grams per second. ma denotes the airflow rate passing through the dehumidification system, typically measured in kilograms per second. $W_{in}$ and $W_{out}$ present the specific humidity of the incoming and outgoing air respectively, given in grams of water vapor per kilogram of dry air, and $\eta_{dehum}$ is the dehumidification efficiency, can

be calculated from the ratio of actual humidity ratio removal to the maximum possible humidity ratio removal, which gauges the system's effectiveness in moisture removal, presented as a dimensionless value.

The sensible heat ratio (SHR) serves as a measure for designing mechanical cooling systems. A decreased SHR indicates greater latent gains, while an increased SHR suggests the opposite (Pillai et al., 2018). SHR was calculated using Equation 3.14:

$$SHR = \text{Sensible load} / \text{Sensible load} + \text{Latent load} \quad (3.14)$$

### 3.3.8 Statistical analyses

#### 3.3.8.1 Statistical analysis between samples

Statistical analyses were performed to evaluate the reproducibility and trend similarities in both the dehumidification and cooling processes. For dehumidification, the inlet and outlet RH values were analyzed using a paired t-test to determine if the differences in RH between the inlet and outlet were statistically significant. A p-value of less than 0.05 indicated that the dehumidification process effectively reduced RH.

For the cooling process, the inlet and outlet temperature values were similarly analyzed to assess the effectiveness of the system. The reproducibility of the results for both dehumidification and cooling was verified by calculating variance, root mean square error (RMSE), and the coefficient of determination ($R^2$). These metrics were used to quantify the goodness-of-fit for the regression models and assess the overall agreement of results across experiments.

#### 3.3.8.2 Uncertainty analyses

Uncertainty analyses were conducted to quantify the errors in measurements of temperature and humidity during the dehumidification and cooling processes. Both systematic errors from the instrumentation and random uncertainties due to the data acquisition and

measurement processes were considered. The overall uncertainty (U) for each variable was calculated as equation 3.15:

$$U = \sqrt{B^2 + P^2} \tag{3.15}$$

where B represents the systematic uncertainty (bias), and P represents the random uncertainty (precision). The random uncertainty P was computed as equation 3.16:

$$P = \sigma \times t \tag{3.16}$$

where $\sigma$ is the standard deviation of the data, and t is the t-distribution value for a 95% confidence level (with t=1.96 for n>200).

Systematic uncertainties were assumed based on the specifications of the measurement equipment used in the experiments. The propagation of uncertainty was evaluated using numerical differentiation to approximate partial derivatives of the involved variables. The propagation formula, equation 3.17, used was:

$$\sigma Q = \sqrt{\left(\frac{dQ}{da}\sigma a\right)^2 + \left(\frac{dQ}{db}\sigma b\right)^2 + \dots} \tag{3.17}$$

where $\delta Q$ is the uncertainty of the resulting parameter $Q$; $\delta a$, $\delta b$, $\delta z$, are the uncertainty of variables $a$, $b$. and $\frac{dQ}{da}$ and $\frac{dQ}{db}$ are the partial derivation of the resulting parameters with respect to a, b respectively.

### 3.4 Results and discussion

#### 3.4.1 Cooling

A novel dehumidification system combining a vortex cooling gun and a cold plate was designed and constructed to enhance moisture control and cooling efficiency. Tests were

conducted to evaluate the system's cooling performance, temperature reduction, and ability to reduce relative and absolute humidity.

Figure 3.3 illustrates the trends in inlet temperature, inlet RH, outlet RH, and outlet temperature over time. The inlet temperature initially dropped rapidly from around 20℃ to 5℃ within 500 s and remained stable. The inlet RH decreased sharply from 80% to 50% in the first 500 s, fluctuated slightly between 50% and 60%, and settles to 50%-55%. The outlet RH decreased quickly from 60% to 30% and stays relatively steady with minor fluctuations. The outlet temperature initially falls from 15℃ to 5℃, then gradually rises to around 10°C over 7000 s. These observations highlight the initial changes and subsequent stabilization in both temperature and RH levels.

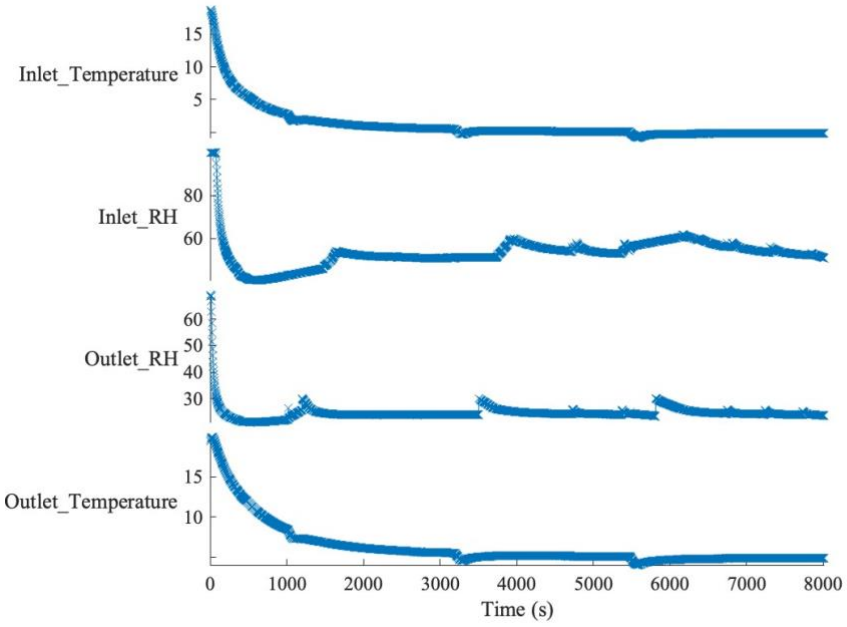


**Figure 3.3.** Temporal variations in inlet and outlet temperature and relative humidity (RH) during the dehumidification process.

### 3.4.2 Dehumidification

The RH at the inlet air was approximately 100% and subsequently stabilizes between 50% and 55%, Figure 3.4. The inlet absolute humidity sensor indicates a decreasing trend, starting just above 14 g $m^{-3}$ and stabilizing at 2 g $m^{-3}$. The outlet absolute humidity sensor starts marginally lower than the inlet values, decreases swiftly to below 2 g $m^{-3}$, and maintains a relatively consistent level for the duration observed. Figure 3.4 delineates a 15% standard deviation (SD) range for both upper and lower humidity bounds. The precipitous decline in both RH and absolute humidity at the outlet signifies effective moisture removal, with the outlet RH rapidly falling below 20%, illustrating the system's proficiency in reducing air moisture content. After initial fluctuations, both the inlet and outlet RH and absolute humidity readings reach stability, suggesting that the system may have achieved a steady operational state, characterized by consistent humidity levels at the input and output. The notable disparity between the inlet and outlet absolute humidity values underscores the system's efficiency in extracting moisture. The significantly lower absolute humidity at the outlet, relative to the inlet, directly reflects the volume of water vapor removed from the air. The ability of the system to sustain a low and stable outlet RH and absolute humidity could prove advantageous for environments requiring stringent control of humidity levels. Furthermore, the minimal variance indicated by the standard deviation lines points to the system's consistent performance over time. This consistent performance is crucial for applications where environmental control is critical to process success. The saturation duration is dependent on the difference between the inlet and outlet humidity ratios with a larger disparity indicating a higher moisture content to be removed, thereby extending the time to reach equilibrium.

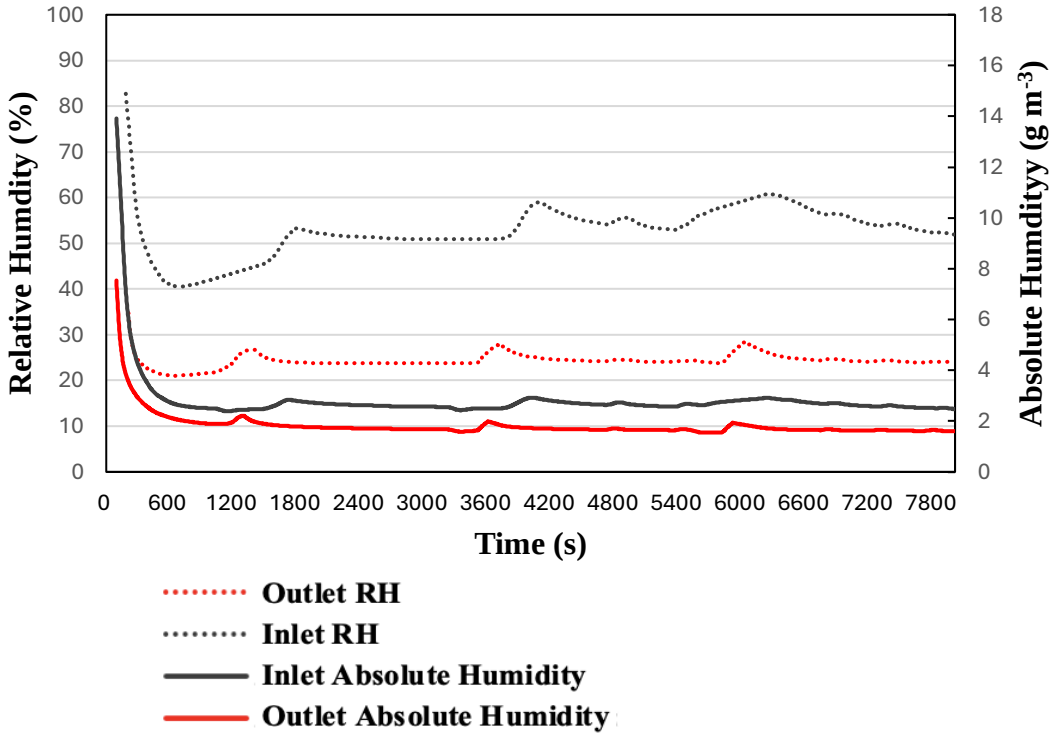


**Figure 3.4.** Comparison of inlet and outlet relative humidity (RH) and absolute humidity measurements over time during dehumidification.

### 3.4.3 Heat and mass transfer effectiveness

Figure 3.5 presents the dynamic response of a dehumidification system, tracking the changes in absolute humidity difference (g $m^{-3}$) and enthalpy difference kj $kg^{-1}$. These metrics are pivotal for evaluating the dehumidifier's performance. The data shows a pronounced decline in the absolute humidity difference, dropping swiftly from a high of about 8 g $m^{-3}$ to stabilize near 1 g $m^{-3}$. This sharp decrease reflects the system's robust initial capacity for moisture removal, subsequently entering a near-steady state with slight fluctuations around 1 g $m^{-3}$.

This increase in the enthalpy difference indicates a gain in energy between the inlet air and outlet air over time. The two parameters exhibit opposing trends in the initial phase, with absolute humidity removal decreasing while the enthalpy difference increases, suggest a transient adjustment period. After this phase, both parameters stabilize, indicating the system

reaches equilibrium and maintains consistent dehumidification and energy transfer. After 1000 s, both parameters stabilize, showing minimal fluctuations over time.

The observed increase in enthalpy ($h_{out}$-$h_{in}$) during the dehumidification process can be explained by the phase change of water vapor directly into ice, which involves the release of latent heat. Unlike conventional HVAC systems, which typically exhibit energy loss during cooling and dehumidification, the phase change process in this system contributes to an energy gain which make it an ideal energy recovery system. This behavior aligns with findings from studies on phase transitions, such as in supercooled silicon, its liquid form has much in common thermodynamically with water, where enthalpy increases during a second-order phase transition due to latent heat release (Sastry & Austen Angell, 2003). Conventional methods rely on energy extraction to achieve moisture removal, where dehumidification typically involves reducing enthalpy or maintaining constant enthalpy (direct evaporative cooling). These methods rely on decreasing air temperature and moisture levels to enhance dehumidification performance, often limited by the need to balance cooling capacity and moisture enrichment (Cheng & Zhang, 2023).

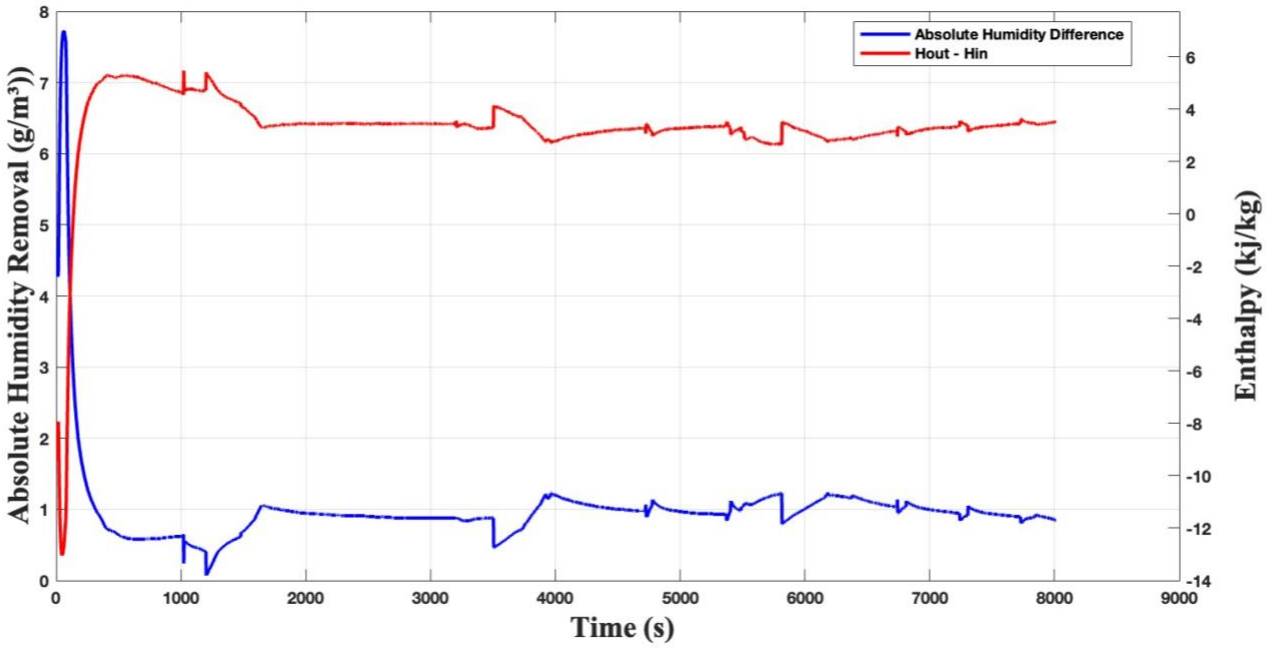


**Figure 3.5.** Dynamics of absolute humidity removal and enthalpy changeover time in the dehumidification process.

The depicted surface of Figure 3.6 demonstrates a downward slope, suggesting that an increase in moisture extraction correlates with a rise in the change in enthalpy (ΔH), typically manifesting as a cooling effect alongside latent heat removal through condensation. The escalating difference in absolute humidity along the X-axis underscores the system's efficacy in moisture removal over time. A greater ΔAH indicates robust performance in converting humid air into a drier state. In the dehumidification process, ΔH is predominantly negative, signifying the extraction of heat from the air, aligning with the cooling effect resultant from moisture condensation—a fundamental element in processing hot and humid air. The outlet humidity conditions, the graph reveals a decline in outlet RH as the absolute humidity difference enlarges. This is considered an optimal point because the system has not only dehumidified the air but also increased the outlet air's capacity to retain moisture. The discernible overall trend on the graph provides a basis for identifying optimal operational conditions that efficiently achieve targeted humidity and temperature levels. Further analysis

of the system's most frequent operational points on the graph could elucidate typical or preferred operating states, offering strategic insights for system optimization and control.

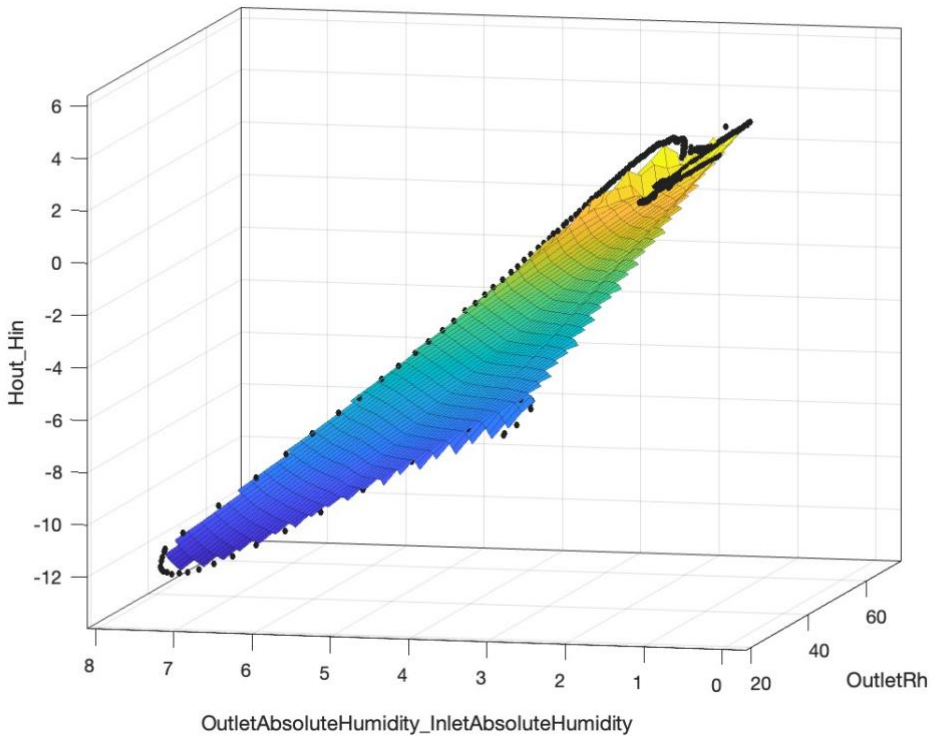


**Figure 3.6.** Relationship between outlet relative humidity, inlet and outlet absolute humidity, and enthalpy changes in dehumidification.

A study reported by Campen et al. (2003) evaluated dehumidification methods for greenhouses, emphasizing that forced ventilation with a heat exchanger is the most efficient and cost-effective method. The experiment demonstrated a significant reduction in RH from approximately 70% to 30% using ice formation on a cold plate. Increased dehumidification rates were observed with higher inlet RH. Both studies highlight the importance of inlet humidity for enhancing dehumidification performance. The results, showing consistent reduction in absolute humidity and enthalpy over time, align with the efficiency trends observed by Campen et al. (2003).

The results show that enhancements in managing both latent and sensible heat loads align with findings Liu et al. (2018), investigated the energy efficiency of counter-flow heat pump driven liquid desiccant systems. Liu et al. conducted experimental tests and system performance evaluations, discovering that increasing water capacity within the system could effectively remove redundant heating, thereby lowering the condensing temperature and enhancing overall performance. They found that the outdoor air humidity ratio had a more substantial impact on system performance than the outdoor air temperature. This observation underscores that inlet air conditions are crucial for optimizing dehumidification efficiency. It noted that the humidity ratio of indoor exhaust air affects system performance more than the temperature of the exhaust air, highlighting the importance of humidity control (Liu et al., 2018).

Figure 3.7 shows higher efficiencies correspond to more negative enthalpy differences. As inlet absolute humidity ($ABH_{in}$) increases, the difference between inlet and outlet enthalpy ($H_{out}$ - $H_{in}$) increases. The surface gradient indicates that higher inlet absolute humidity and efficiency are associated with increase in enthalpy difference, reflecting a linear interaction between efficiency and absolute humidity impacting enthalpy change. High inlet absolute humidity necessitates greater energy removal to condense the moisture, enhancing system performance. The system's efficiency improves with higher humidity levels, allowing more latent heat removal as more ice crystals are created on the surface of the cold plate. This results in a positive enthalpy difference, indicating effective energy transfer. Efficient systems extract more energy while processing humid air, aligning with the thermodynamic principles of dehumidification. The trends suggest that higher inlet absolute humidity improves system efficiency by increasing the amount of energy removed through latent heat condensation.

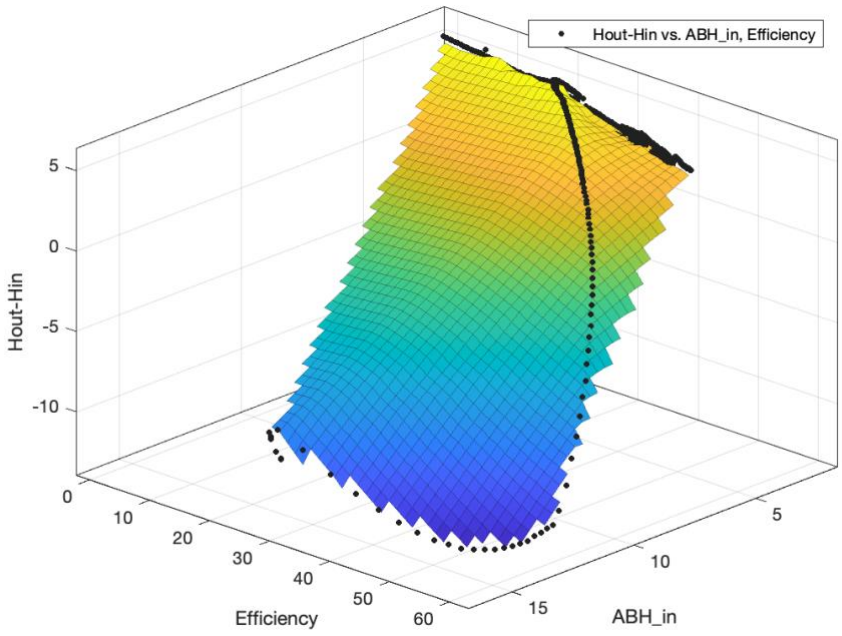


**Figure 3.7.** Relationship between enthalpy change, absolute humidity at Inlet ($ABH_{in}$), and dehumidification efficiency.

Figure 3.8 shows the relationship between enthalpy difference ($H_{out}$ - $H_{in}$), $ABH_{in}$, and efficiency. $ABH_{in}$ ranges from 1 to 16 g $m^{-3}$ efficiency from 0% to 60%, and enthalpy difference from -15 to 10 kj $kg^{-1}$. The plot highlights that higher $ABH_{in}$ values correspond to more negative enthalpy differences, with varying efficiency levels.

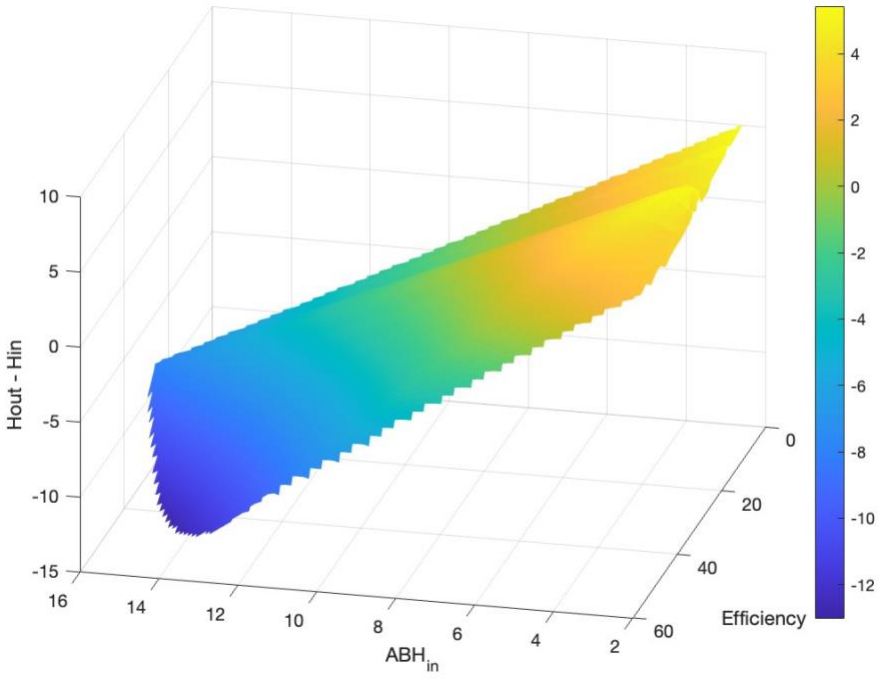


**Figure 3.8.** Correlation of Enthalpy Change with Inlet Absolute Humidity ($ABH_{in}$) and Dehumidification Efficiency

The polynomial regression models for efficiency and MRR were developed using key variables including inlet temperature ($T_{in}$), inlet relative humidity ($RH_{in}$), inlet pressure ($P_{in}$), outlet temperature ($T_{out}$), outlet relative humidity ($RH_{out}$), outlet pressure ($P_{out}$), $ABH_{in}$, the difference in absolute humidity ($ABH_{in}$ - $ABH_{out}$), enthalpy difference ($H_{out}$ - $H_{in}$), MRR, inlet enthalpy ($H_{in}$), outlet enthalpy ($H_{out}$), airflow, and time. For efficiency, the model achieved an R-squared value of 0.999. For MRR, the model achieved an R-squared value of 1.000. These models demonstrate the influence of various factors on the efficiency and moisture removal capabilities of the HVAC system, highlighting the critical predictors and their respective impacts.

The observed freezing of water droplets appears surface-driven and highly influenced by air RH, where increased humidity at specific temperatures enhanced the freezing process. This

surface phenomenon, attributed to changes in surface entropy and energy (J. L. Pérez-Díaz 2016). It can draw parallels regarding the impact of relative humidity on phase changes.

Unlike traditional systems where chillers expend significant energy to lower air temperature and condense moisture, the ice formation process inherently cools the air as it releases latent heat, reducing the load on the chiller and thereby decreasing energy consumption. This could offset the need for external heating sources, further enhancing the system's net energy efficiency (Chua et al., 2013).

### 3.4.4 Moisture removal rate (MRR)

The results show that has a higher inlet RH which leads to enhanced ice formation on the cold plate, leveraging the latent heat of fusion to efficiently remove moisture from the air. Inlet absolute humidity is a critical parameter in assessing the dehumidification process (Figure 3.9). The scatter plot of $ABH_{in}$ versus MRR illustrates that $ABH_{in}$ ranges from approximately 2 to 18 g $m^{-3}$, while MRR varies between 0.005 and 0.025 g $m^{-3}$ Significant data points include an $ABH_{in}$ of 11.65 g $m^{-3}$ with an MRR of 0.022 g $m^{-3}$ .The trendline in the plot reveals a positive correlation between $ABH_{in}$ and MRR, indicating that MRR slightly increases as $ABH_{in}$ increases. Yang et al. (2015) reported that both dehumidification effectiveness and MRR increased significantly with the growth of desiccant flow rate. In our study, a higher inlet absolute humidity similarly results in higher MRR, which can be attributed to the increased potential for moisture removal due to higher absolute humidity levels (Yang et al., 2015). Luo et al. (2011) examined the dehumidification performance of the ionic liquid [EMIM]BF4 compared to the traditional desiccant LiBr under varying air flow rate, solution flow rate, and air humidity conditions. Their key findings indicated that the dehumidification rate improved with increases in air flow rate, solution flow rate, and air humidity. The novel experiment demonstrated that higher inlet RH led to more effective dehumidification through enhanced ice

formation, paralleling Luo et al. (2011), which showed that higher air humidity increased the driving force for mass transfer, thereby enhancing dehumidification rates.

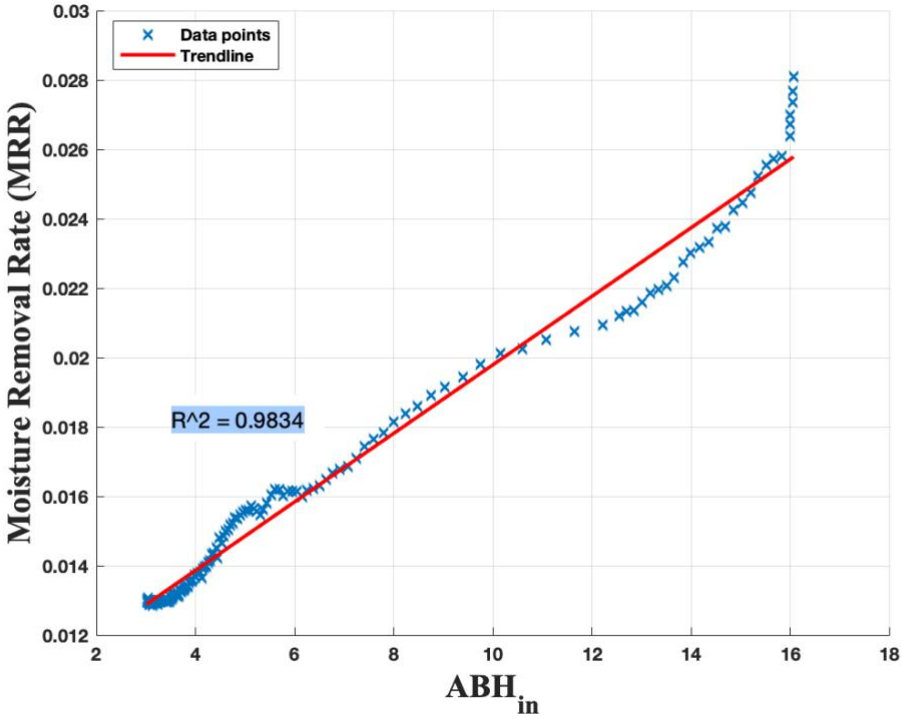


**Figure 3.9.** Scatter plot of inlet absolute humidity ($ABH_{in}$) vs. moisture removal rate (MRR) with trendline.

A study by Sayegh et al. (2011) highlights that a hybrid system achieves better dehumidification at higher air flow rates due to the desiccant wheel's efficiency. This enhanced performance is attributed to the desiccant wheel's efficiency in handling higher humidity loads, resulting in better dehumidification performance. Similarly, the current study's results indicate that higher $ABH_{in}$ enhances the dehumidification process through increased ice formation, as evidenced by the positive correlation between $ABH_{in}$ and MRR. The analysis shows that as $ABH_{in}$ increases, the MRR increases, indicating more efficient moisture removal. The latent heat released during the ice formation contributes to the system's overall efficiency, making it more effective in reducing relative humidity (Gao et al., 2011).

Data reported herein illustrate the relationships between total heat ($Q_{total}$) and environmental factors such as $RH_{in}$ and inlet temperature, Figure 3.10 The linear regression model for $Q_{total}$ versus inlet RH demonstrates a substantial positive correlation, evidenced by an R-squared value of 0.81 and 0.94, indicating that total heat output increases with higher RH. In contrast, the relationship between $Q_{total}$ and inlet temperature are characterized by a polynomial fit with an R-squared value of 0.81, reflecting a significant non-linear rise in total heat as temperature increases. These findings emphasize the critical role both temperature and humidity play in determining the thermal dynamics of the system, showcasing the intricate interactions that govern system efficiency.

### 3.4.5 Influence of inlet temperature and relative humidity on total heat transfer

The polynomial fit results for $Q_{total}$ as a function of inlet RH and inlet temperature reveal insights into HVAC system performance in humid and warm conditions, Figure 3.10. The 3rd-degree polynomial fit for inlet RH (with an $R^2$ of 0.81) indicates a pronounced non-linear increase in $Q_{total}$ as RH surpasses 70%, reflecting the sharp rise in latent heat load in higher humidity environments.

The dehumidification process in this system is governed by both latent and sensible heat transfer mechanisms. As hot and humid air, with inlet temperatures between 5°C to 17°C and RH from 50% to 95%, comes into contact with the cold plate, water vapor condenses, forming ice crystals and releasing latent heat. This process is reflected in the rise of $Q_{total}$, which increases from 2 kW to over 12 kW as RH increases from 50% to 95%, highlighting the increased latent heat load. Sensible heat transfer occurs as the air cools, leading to a drop in outlet temperature. With increasing inlet temperature from 5°C to 17°C, $Q_{total}$ rises from 4 kW to over 15 kW, indicating the system's high responsiveness to temperature changes. Polynomial regression models show correlations, with $R^2$ values of 0.94 for inlet temperature and 0.81 for

inlet RH, confirming the system's sensitivity to both variables and its effective handling of increased thermal loads.

This trend aligns with thermodynamic principles, where the energy required to condense and remove moisture from the air significantly increases the overall heat load on the system (Chua et al., 2013). These findings are consistent with existing studies on latent heat transfer in air handling units and emphasize the importance of humidity control in optimizing energy efficiency, particularly in humid climates. This will be essential for addressing HVAC system design strategies, especially in regions where high relative humidity contributes heavily to total energy consumption.

In the case of inlet temperature, the 3rd-degree polynomial fit ($R^2 = 0.94$) shows a rapid increase in $Q_{total}$ from 5°C to 15°C, followed by a levelling off as temperatures continue to rise. This steep increase reflects the rise in sensible heat load at higher temperatures, while the plateau suggests that the system may approach a stabilization point as it handles the increased thermal energy. These observations align with studies on the enthalpy of humid air, where temperature has a pronounced effect on total heat loads in HVAC systems. As both inlet RH and temperature rise, the total heat load on the system increases exponentially, but the system continues to maintain effective heat removal. This results in RH reductions at the outlet, with the final RH decreasing by up to 30%, and temperature reductions of over 10°C in the air exiting the system. These results statistically affirm the system's ability to handle high thermal loads, while efficiently reducing both moisture content and temperature. The correlation between temperature and $Q_{total}$ underscores the necessity of precise temperature and humidity regulation for improving energy efficiency in building climate control systems, as demonstrated in psychrometric analyses and research focused on sustainable building design.

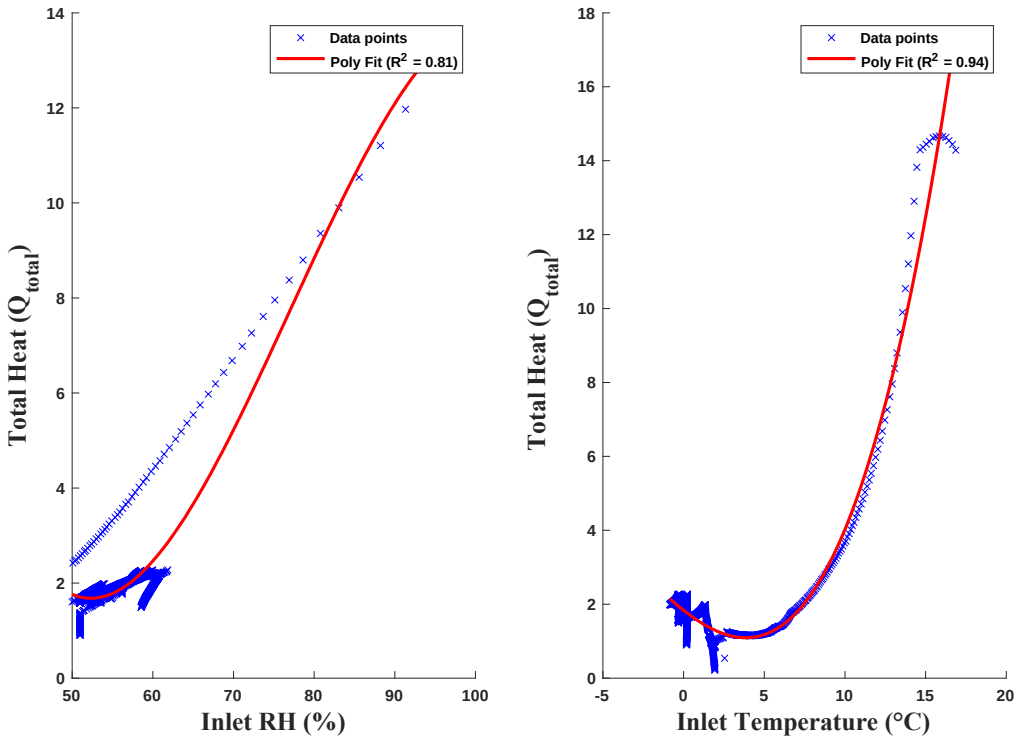


**Figure 3.10.** Comparative analysis of total heat ($Q_{total}$) (kj) with inlet relative humidity and temperature demonstrating varied correlations and impact on system efficiency.

Compared to the dynamics of RH in natural cloud formations, the observations from a previous study on RH in ice clouds offer a foundational comparison. It was observed that RH in mixed-phase clouds is typically close to saturation over water, even at temperatures ranging from -5℃ to -35 ℃. In contrast, in ice clouds, relative humidity can deviate from saturation over both ice and water, influenced by temperature and ice content. Moreover, the relative humidity in ice clouds tends to increase as temperature decreases (Korolev & Isaac, 2006). Findings from this preceding work on heat transfer in desiccant-coated microchannel heat exchangers offer insights that align closely with experimental observations of ice crystal formation on a cold plate for dehumidification. The study highlights enhancements in dehumidification capacity through modifications in airflow velocity and microchannel

architecture, which effectively manage both sensible and latent heat (Wang et al., 2021). Similarly, experimental results demonstrate a dependency of RH on phase changes, particularly when ice forms on the cold plate, leading to a reduction in relative humidity. This behavior mirrors that observed in ice clouds, where the relative humidity is not always at saturation and varies with temperature. Li et al. noted that while indirect evaporative cooling could further decrease the temperature, it introduces additional energy from the outdoor air, which they excluded from their analysis for ideal efficiency (Li et al., 2010). Similarly, this study focuses on optimizing internal system parameters without incorporating external energy inputs, to maintain energy efficiency in the dehumidification process.

In a controlled experiment, as ice accumulates on the cold plate, there is a clear trend of relative humidity reduction, aligning with the theoretical framework proposed by Korolev and Mazin (Korolev & Mazin, 2003). This comparative analysis underscores the effectiveness of ice formation in artificially controlled environments for dehumidification, drawing parallels with natural phenomena observed in cloud physics. The use of a vortex cooling gun and cold plate in this system represents a novel approach not widely explored in recent years. This research not only reaffirms the potential of such technologies to enhance the efficiency of HVACs systems and manage condensing temperatures, extending the discussion to the modern context where energy efficiency is increasingly crucial.

### 3.4.6 Reproducibility and uncertainty of data

The reproducibility of the experimental results was evaluated by comparing the cooling and dehumidification (MRR) processes across multiple trials. Key metrics, including R-squared ($R^2$), RMSE, standard deviation, uncertainty of maximum value, and propagated uncertainty, are summarized in Table 3.1.

**Table 3.1.** Calculation of statistical parameters

| Metric | Cooling Analysis | MRR Analysis |
|---|---|---|
| **R-squared ($R^2$)** | 0.9984 | 0.98345 |
| **RMSE** | 0.10907 | 0.00054086 |
| **Standard Deviation** | 2.7585 | 0.0042183 |
| **Uncertainty of Max Value** | ±5.4297 | ±0.50007 |
| **Propagated Uncertainty** | 4.1484 | 0.00057933 |

The cooling process exhibited a high degree of reproducibility, as evidenced by the R-squared value of 0.9984, indicating a strong linear relationship between the inlet and outlet temperature values. The RMSE of 0.10907 demonstrates minimal deviation between observed and predicted values, confirming the accuracy of the model. The standard deviation of 2.7585 further supports the consistency of measurements across multiple trials.

The uncertainty associated with the maximum value for cooling was ±5.4297, which accounts for the variability inherent in the measurement system and possible instrumental errors. The propagated uncertainty, derived through numerical differentiation and uncertainty propagation methods, was 4.1484, providing an additional assessment of the reliability of cooling process measurements.

The analysis of MRR also demonstrated a high degree of accuracy, with an R-squared value of 0.98345, indicating a strong fit for the linear regression model applied. The RMSE of 0.00054086 suggests a very low level of residual error, highlighting the model's robustness in predicting MRR. The standard deviation for MRR was 0.0042183, demonstrating consistency in the collected data. The uncertainty of the maximum value for MRR was ±0.50007, suggesting minor variability, which is within an acceptable range for this type of experimental

setup. Additionally, the propagated uncertainty was calculated as 0.00057933, further indicating the high precision and reliability of the MRR measurements

### 3.5 Conclusion

This experimental proof-of-concept investigation of a novel dehumidification system that uses ice formation on a cold plate has demonstrated enhanced air moisture removal efficiency. Through the methodical adjustment of inlet air conditions and the strategic incorporation of a vortex cooling gun and cold plate, the system efficiently facilitated the formation of ice crystals, which in turn led to a marked reduction in RH. Analyses showed a consistent decrease in RH as ice formed over the cold plate, indicating that the phase change effectively extracted moisture from the air. These attributes may make this novel approach to dehumidification particularly suitable for applications in climates where rapid and efficient humidity control is necessary. The system's ability to rapidly condense moisture and its efficient thermal dynamics suggest potential scalability for industrial applications where air quality and climate control are critical. The key findings are listed as:

- Temperature: The inlet temperature rapidly decreased from about 20°C to just below 5°C within the first 1000 seconds and then stabilized, demonstrating the system's efficiency in heat extraction.
- Relative Humidity (RH): Initially at 80%, inlet RH quickly dropped to around 50% early in the experiment, with outlet RH further reducing to about 30%, illustrating effective moisture extraction.
- Absolute Humidity: There was a notable reduction from initial readings of approximately 14 g $m^{-3}$ to 2 g $m^{-3}$ affirming the system's quick moisture removal capability.
- Moisture Removal and Enthalpy: The system lowered enthalpy by up to 20 kj $kg^{-3}$, beneficial for applications needing both cooling and dehumidification.

Efficiency: A positive correlation was observed between the moisture removal rate (MRR) and higher inlet absolute humidity, indicating more efficient dehumidification at higher humidity levels.

**Connecting text**

Chapter 3 details the experimental design and methodology employed in this research. This chapter describes the setup, including the innovative use of a vortex cooling gun and cold plate to achieve moisture removal, and outlines the specific procedures for each experimental phase. The careful design of this experimental system draws on the theoretical foundations established in the previous chapter.

# CHAPTER 4

## Ice Formation for Enhanced Dehumidification: An Innovative Approach to Moisture Control

Sheida Rezaei[1], Sarah MacPherson[1], Valérie Orsat[1], Mark Lefsrud[1]*

[1]Department of Bioresource Engineering, Macdonald Stewart Building, Macdonald Campus, McGill University, 21111 Lakeshore Road, Ste-Anne-de-Bellevue, QC, H9X3V9

***Corresponding author:** mark.lefsrud@mcgill.ca

**4.1 Abstract**

Global warming has escalated energy consumption in cooling, emphasizing the pivotal role of heating, ventilating, and air-conditioning (HVAC) systems in providing comfort and indoor air quality. However, conventional HVAC systems struggle with excess moisture during high humidity periods. This follow-up study aimed to examine the dehumidification capacity of a newly developed cooling system novel inspired by natural fog formation, employing a vortex cooling gun and a cold plate, to assess the system's performance under varied loads of relative humidity (RH), each up to 60%. The system was challenged by humidity up to 90%, this method can extract moisture from saturated vapor, transforming it into fog or ice particles. By manipulating the temperature, relative humidity, and pressure, we achieved a remarkable temperature reduction from 30°C to 4°C within 40 min, concurrently reducing indoor relative humidity from 100% to 19%, employing a vortex cooling gun and a cold plate. This innovation may offer a prospective solution to offers energy-efficient humidity control for HVAC systems in hot and humid climates.

Understanding energy efficiency helps optimize the energy consumption involved in extracting moisture from indoor air and releasing it outdoors.

**Key words:** climate control, dehumidification, energy consumption reduction, indoor air quality

## 4.2 Introduction

Air-conditioning systems are essential for maintaining daily functionality and achieving thermal comfort, particularly in regions with high temperatures and humidity. The Indoor Air Quality (IAQ) of these systems depends on the efficacy of air filters, along with the rates of ventilation and exfiltration, and is crucial in establishing healthy conditioned environments (Allam & Elsaid, 2020). Addressing high humidity levels in climate control presents significant challenges and high energy demands, particularly in regions characterized by hot and humid climates. High humidity in buildings can cause several serious issues, such as the growth of mold and mildew, which thrive in damp environments. Additionally, it can worsen problems like fungal growth and leaks. This can result in deterioration of building materials (Guieysse et al., 2008). Ma et al. studied the relationship between COVID-19 spread and climatic factors such as temperature and humidity from January to February 2020. They found that weather conditions significantly influence infectious disease transmission. While temperature and air movement positively correlated with virus transmission rates, absolute humidity showed a negative correlation (Elsaid & Ahmed, 2021). Particularly within HVAC systems, posing potential risks to indoor air quality and structural integrity. Effectively managing and controlling humidity levels is essential for mitigating these adverse effects and maintain a healthy and comfortable environment. When it comes to energy use in buildings, about 10-15% of the total energy consumed is dedicated to maintaining humidity levels, particularly in tropical regions (Guan et al., 2020). Global warming increases energy demand, mainly due to rising cooling needs, outweighing reductions in heating demand (Santamouris, 2015). Meanwhile, AI and data centers drive electricity consumption, sometimes surpassing climate-driven demand in certain regions (Masanet et al., 2020). The net impact depends on renewable adoption, efficiency improvements, and regional energy policies.In hot and humid regions,

constructing buildings with efficient insulation and controlled airflow is difficult; a s we reduce the sensible heat load by improving windows, insulation, and positioning air ducts indoors, the latent heat load increases. Traditional cooling systems may have difficulty maintaining humidity within the desired range, which, according to ASHRAE standards, should be below 65% (Heating et al., 2001; Rudd et al., 2005). In hot and humid regions such as South China, a substantial portion, approximately 25%, of the overall energy utilized for air conditioning is allocated to moisture regulation through independent humidity control systems. To further mitigate energy consumption associated with the treatment of fresh air, it is imperative to integrate energy recovery mechanisms with independent humidity control systems (Zhang, 2006). Outdoor temperature and humidity's impact has been studied extensively. Chun et al. (2021) found that the cooling limit of dew point evaporative cooling aligns with the inlet air's dew point temperature. In cases of low latent heat load, slight dehumidification may not adequately meet indoor cooling needs, hindering the system's ability to provide sufficiently cool air. Enhanced dehumidification efficiency can boost the coefficient of performance (COP) of cooling systems while maintaining a constant cooling capacity ratio (Chun et al., 2021).

The core concept of cooling dehumidification involves the transition of water vapor from moist air into liquid form due to a drop in air temperature below the dew point. This process is facilitated by a cooling dehumidification system, which typically consists of both a vapor compression refrigerator (Ariwibowo & Darmanto, 2020) and an air cycle refrigerator (Kikuchi et al., 2005). The vapor compression refrigerator utilizes refrigerants such as freon (Sasongko et al., 2021) to decrease the air temperature to the dew point under atmospheric pressure, while the air cycle refrigerator works by pressurizing the air to raise the dew point temperature, thereby aiding in the dehumidification process. These distinct mechanisms collectively enable effective regulation of humidity levels in various settings (Yang & Yang, 2021).

Water ice is widely prevalent on the Earth's surface and holds significant importance in various meteorological, biological, environmental, chemical, and physical phenomena. Despite our long-standing knowledge of the material properties of ice, our comprehension of ice crystal formation remains relatively limited. The process of ice formation, whether from liquid water or water vapor, can markedly enhance the dehumidification process, akin to natural environmental mechanisms. When a cloud droplet undergoes freezing, initiating the formation of a nascent snowflake, the crystal starts to expand by assimilating water vapor present in its vicinity (Libbrecht, 2017).

The objective of this study was to investigate and optimize the techniques for controlling relative humidity (RH) in tropical climates using phase change properties of water to convert excess humidity into ice crystals. By focusing on the transformation of humidity into solid form, this approach seeks to enhance the efficiency of moisture absorption significantly, thus offering a targeted method for maintaining desired humidity levels within these challenging environments. This method provides a practical solution for humidity management, leveraging the natural phase transitions of water to improve indoor environmental conditions.

**4.3 Materials and methods**

In this experimental setup, two cylindrical PVC conduits, each measuring 0.10 m in diameter, were aligned to flank a circular chamber crafted from hard plastic, with a diameter of 0.33 m. These conduits served to facilitate the connection to a booster fan (LFANXBOOSTER6, 6-inch, 240 CF, iPower, Irwindale, CA, US) with a diameter of 0.1524 meters. The output regions of these conduits were insulated using fiberglass pipe wrap, measuring $0.03 \times 0.01 \times 0.25$ meters. Moisture regulation within the chamber was managed by a large model ultrasonic mist humidifier, Lacidoll ultrasonic mist humidifier ($27 \times 27 \times 63$ cm; Lacidoll, Cerritos, CA, US), which was capable of adjustable moisture output. For generating

a cold air stream inside the chamber, a compact Vortex cooling gun (model 3404, EXAIR LLC) was utilized. The system's cooling was further enhanced by an aluminum cold plate (ATS-CP-1003-DIY, 0.202 × 0.13 × 0.02 m) with a flow rate of 4 L per minute, capable of transferring 1000 watts of heat while maintaining a temperature difference of 6.8°C between the cold plate base and the fluid entering it. Positioned centrally within the chamber, the cold plate was connected to a circulator bath which employed Heated Immersion Circulators (model 4100 R20, Fisher Scientific Isotemp®) providing both heating and cooling functions, Figure 4.1.

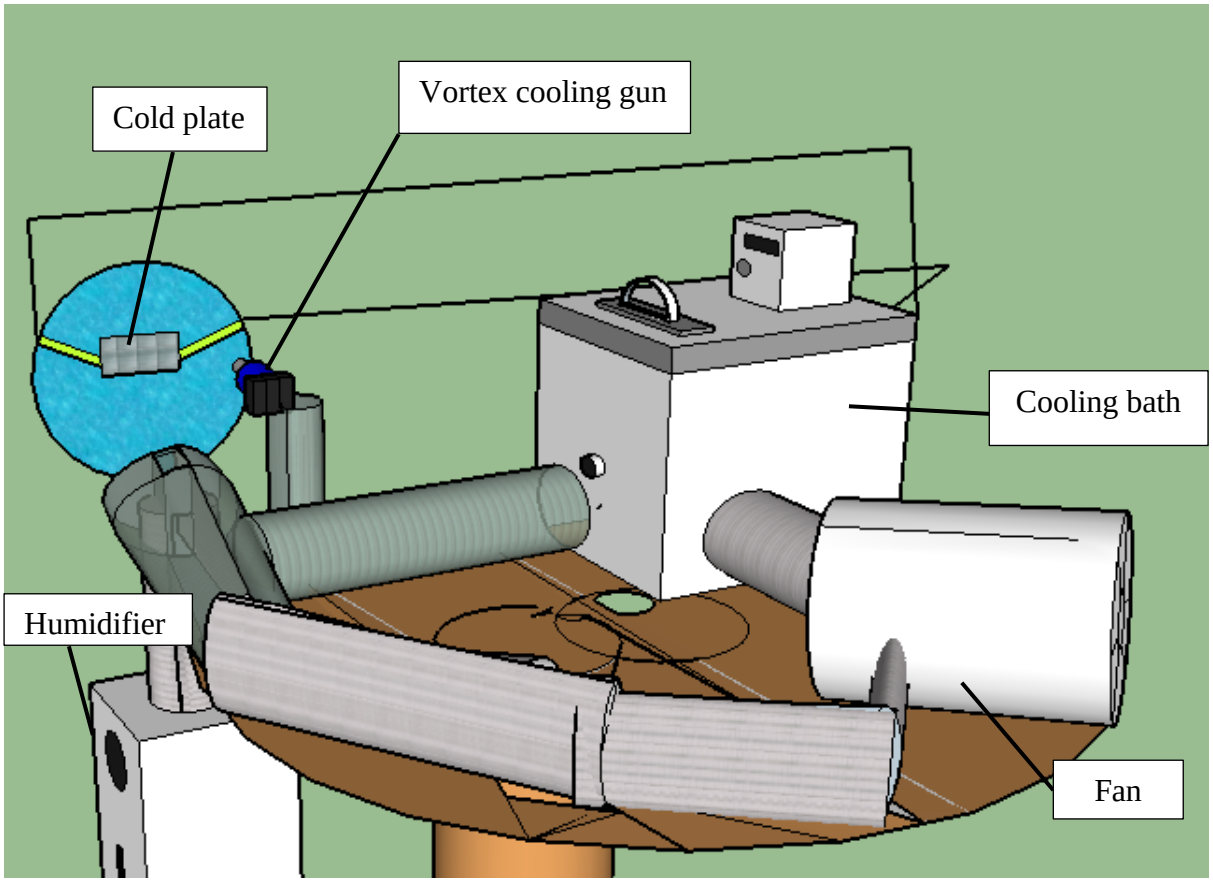


**Figure 4.1.** Schematic of the design of the dehumidification system

Humidity variations produced by the ultrasonic humidifier were directed to the vortex gun and the cold plate. The experiment focused on monitoring several key variables: RH, temperature, and pressure. These were accurately measured using four strategically placed

BME280 I2C sensors (Raspberry pi: BME280, Adafruit Industries, New York, NY, US) within the setup. The sensors were positioned at the inlet for humid air, the outlet for dry cold air, near the cooling devices, and in an external location to assess ambient environmental conditions.

The key parameters used to evaluate the effectiveness of dehumidification are the moisture removal rate, expressed in grams per second, and the dehumidification efficiency, determined through Equations (4.1) and (4.2) respectively (Kumar et al., 2023):

$$MRR = m_a(W_{a\_in} - W_{a\_out}) \quad (4.1)$$

$$\eta_{dehum} = (W_{a\_in} - W_{a\_out}) / (W_{a\_in}) \quad (4.2)$$

In this equation, MRR represents the Moisture Removal Rate, measured in grams per second. $m_a$ denotes the airflow rate passing through the dehumidification system, typically measured in kilograms per second. $W_{in}$ and $W_{out}$ present the specific humidity of the incoming and outgoing air respectively, given in grams of water vapor per kilogram of dry air. $\eta_{dehum}$ the dehumidification efficiency, which gauges the system's effectiveness in moisture removal, presented as a dimensionless value.

### 4.3.1 Experimental setup

The experimental arrangement for dehumidification comprises two primary elements: a vortex cold gun and a cold plate. Initiated by an ultrasonic humidifier, humid air is introduced into the system and directed through a duct where it first interacts with the chilled, dry output from the vortex cold gun. Following this, the air is channeled towards the cold plate, strategically located to continue the thermal exchange. To effectively monitor the environmental variables throughout this process, sensors S1 to S4 are meticulously positioned. Sensor S1 is installed at the system's entry point where the humid air is fed in, S2 is placed

adjacent to the cold plate, S3 in the transition zone between the cold gun and the cold plate, and S4 at the system's outlet, enabling a comprehensive data capture of relative humidity, temperature, and air pressure throughout the dehumidification stages, Figure 4.2.

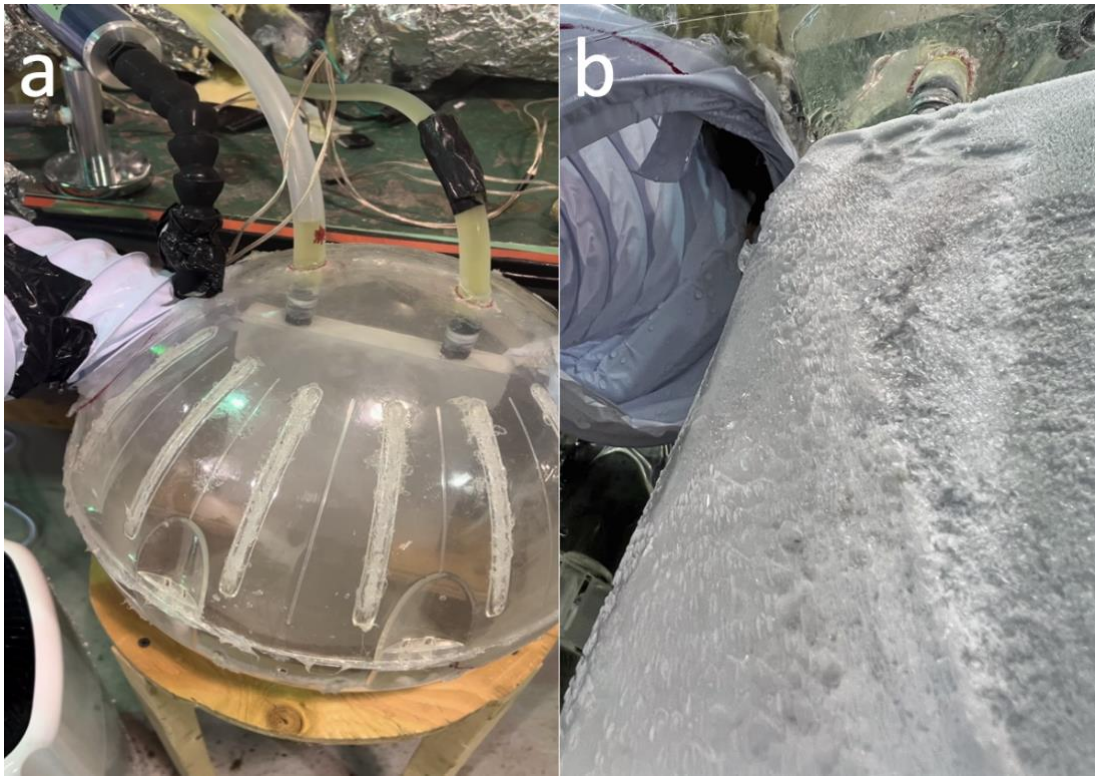


**Figure 4.2.** Dehumidification system overview, (a) Exterior view of the circular chamber with a cold plate installed inside, (b) Interior view showing ice crystals formed on the surface of the cold plate.

## 4.5 Results

### 4.5.1 Cooling

This study investigates the impact of relative humidity on system efficiency, focusing on optimizing performance through the precise adjustment of variables in accordance with thermodynamic balancing principles. The main objective is to to optimize system efficiency by adjusting operational parameters to suit different levels of relative humidity. A series of

experiments were conducted, each designed to explore different humidity settings and their effects on the system's performance, guided by the findings from initial experimental data. At the outset, the temperature was set at 32°C with a RH of 75%, maintained at a pressure of $10^5$ Pa. After running the system for 30 min, rh decreased by 30%, fluctuating between 20% and 30%. Figure 4.3 illustrates the performance of a dehumidification system over time, demonstrating a rapid initial decline in outlet temperature from approximately 30°C to slightly above 5°C within the first 10 min, followed by a more gradual decrease and eventual stabilization around 5°C. This trend suggests the system's approach to thermal equilibrium, where the heat transfer from the incoming hot and humid air—kept constantly saturated at nearly 100% RH—is balanced by the cooling effects of the vortex gun and cold plate. The difference in absolute humidity between the inlet and outlet initially stabilizes at around 2 g $m^{-3}$, maintained throughout the experiment by the system. This data underscores the system's ability to consistently manage temperature and humidity under controlled conditions. The rapid temperature drop within the initial 5 min highlights the system's swift cooling capability, likely due to the immediate response of the cooling mechanism. The subsequent gradual temperature decline indicates a sustained cooling effect, influenced by factors such as heat dissipation and system efficiency. Variations in RH are displayed in the graph; these are likely caused by the intermittent operation of the humidifier, which lacks a consistent humidity load. consequently, the system displays fluctuating trends, showing both upward and downward movements. The system successfully counteracted these fluctuations by improving its moisture absorption capacity.

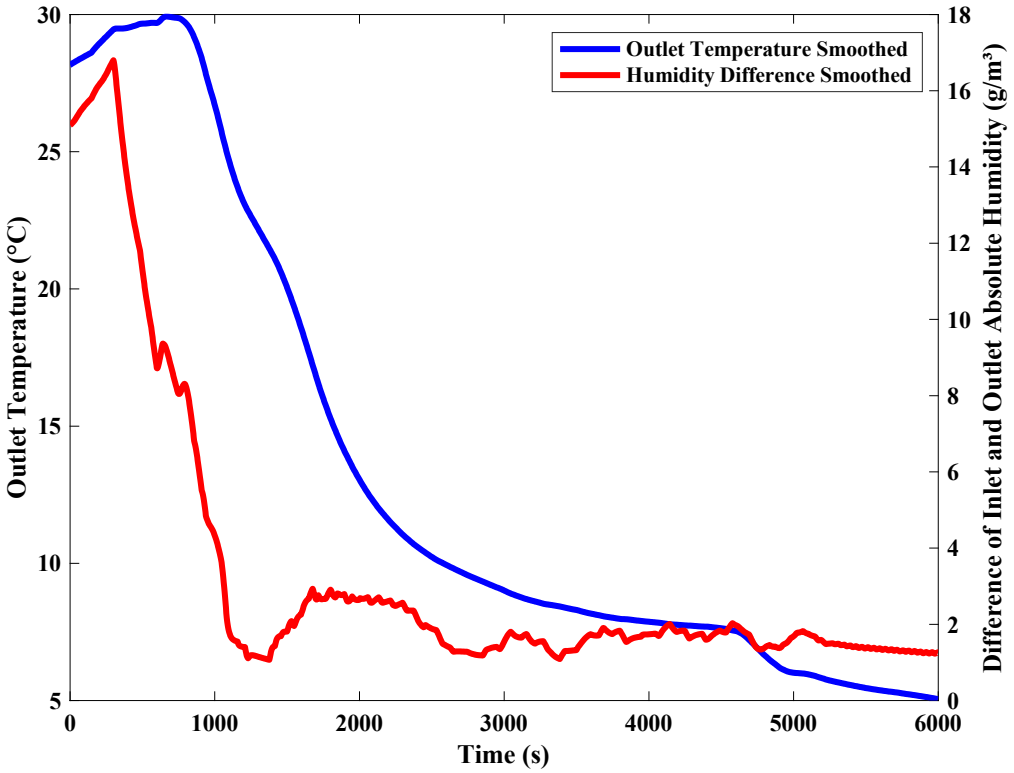


**Figure 4.3.** The changes in temperature (°C) and absolute humidity (g/m³) across different relative humidity conditions during the experiment.

To assess the system's efficacy in managing fluctuations in RH, a series of experiments were conducted wherein different moisture loads were introduced into the chamber. Across each trial, there was a notable reduction in RH, declining from 100% to approximately 30%, achieved within a consistent timeframe of approximately 3 min. Notably, the temperature within the chamber was controlled at 9°C, a departure from the initial ambient temperature of 32°C. This deliberate temperature adjustment was instrumental in facilitating precise moisture regulation, leveraging the heightened cooling efficiency afforded by the cold fog system at lower temperatures around 6°C. These findings underscore the system's robust capability to

effectively modulate relative humidity levels across varying moisture loads, demonstrating its potential for reliable humidity control in dynamic environmental conditions.

### 4.5.2 Dehumidification

Figure 4.4 shows how RH was controlled at temperatures lower than 10°C. During the experimental trials, different amounts of RH up to 60 % continuously entered to the system, the system even was subjected to a maximum humidity level of 100%. In each trial, the system promptly responded to this input and effectively regulated the humidity, swiftly reducing it to less than 30%. The graph indicates that as the humidity rate rises, the formation of ice on the cold plate's surface is accelerated. Consequently, the humidity ratio across the humidifier sees an increase, leading to more effective dehumidification. This process enables the system to condense a greater amount of water vapor. Given that the inlet feed water flow rate remains largely unchanged. This consistent performance underscores the system's ability to promptly and reliably control humidity levels in varying environmental conditions. The graph demonstrates the dehumidification system's efficiency, where significant peaks in inlet RH are effectively managed, even under conditions of fully saturated air.

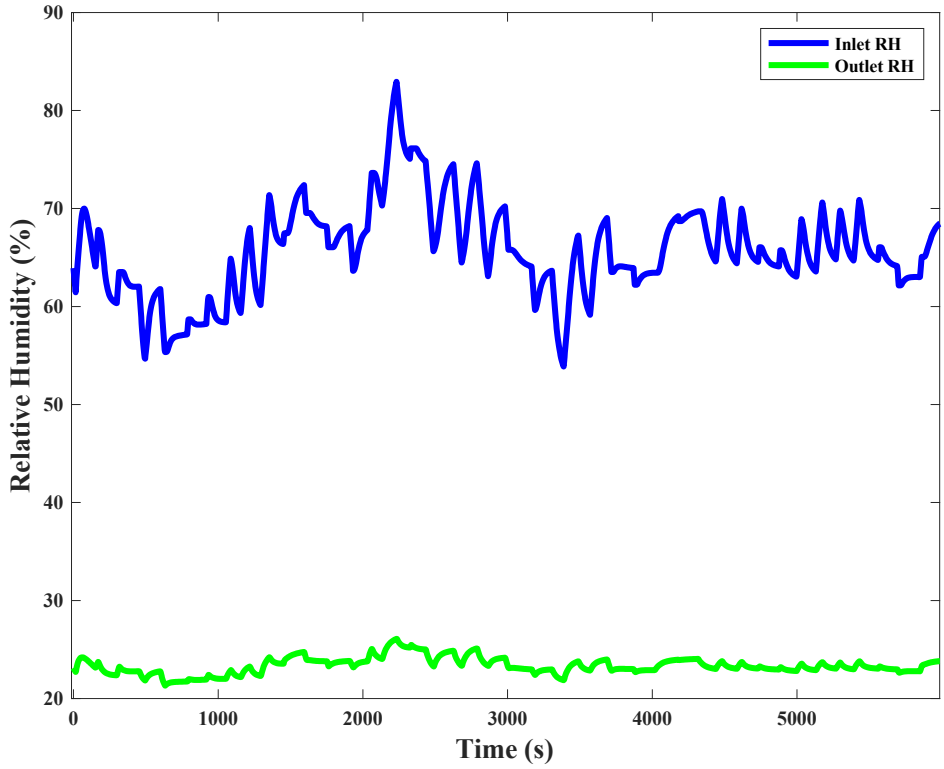


**Figure 4.4** RH performance. Achieving less than 30% RH from 100% RH input.

### 4.5.3 Heat and mass transfer effectiveness

Figure 4.5 shows that the mean efficiency of dehumidification was approximately 40%, with the most notable efficiency reaching around 60%. This indicates that, on average, the dehumidifier effectively reduced the moisture content in the air, with some instances demonstrating even higher efficacy. Specifically, the specific humidity of the air decreased from 23 g $kg^{-1}$ at the inlet to 2 g $kg^{-1}$ at the outlet, and from 19 g $kg^{-1}$ to 1.5 g $kg^{-1}$, respectively. After reaching this low point, the curve gradually ascends, signaling an increase in the rates of moisture removal. The variability observed in the efficiency coefficient ($\eta_{dehum}$) can be attributed to fluctuations in incoming moisture from the humidifier. These fluctuations reflect the system's ability to adapt to real-world conditions where incoming humidity levels are not constant. Despite this variability, the efficiency of the system consistently maintains an upward

trend, hovering around 40%. This suggests that the system retains its effectiveness in regulating humidity levels despite fluctuations in input moisture levels.

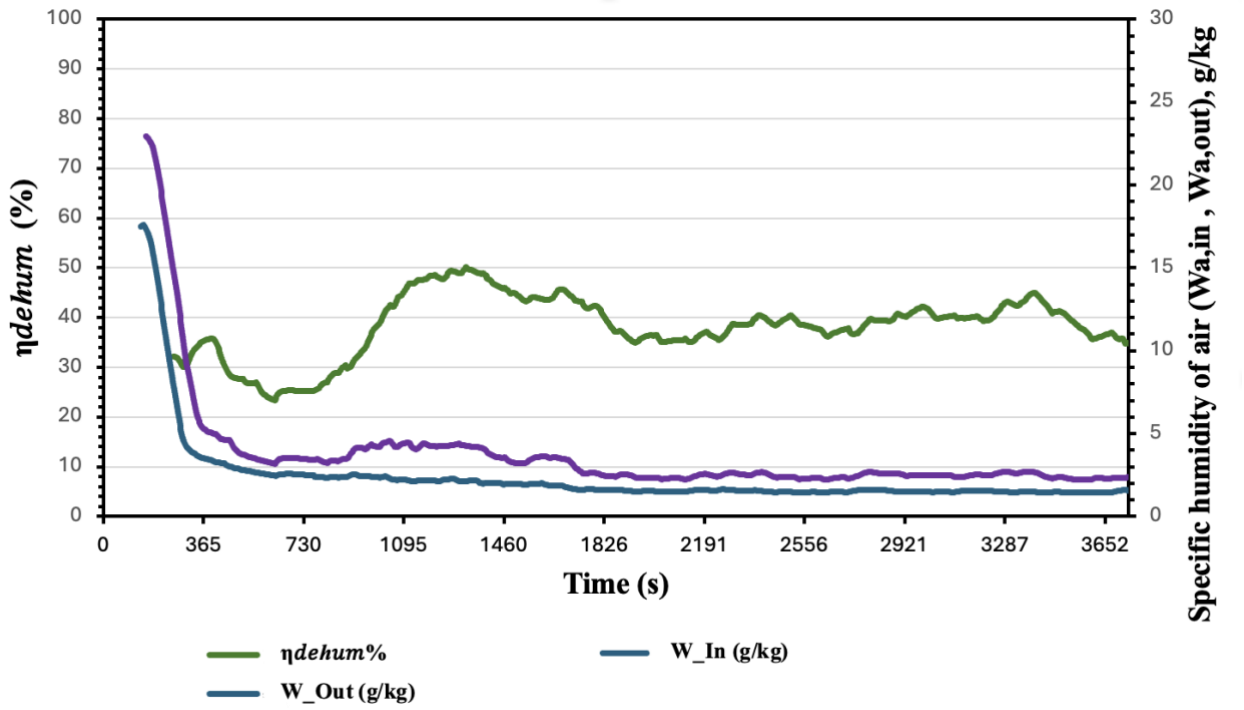


**Figure 4.5.** Effect of inlet-specific humidity of air dehumidification efficiency.

The dehumidification efficiency exhibits a generally increasing trend as the inlet absolute humidity rises from approximately 3 g $m^{-3}$ to about 16 g $m^{-3}$, Figure 4.6 The efficiency reaches a peak of around 50%. This observation implies that the dehumidification process becomes more efficient as the air's moisture content increases, likely due to enhanced mass transfer driven by higher humidity levels. Similarly, MRR tends to increase with the inlet absolute humidity, achieving a maximum of approximately 0.2 g $s^{-1}$, which coincides with the peak in dehumidification efficiency. As the inlet absolute humidity increases, the vapor pressure difference between the air and the condensing surface of the cold plate rises, strengthening the

driving force for mass transfer. This increased driving force enhances both the dehumidification efficiency and the MRR up to a certain threshold.

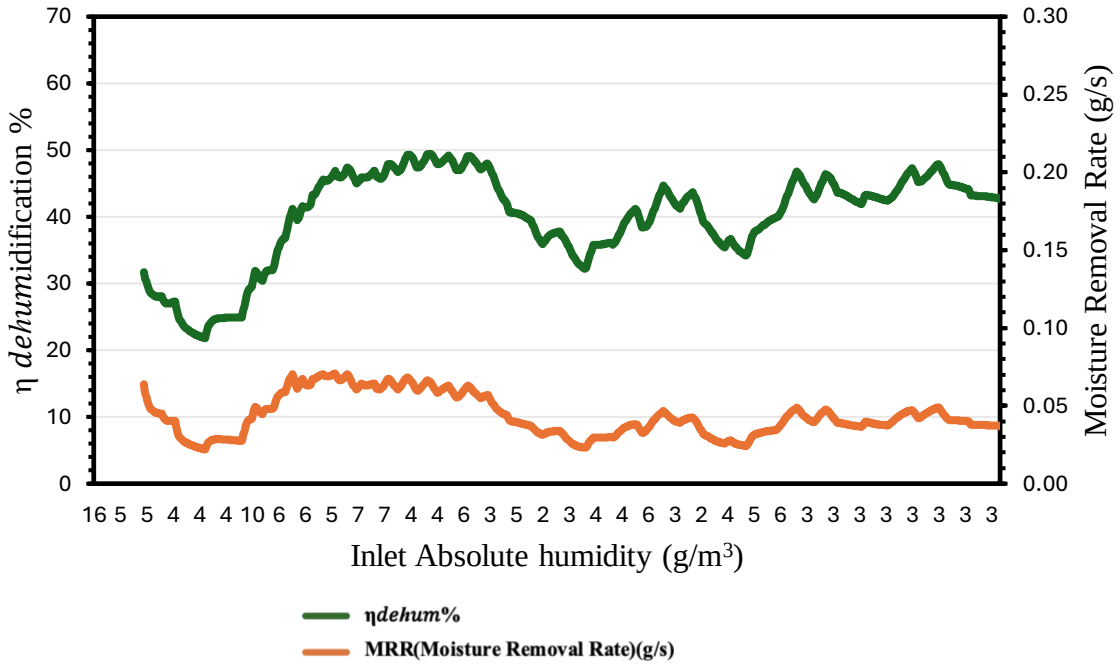


**Figure 4.6.** Moisture removal rate and efficiency vs. Inlet absolute humidity: of cold plate and ice crystal formation.

### 4.6 Discussion

This study looks at the same parameters but also closely considers the efficiency of the system in each cycle with different input of RH. The main objective is to achieve optimum performance by adjusting the variables based on the thermodynamic balancing concept. A series of experiments were conducted, each designed to explore different RH settings and their effects on the system's performance, guided by the findings from initial experimental data.

As ice crystals merge and expand into larger flakes, they serve as nuclei, attracting and condensing supercooled droplets found in the surrounding air. This process leads to a greater buildup of ice on the cold plate's surface, contributing significantly to the dehumidification process by effectively extracting moisture from the air. The attraction and condensation of

supercooled droplets onto the ice crystals not only improve dehumidification but also play a vital role in lowering RH levels in the environment. Additionally, the formation of cold fog around the cold plate serves as an additional indication of the system's effectiveness in removing moisture and controlling humidity. When humid air is cooled, its capacity to retain moisture diminishes due to the decrease in temperature. Cooler air inherently possesses a reduced ability to hold water vapor. As the air cools further, it eventually reaches a point where it becomes saturated with moisture, leading to condensation. If the temperature drops below the freezing point and the dew point follows suit, the water vapor in the air undergoes direct condensation into ice crystals without transitioning through a liquid state. In dehumidifiers, particularly those operating within open systems, the refrigerated cold plates serve as prime locations for this phenomenon. These cold surfaces facilitate deposition, wherein water vapor bypasses the liquid phase and directly forms solid ice crystals. The accumulation of ice crystals on the cold plates hinders the efficiency of the dehumidification process by reducing the available surface area for further condensation. Another significant outcome of this process is the formation of icy fog, characterized by a mixture of ice crystals, water vapor, and liquid water droplets at lower temperatures. This underscores the simultaneous occurrence of freezing and deposition under specific environmental conditions, emphasizing the intricate relationship between temperature, humidity, and phase transitions in atmospheric processes.

Following the activation of the vortex and cold plate systems, the initial temperature registered approximately 9°C, signifying the successful integration of these components to attain the intended cooling effect. Subsequently, over a duration of one and a half hours, the temperature exhibited a gradual decline, reaching approximately 6°C. This progressive reduction in temperature indicates the sustained efficacy of the system in maintaining cooling capacity and operating efficiently over an extended timeframe. Despite the temperature decrease to 6°C, the system exhibited proficient control over RH levels, as evidenced by the

preservation of RH within the targeted range. This observation accentuates the system's resilience and adaptability, showcasing its capability to uphold consistent humidity regulation even under lowered temperatures.

The upward trend in Figure 4.4 suggests that the formation of ice crystals plays a contributory role in augmenting the absorption of moisture, particularly at lower temperatures. Such findings shed light on the intricate dynamics of moisture removal mechanisms, emphasizing the importance of temperature regulation and ice crystal formation in enhancing dehumidification processes, suggesting that the system operates most effectively at higher humidity levels. These reductions underscore the effectiveness of the dehumidifier in removing moisture from the air passing through it. In the investigation of moisture removal rates at various outlet air temperatures, the observed curve in figure distribution unveils a distinct pattern characterized by a sharp decline to a minimum value. This phenomenon underscores the efficient absorption of humidity by the cold plate under colder conditions.

## 4.7 Conclusion

The combination of experimental data with the previously discussed results reveals the effectiveness and potential uses of the innovative dehumidification method inspired by natural fog formation. Through a series of experiments assessing its performance under various moisture loads, consistent and substantial decreases in RH were observed. RH levels decreased from 100% to approximately 40% within an average timeframe of three minutes. This rapid and accurate adjustment of RH highlights the system's strong ability to manage changes in moisture levels, demonstrating its reliability in controlling humidity in dynamic environmental conditions. The analysis of dehumidification efficiency and moisture removal rates as functions of inlet absolute humidity reveals that the system performs optimally under conditions of higher

humidity. This correlation underscores the system's ability to leverage increased humidity for enhanced moisture extraction, thus improving its overall efficiency and performance.

The proposed dehumidification approach not only offers a more effective means of controlling indoor humidity but also presents a significant advancement in energy-efficient HVAC technology. Additionally, precise temperature control within the experimental chamber played a crucial role in improving the system's moisture regulation efficiency. By capitalizing on the enhanced cooling efficiency of the cold fog system at lower temperatures, the deliberate temperature control allowed for precise management of moisture levels, resulting in the observed reductions in RH across different moisture load scenarios.

**Connecting text**

Chapter 4 presents the first set of results, focusing on temperature and humidity reduction achieved through the novel dehumidification system. The findings here establish the baseline performance of the system under controlled conditions and highlight the system's ability to achieve significant reductions in relative humidity and absolute humidity, as initially anticipated in the objectives.

# CHAPTER 5

## COMSOL Multiphysics Simulation and Performance Analysis of a Dehumidification System in Controlled Environment Conditions

Sheida Rezaei[1], Valerie Orsat[1], Mark Lefsrud[1]*

[1]Department of Bioresource Engineering, Macdonald Stewart Building, Macdonald Campus, McGill University, 21111 Lakeshore Road, Ste-Anne-de-Bellevue, QC, H9X3V9

***Corresponding author:** mark.lefsrud@mcgill.ca

## 5.1 Abstract

In the quest for efficient air dehumidification in controlled environments, the integration of innovative cooling technologies, such as vortex cooling coupled with cold plates, presents a viable solution. This study develops a comprehensive computer model using COMSOL Multiphysics to elucidate the transient mass and heat transfer dynamics in a novel dehumidification system. The model is established in a two-dimensional (2D) framework considering the conservation of mass, momentum, and heat, tailored to the specifics of the cooling mechanisms involved. It utilizes the Linear Driving Force (LDF) model to characterize the moisture removal properties under various operational conditions. The applicability of the LDF model is further validated by a parametric analysis exploring system responses to changes in inlet temperature, relative humidity, and operational configurations. Parameters such as inlet air velocity, humidity levels, and cooling surface dimensions are varied to gauge their impact on the system's dehumidification efficiency. Results indicate optimal performance at specific operational thresholds, notably an inlet velocity of 0.3 m $s^{-1}$, a relative humidity of 50%, and a cooling surface area effectively managed by the cold plate design. The model's predictions align closely with experimental data, confirming its potential utility in optimizing real-world applications of such dehumidification systems. This study not only reinforces the theoretical understanding of complex dehumidification dynamics but also provides a practical framework for enhancing system design and efficiency.

## 5.2 Introduction

Dehumidification technologies are critical in environments where control of humidity is essential for operational reliability and safety, such as in data centers and industrial applications. Traditional methods like heating, ventilation, and air conditioning (HVAC) systems have been the primary strategies for controlling air quality and humidity. However,

these systems often consume substantial energy, prompting the need for more efficient solutions (Geraldini & Spa).

In high-temperature and high-humidity environments, effective humidity control is crucial for ensuring equipment safety and comfort within enclosed spaces like prefabricated chambers. Lin et al. (2023) conducted numerical simulations to analyze the effects of thermal dissipation and air supply on condensation, revealing that an increase in load power inhibits condensation (Lin et al., 2023).

Recent advancements have focused on integrating multi-physical field approaches to optimize dehumidification processes. This includes the use of numerical simulations to better understand the dynamics of air flow, temperature, and humidity within controlled environments (Lin et al., 2023). The performance of isothermal dehumidifiers in nuclear waste storage indicates that managing humidity is not only about comfort but also about preventing corrosion and ensuring the structural integrity of storage facilities (Geraldini & Spa).

Vivekh et al. (2023), have employed advanced three-dimensional mathematical models to meticulously analyze the air dehumidification performance of desiccant wheels. This research utilized COMSOL Multiphysics to simulate the intricate interplay of temperature, humidity, and chemical reactions within the desiccant wheel, providing insights that surpass the capabilities of traditional models. Their work demonstrates the model's enhanced accuracy in predicting desiccant wheel performance under various operational conditions (Vivekh et al., 2023).

Efficient humidity control is paramount in environments where precise moisture levels are crucial. This research centers on modelling a dehumidification system using COMSOL Multiphysics (Multiphysics, 1998) to evaluate its performance under various operational conditions and enhance its design for better efficiency. A simulation model was created to evaluate different variables that may impact the performance and improve the efficiency of the

system. This model facilitates forecasting the temperature distribution and accurate humidity profiles throughout the test segment.

### 5.3 Materials and methods

The primary focus of this study was to analyze the dehumidification and heat transfer characteristics within a cooling chamber, modeled using COMSOL Multiphysics. The geometry of the chamber, as shown in the schematic diagram, figure 5.1, was designed with a circular cross-section, a centrally located cold plate, and specific inlets and outlets for airflow. The cold plate, represented by the grey region at the center, acts as the primary cooling and dehumidification surface. The hot and humid air enters the chamber through a larger inlet on the left, while a vortex cooling gun supplies cold air through a smaller entrance on the top-left. The mixed air exits through a designated outlet on the right side.

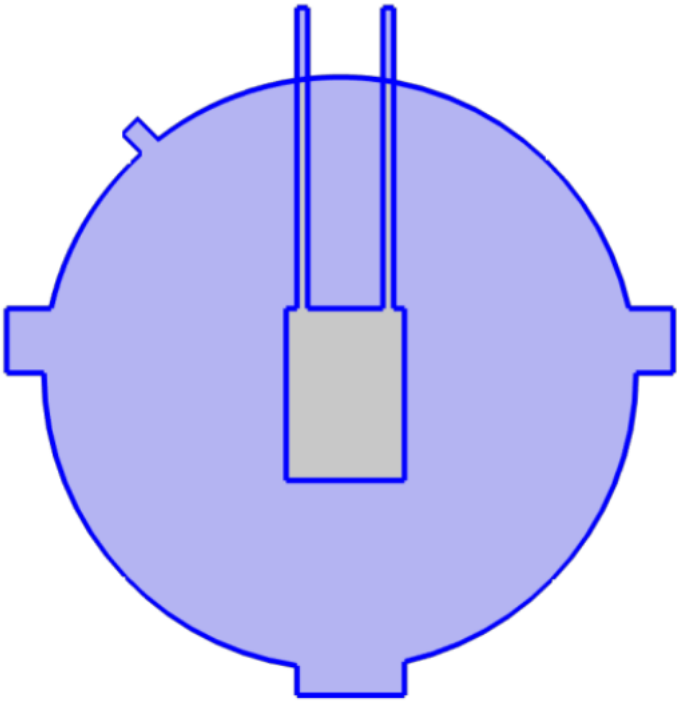

**Figure 5.1.** Schematic of the Cooling Chamber with Cold Plate and vortex cooling gun.

### 5.3.1 Governing equations

1. Convective Heat Transfer with Moist Air

This section involves equations governing the movement and temperature change of air due to the vortex cooling gun. The convective heat transfer equations would account for the velocity of the air ($u_g$ for gas phase) and the change in temperature ($\nabla T$) across the domain. This is crucial for modelling how effectively the cold air from the vortex gun can reduce the air temperature around the cold plate, facilitating dehumidification.

2. Moisture Transport Equations

Moisture transport equations would be essential to understand how water vapor moves within the setup, especially from the hotter regions towards the cold plate where condensation can occur. These equations would involve gradients of moisture concentration and include terms for diffusion and advection of moisture due to air movement induced by the cooling gun.

3. Equations Involving Phase Change (mentioned as $Q_{evap}$ in the primary heat transfer equation)

In the dehumidification process, the phase change from vapor to liquid on the cold plate's surface is a critical aspect. Equations that include $Q_{evap}$ terms would model the latent heat release due to condensation, which is vital for evaluating the efficiency of the dehumidification process. These would be directly related to the surface temperature of the cold plate and the surrounding air's humidity and temperature.

4. Energy Balance and Porosity Effects

Since the cold plate might have a structure to enhance condensation or moisture capture, any equations discussing porosity effects on fluid flow and thermal properties would be relevant. These would detail how the structure of the cold plate influences the heat and mass transfer, incorporating terms from Darcy's law or modified forms of it to account for the viscous flow through porous media.

5. Boundary Conditions and External Cooling Influences

Equations detailing boundary conditions around the edges of the circle, especially where the cooling gun introduces cold air, would be crucial. These would specify how external cooling affects the internal flow and thermal gradients, potentially modelling how effectively the introduced cold air mixes with the internal air, its path, and its impact on overall temperature distribution within the circle.

### 5.3.2 Convective heat transfer in moist air

$$(\rho c_p)\frac{\partial T}{\partial t} + (\rho_g c_{pg} u_g) \cdot \nabla T + (\rho_l c_{pl} u_l) \cdot \nabla T + \nabla \cdot (k_{eff} \nabla T) = Q + Q_{evap} \quad (5.1)$$

Where :

$(\rho c_p)\partial t/\partial T$ is This term represents the transient heat storage in the air, where $\rho$\rho$\rho$ is the air density, cp is the specific heat capacity, and $\partial T/\partial t$ is the rate of temperature change over time. $(\rho_g c_{pg} u_g)\cdot\nabla T$ is Convective heat transfer by the gaseous phase, incorporating the density of the gas ($\rho_g$), the specific heat at constant pressure ($c_{pg}$) and the velocity vector ($u_g$). $(\rho_l c_{pl} u_l)\cdot\nabla T$ is Convective heat transfer by the liquid phase, similar to the gaseous phase but for the liquid components. $\nabla\cdot(k_{eff}\nabla T)$ is Conductive heat transfer across the medium, where $k_{eff}$ is the effective thermal conductivity. Q + $Q_{evap}$ is Internal heat generation (Q) and the heat associated with phase changes, specifically evaporation or condensation ($Q_{evap}$).

### 5.3.3 Moisture transport equation

$$\frac{\partial(\rho_v)}{\partial t} + \nabla \cdot (\rho_v u) = S \quad (5.2)$$

Where $\partial(\rho v)/\partial t$ is Rate of change of vapor density ($\rho_v$), indicating how moisture content in the air changes over time. $\nabla\cdot(\rho_v u)$ is Divergence of the moisture flux, representing

how moisture moves through the air due to air currents (u). S is Source term for moisture, which could include evaporation or condensation sources.

### 5.3.4 Phase change equation

$$Q_{cond} = hA(T_{surf} - T_{air}) \tag{5.3}$$

Where $Q_{cond}$ is Heat transfer due to condensation, a key part of the dehumidification process on the cold plate, H is the heat transfer coefficient, which quantifies the effectiveness of the cold plate at condensing moisture, A is the surface area of the cold plate and ($T_{surf}$−$T_{air}$) is the temperature difference between the surface of the cold plate ($T_{surf}$) and the air ($T_{air}$), driving the condensation process.

### 5.3.5 Laminar flow equation

$$\frac{\partial(\rho \mathbf{u})}{\partial t} + (\mathbf{u} \cdot \nabla)(\rho \mathbf{u}) = \nabla \cdot [-pI + \mathbf{K}] + \mathbf{F}\ \nabla \cdot (\rho \mathbf{u}) = 0 \tag{5.4}$$

Where ρ is fluid density, u is fluid velocity vector. ∂(ρu)/∂t is temporal change in momentum, (u·∇)(ρu) is convective transport of momentum, p is fluid pressure, I is identity matrix, K is stress tensor incorporating viscous stresses, F is external force fields (e.g., gravitational forces) and ∇·(ρu) = 0 : continuity equation asserting mass conservation.

### 5.3.6 Moisture transport in air equation

$$\frac{\partial M}{\partial t} + \mathbf{u} \cdot \nabla M = -\nabla \cdot \mathbf{g}_w + S\ \mathbf{g}_w = -D \nabla M\ C_v = \phi_w C_{sat} \tag{5.5}$$

Where M is moisture content or specific humidity, $g_w$ is moisture flux vector, D is diffusivity of moisture in air, ∇M is gradient of moisture content, S is source/sink term for

moisture, $C_v$ is vapor concentration, $\phi_w$ is relative humidity and $C_{sat}$ is saturation vapor concentration (Datta, 2007).

### 5.4 Numerical model

The system's performance, driven by coupled heat and moisture transfer, is simulated within COMSOL Multiphysics, reflecting the setup's actual operating conditions.

#### 5.4.1 System geometry and material properties

The simulation domain features a cylindrical chamber with a centrally positioned cooling mechanism. Properties such as thermal conductivity and moisture permeability align with experimental configurations.

#### 5.4.2 Boundary conditions and simulation setup

Boundary conditions replicate the real operational environment with specific focus on inlet air properties and cooling surface temperatures. Simulations dynamically track temperature and humidity changes, offering insights into the system's responsiveness.

### 5.5 Results

#### 5.5.1 Analysis of airflow dynamics and dehumidification efficiency in a cold plate cooling system

The velocity magnitude plot from the COMSOL simulation, captured at 5000 seconds, provides critical insight into the airflow patterns and dehumidification efficiency of the system (Figure 5.2). The figure shows the velocity distribution within the chamber, with the color scale representing velocity in meters per second (m $s^{-1}$). The hot and humid air at a temperature of 30 °C and relative humidity (RH) of 100% enters from the left through a larger opening with the airflow of 2 m $s^{-1}$, which corresponds to the high-velocity region marked in red. This high velocity indicates the strong influx of hot air, which is essential for ensuring that the humid air is directed towards the central cold plate. Simultaneously, the cold air from the vortex cooling gun enters from the top-left entrance, with a similar high-velocity region, 5 m $s^{-1}$, forming due to the forced cold air flow. The convergence of these two streams creates a critical mixing zone

before the air reaches the cold plate, allowing the hot and humid air to be effectively exposed to the cooling surface.

At the cold plate, with the temperature of -10 °C located at the center of the circular chamber, the velocity magnitude decreases significantly, as depicted by the blue region. This drop in velocity aligns with the expected behavior where the humid air encounters the cold plate, loses heat, and condenses moisture, forming ice crystals on the surface. The low-velocity region around the cold plate suggests that latent heat release and moisture removal are occurring, resulting in cooler, slower-moving air. Furthermore, the exit airflow on the right side of the chamber also shows reduced velocity, indicating that the air leaving the system has been dehumidified and cooled. This lower velocity reflects the reduced energy content of the air after undergoing the cooling and dehumidification process, demonstrating the system's effectiveness in lowering the temperature and humidity of the air. The velocity gradient observed from the entrances to the exits aligns with the system's design objectives, confirming that the cold plate serves as the focal point for energy and moisture extraction. This velocity analysis supports the successful functioning of the system in meeting the cooling and dehumidification targets and validates the results when compared with experimental data from MATLAB simulations.

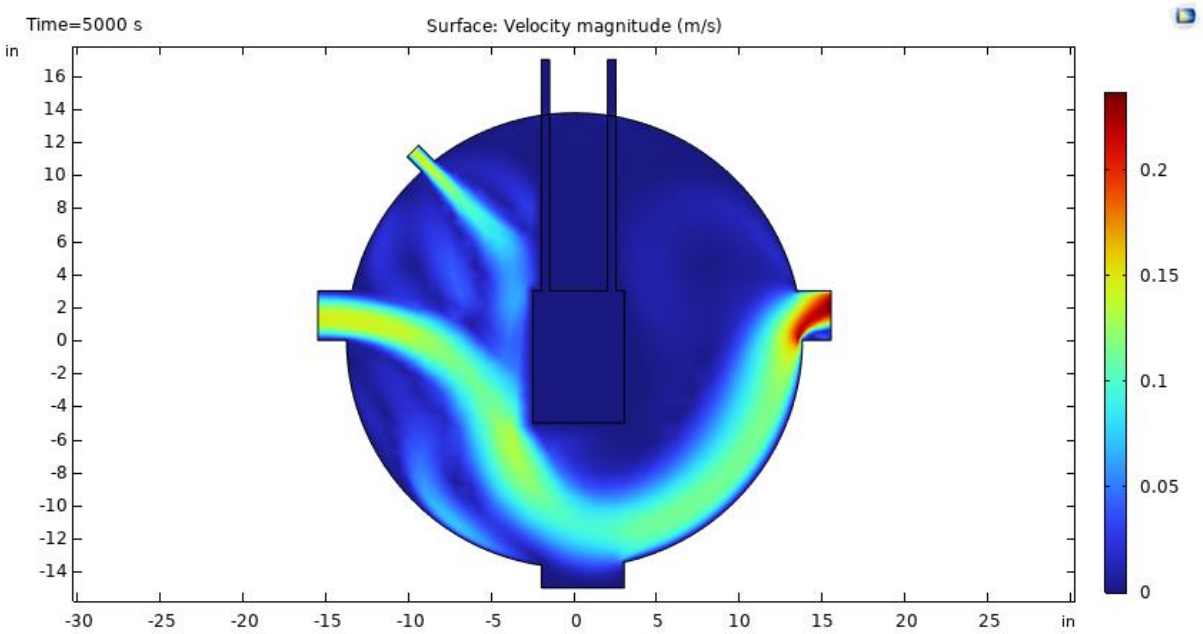


**Figure 5.2.** Velocity magnitude distribution (m/s) at 5000 seconds, illustrating airflow patterns, mixing regions, and dehumidification around the cold plate in the cooling chamber.

### 5.5.2 Analysis of relative humidity distribution in the cooling chamber

The high RH near the inlet reflects the humid air entering the chamber, where it contacts the cold plate, maintained below the dew point (Figure 5.3). This induces condensation, turning water vapor into ice crystals on the plate's surface and releasing latent heat. This process reduces the moisture content, lowering the RH from 100% at the inlet to approximately 30% at the outlet, demonstrating effective dehumidification. The cold plate acts as a heat sink, removing both latent heat from condensation and sensible heat, thus decreasing RH and temperature.

The system reduces the total enthalpy of the incoming air through moisture removal and cooling. The cold plate, operating based on psychrometric principles, encourages continuous condensation due to the vapor pressure gradient between the humid air and its surface. The system efficiently manages heat and mass transfer, enabling steady dehumidification by simultaneously removing moisture and lowering air temperature. The cold plate’s placement

and heat exchange efficiency with the incoming air are critical to the system's performance, further supporting analysis through mass transfer models in humid air systems.

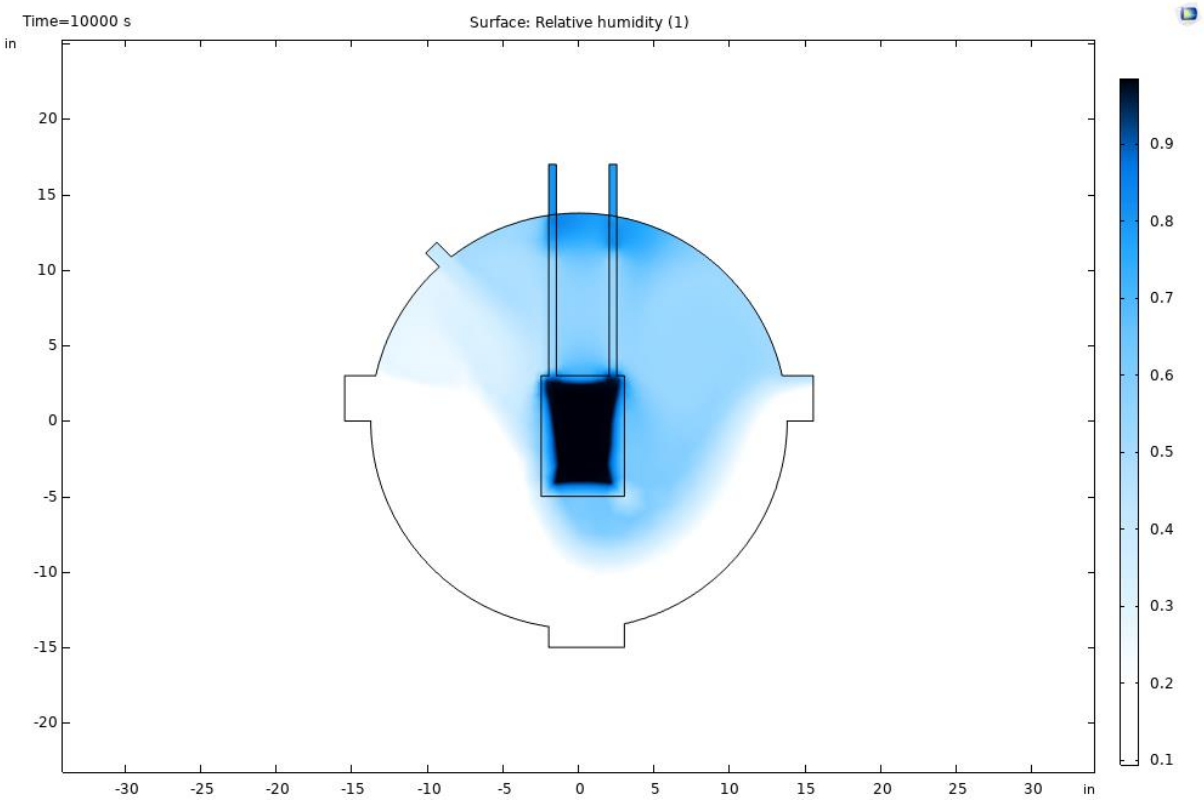


**Figure 5.3.** Relative humidity distribution illustrating dehumidification with higher RH at the hot and humid air inlet and condensation on the central cold plate.

### 5.5.3 Moisture removal efficiency in porous medium: a time-based analysis

Figure 5.4 illustrates the moisture content in a chamber over time, revealing the dynamic behavior of moisture removal during the dehumidification process. The graph shows a consistent downward trend in moisture content, indicating a continuous reduction of moisture within the medium. This behavior is indicative of the effectiveness of the dehumidification system, where the mass transfer of water vapor is driven out of the medium over time.

The moisture removal is observed to be steady throughout the simulation period, with a rapid initial decrease, suggesting that a higher moisture removal rate is achieved at the start.

This initial efficiency can be attributed to a larger concentration gradient between the cold plate and the surrounding air, which promotes faster diffusion and removal of moisture. As time progresses, the rate of moisture removal gradually decreases, likely due to the reduced moisture gradient and diminished driving force for vapor diffusion. This trend aligns with the expected behavior in mass transfer processes, where the removal rate decreases as the system approaches equilibrium.

The consistent reduction in moisture content throughout the simulation, without significant fluctuations, indicates that the operation parameters, such as temperature and flow conditions, are well-regulated. This allows for a steady-state mass transfer within the system. The controlled decline in moisture content over time supports the efficiency of the dehumidification system and demonstrates that the process can maintain a stable and sustained moisture removal capability, which is crucial for applications requiring precise control of humidity within materials or enclosed environments.

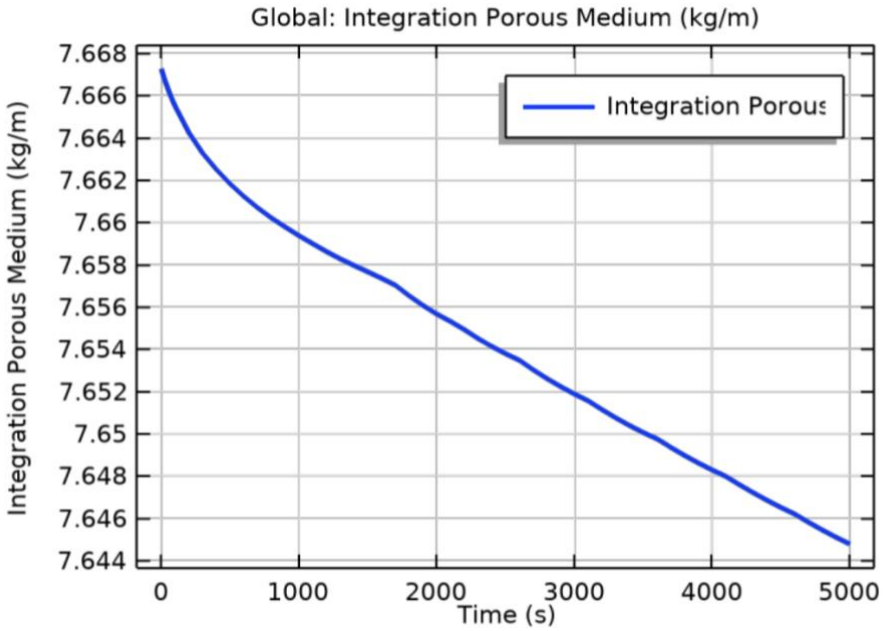


*Global: Integration Porous Medium (kg/m)*

**Figure 5.4.** Time-based reduction in moisture content within the porous medium, demonstrating consistent dehumidification performance over the 5000-second period.

### 5.5.4 Mass balance analysis and system stabilization

The mass balance, Figure 5.5 shows that the system quickly stabilizes after initial fluctuations, achieving a near-zero mass balance that suggests the attainment of a steady-state. This equilibrium implies effective mass conservation, where the inflow and outflow rates are balanced. Initially, the total net moisture is high, indicating a significant moisture presence, which decreases sharply early on, reflecting rapid moisture removal and an efficient dehumidification process. Over time, the moisture reduction becomes more gradual, consistent with continued condensation and moisture extraction. The total accumulated mass displays a continuous, linear decline, suggesting uninterrupted and steady mass removal throughout the simulation. Meanwhile, the total mass source initially fluctuates but then stabilizes, indicating

a balance between mass input and removal. Overall, the steady mass balance and the decline in both net moisture and accumulated mass confirm the system's effectiveness in managing moisture removal and mass conservation, highlighting its capacity to maintain controlled humidity levels over time.

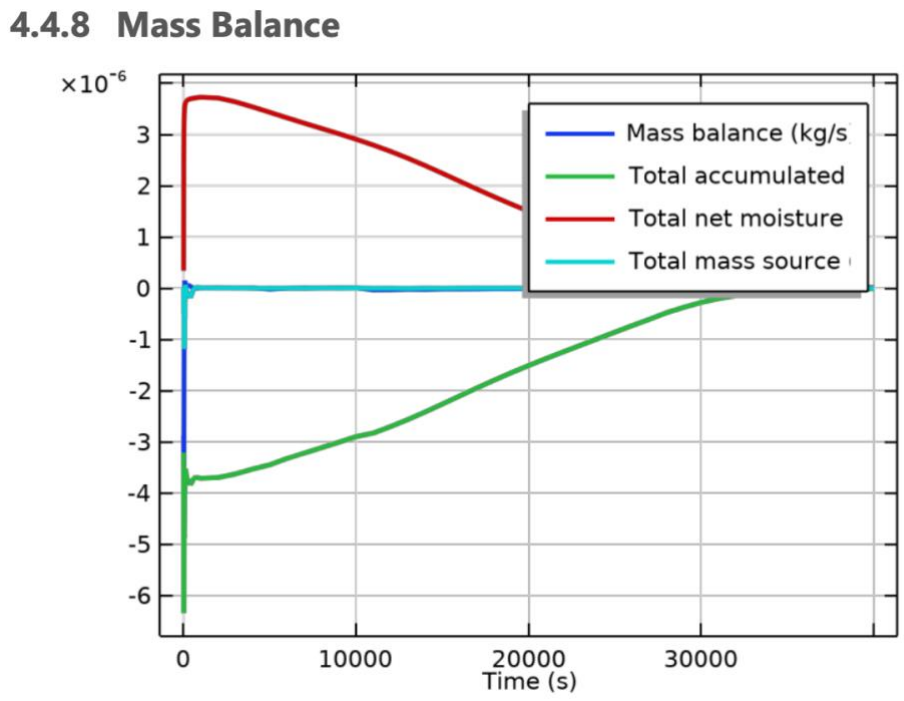


**Figure 5.5.** Mass balance analysis over time, showing stable system performance with consistent moisture removal and near-zero mass balance, indicating effective mass conservation and dehumidification.

### 5.5.5 Analysis of temperature distribution in the cooling chamber

The temperature distribution within the cooling chamber shows a clear transition from higher temperatures near the hot air inlet to significantly lower temperatures around the cold plate, Figure 5.6. The colder regions on the cold plate's surface indicate areas where ice crystals have formed, demonstrating effective moisture condensation. This phase change occurs as the humid air comes into contact with the cold plate, which is maintained below the dew point

temperature. The pipes entering the cold plate from the top side are visible with lower temperatures due to the circulating fluid inside, which is maintained at -10°C, further enhancing the cooling effect.

The system exhibits a strong temperature gradient, with rapid heat loss through convection as the hot air interacts with the cold plate. The steep temperature drop near the plate suggests efficient heat transfer, ensuring both latent heat removal from condensation and the phase change from water vapor to ice, along with sensible heat removal through temperature reduction. The temperature decreases from 30°C at the inlet to around 0°C near the cold plate, indicating significant cooling. The smooth transition in temperature as air moves from the hot inlet to the cooler outlet demonstrates the system's capacity to maintain consistent thermal regulation and dehumidification, effectively reducing both humidity and temperature in the outlet air.

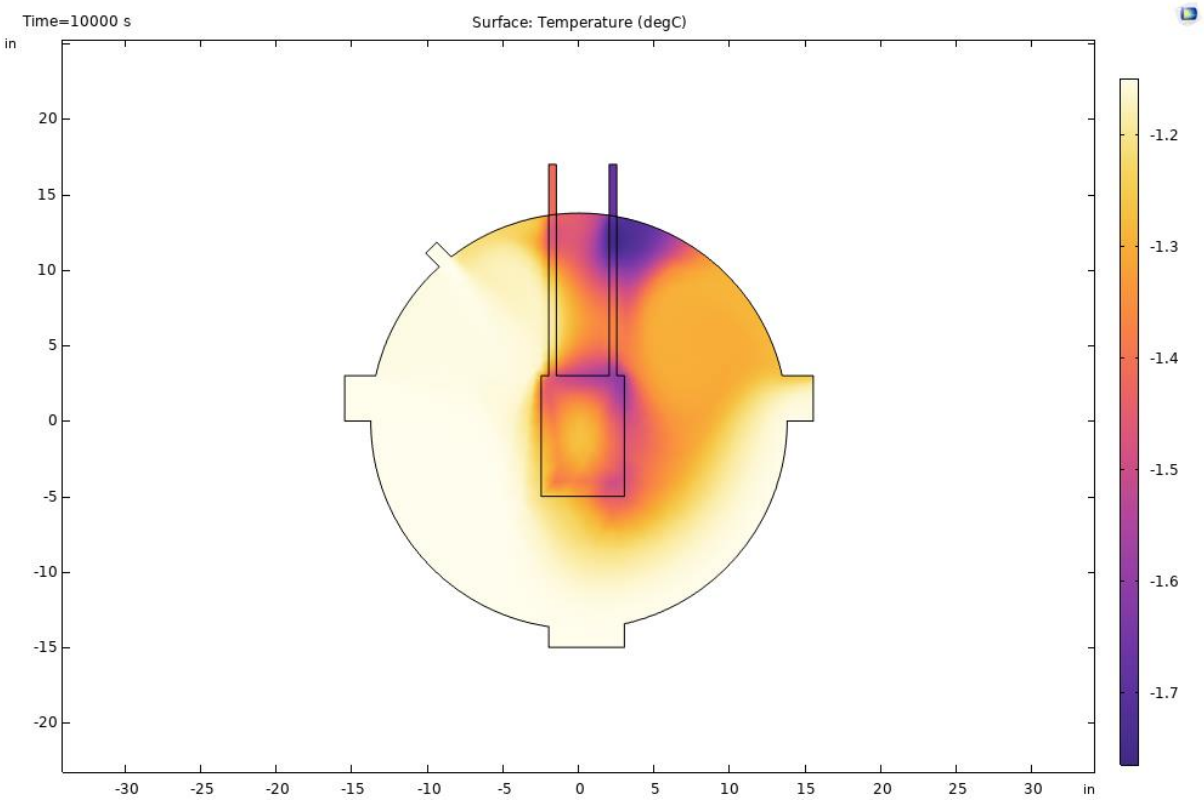


**Figure 5.6.** Temperature distribution in the cooling chamber, with higher temperatures at the inlet and lower temperatures near the cold plate indicating effective cooling and ice crystal formation.

### 5.6 Performance under varying conditions

The system exhibits robust humidity control across various thermal loads and airflow rates, with optimal performance at higher air velocities which promote more effective moisture contact with the cooling surfaces.

### 5.7. Discussion

Simulations pinpoint essential enhancements, especially in air flow management within the chamber to maintain consistent humidity control. The potential for system scaling is also discussed, considering the need to sustain airflow and cooling efficacy.

The results of this study demonstrate that the cold plate cooling system is highly effective in achieving dehumidification through the management of airflow and temperature reduction. Compared to conventional HVAC dehumidification methods, which typically rely on cooling air below the dew point and subsequent reheating (Nada et al., 2015a; Yuan et al., 2005), the cold plate system provides a more energy-efficient approach by leveraging targeted condensation and latent heat release directly on the cooling surface. The system achieves a substantial reduction in relative humidity from 100% to 30%, which is comparable to or exceeds the performance of other advanced systems reviewed in the literature.

Nada et al. (2015a) and Yuan et al. (2005) used hybrid humidification-dehumidification methods integrated with vapor compression cycles, producing fresh water while maintaining air conditioning. However, these approaches required additional steam boilers and energy-intensive heating components, which add complexity and high energy consumption. In contrast, the cold plate system demonstrated in this study achieves moisture removal without the need for excessive auxiliary heating, thereby reducing overall energy consumption. Moreover, the cold plate setup simplifies the process by directly controlling temperature and humidity in a compact manner (Nada et al., 2015a; Yuan et al., 2005).

Similarly, Gao et al. (2008) and Habeebullah (2010) investigated desalination systems combined with dehumidification, using heat pumps for enhanced performance. These studies highlighted the effectiveness of using heat pumps and renewable energy sources in maintaining dehumidification efficiency. However, the systems still faced challenges with waste heat recovery and energy utilization. The cold plate system presented here operates with a focus on thermal efficiency, but differentiates itself by achieving effective condensation directly on the cooling surface at temperatures of approximately -10 °C, without energy losses from waste heat (Gao et al., 2008; Habeebullah, 2010).

When compared to other alternative HVAC methods, such as desiccant-based dehumidification and chilled beam systems, the cold plate cooling system offers distinct advantages. Desiccant dehumidification methods, which rely on hygroscopic materials to absorb moisture, are effective in reducing humidity but often require substantial energy for desiccant regeneration, leading to higher operational costs. Chilled beam systems, which use convective cooling to condition indoor spaces, provide efficient temperature control but may struggle to effectively manage high latent loads in humid environments. The cold plate system, in contrast, directly condenses moisture onto a cold surface, making it particularly effective in managing both latent and sensible loads with lower energy requirements.

The energy efficiency of the cold plate cooling system also compares favorably with hybrid dehumidification systems. Hybrid systems, which combine vapor compression with additional humidification or dehumidification techniques, often require complex energy-intensive processes, such as the use of steam boilers or auxiliary heating units (Nada et al., 2015a). While these systems can achieve effective dehumidification, they do so at the cost of increased energy consumption. In contrast, the cold plate cooling system simplifies the process by eliminating the need for auxiliary components, thereby reducing the overall energy usage. The ability to directly achieve moisture removal through condensation at temperatures as low as -10 °C enhances its energy efficiency compared to hybrid systems that face challenges related to waste heat and additional heating requirements.

The stability of moisture removal over the 5000-second duration further highlights the robustness of the cold plate cooling approach. Compared to the solar-driven dehumidification systems discussed by S. A. Nada et al. (2015) and studies utilizing dual purpose solar collector (DPSC) (Rajaseenivasan & Srithar, 2017b), which depend on environmental conditions and often experience fluctuating performance, the cold plate system provides consistent moisture

removal irrespective of external factors. This stability is critical for controlled environments where precise humidity regulation is required.

The current findings also align with studies that emphasize the importance of coupling heat and moisture transfer for optimal dehumidification, such as the work on solar bubble column systems (Srithar & Rajaseenivasan, 2017) and biomass-powered dehumidification (Rajaseenivasan & Srithar, 2017a). However, the use of a cold plate offers a more direct and controllable solution, achieving condensation via rapid temperature reduction and effectively leveraging the latent heat release to further enhance performance.

The cold plate cooling system demonstrates

t advantages in energy efficiency, simplicity, and stable dehumidification performance when compared to existing hybrid, desiccant, chilled beam, and solar-based dehumidification solutions. Future research will focus on experimental validation to corroborate these findings and explore opportunities for optimizing individual system components, such as the cold plate configuration and airflow dynamics, to further enhance moisture removal efficiency and reduce energy consumption.

### 5.8. Conclusion

The study demonstrates the efficacy of the cold plate cooling system in achieving dehumidification through controlled airflow dynamics and temperature reduction. Velocity analysis reveals an initial 5 m/s for hot and humid air and 2 m $s^{-1}$ for the vortex cooling gun, effectively facilitating the air mixing and cooling process. Relative humidity decreases from 100% at the inlet to 30% at the outlet, indicating substantial moisture removal. Moisture removal efficiency is maintained consistently over 5000 seconds, reflecting stable system performance. The temperature distribution shows a reduction from 30 °C at the inlet to approximately 0 °C at the outlet. These results, derived through COMSOL Multiphysics simulations, validate the system's capacity to regulate temperature and humidity effectively.

The COMSOL Multiphysics modelling confirms the system's dehumidification potential for moisture control in targeted environments. Future work will emphasize experimental validation and component optimization to further enhance system performance. Beyond time limit, challenges include replicating complex boundary conditions (e.g., moisture transport and ice crystallization) in a controlled lab with advanced sensors. Additionally, the study likely prioritized numerical optimization before investing in costly prototyping.

# CHAPTER 6

## Discussion, future studies and conclusions

### 6.1 General discussion

The focus of this research was on the development, testing, and performance evaluation of an innovative HVAC dehumidification system, designed to address the limitations of conventional humidity control methods. This system combines a vortex cooling gun with a cold plate to facilitate rapid cooling and moisture removal from humid air, a novel approach aimed at increasing energy efficiency while maintaining precise humidity control. Unlike traditional dehumidification systems that rely heavily on energy-intensive refrigeration cycles, this design utilizes phase-change processes, enabling the effective removal of moisture through ice crystal formation.

This doctoral research began with a thorough examination of current dehumidification technologies, exploring their limitations in handling high humidity levels, energy consumption, and effectiveness in varied environmental conditions. Most conventional systems are optimized for temperature control rather than humidity, resulting in less efficient performance in high-moisture settings. In contrast, this research introduces an approach that addresses these challenges by focusing on rapid temperature reduction and enhanced moisture removal through direct contact cooling, significantly lowering RH without excessive energy use.

While traditional systems primarily focus on lowering air temperature to condense moisture, this system was designed with a more dynamic approach, capitalizing on the principles of phase transition. Initial findings demonstrated that integrating the vortex cooling gun and cold plate not only improved moisture extraction but also allowed for sustained dehumidification even in high-humidity environments. The research thus provides new insights into HVAC system design, showing that advanced cooling techniques can yield substantial gains in both energy efficiency and dehumidification performance.

In this study, the dehumidification system utilized a vortex cooling gun and a cold plate to test the cooling, dehumidification, and energy efficiency of this novel HVAC design. Airflow and temperature variables were carefully adjusted to analyze the system's performance under different humidity conditions. The vortex cooling gun directed high-speed, cold air towards the hot and humid airflow, creating rapid temperature reduction, while the cold plate provided a condensation surface for moisture extraction.

The experiment involved setting the inlet air temperature between 25°C and 30°C, while maintaining a steady airflow rate. During the initial cooling phase, the temperature reduction was gradual until it reached approximately 5°C, a sharp increase in cooling efficiency occurred. This effect is due to the combined cooling mechanisms of both the vortex gun and the cold plate, which allowed for rapid phase transitions at lower temperatures.

The cooling gun enabled the controlled movement of air, transferring heat from the moist air to the vortex cooling mechanism and then to the cold plate. As the air temperature dropped below the dew point, moisture condensed on the cold plate surface, forming ice crystals. The cooling process was primarily driven by convective and conductive heat transfer, with convection playing a dominant role as the air moved swiftly through the system. Radiation was not considered significant for heat transfer in this context, given the low temperatures and the specific design, which focused on direct contact cooling.

Throughout the experiment, the airflow was approximately between 0.3 and -1 m $s^{-1}$. At lower temperatures, the air was able to carry heat away effectively, with most of the heat transfer occurring through convective processes. As the air temperature approached 10°C, there was a shift in the heat transfer profile, where conduction between the cold plate and the adjacent air layers became more prominent. The temperature reduction rate was steeper between 10°C and 5°C, demonstrating the system’s efficiency in achieving low humidity at lower temperature thresholds.

The placement and configuration of the vortex gun and cold plate also influenced the heat transfer characteristics. When both components were optimally aligned, there was greater heat absorption from the moist air, allowing for faster condensation and enhanced dehumidification efficiency. This setup effectively utilized the energy in the cooling cycle, showing potential for reducing HVAC operational costs by achieving high moisture removal rates at low energy inputs.

The novel dehumidification system demonstrated a robust ability to handle high humidity loads through effective moisture removal, stable heat transfer, and adaptable humidification control. The relationship between the inlet absolute humidity and the MRR was positively correlated, with MRR increasing proportionally as inlet absolute humidity rose. This response highlights the system's design efficiency, particularly in high-humidity environments, and was validated through polynomial regression, which confirmed a high correlation, underscoring the system's reliability in maintaining effective moisture control.

In terms of heat transfer, the total heat extracted from the air was calculated based on both sensible and latent heat contributions. The results showed higher total heat removal rates at elevated humidity and temperature levels, aligning with peak MRR measurements. Polynomial regression analysis further confirmed a strong correlation between total heat transfer and relative humidity, with $R^2$ values above 0.8, reinforcing the system's reliability in dynamic conditions. The enthalpy difference between the inlet and outlet air provided insights into cooling efficiency, with the average heat extraction rate stabilizing after the initial cooling phase, indicating the system's capacity to sustain performance over time.

Throughout the testing, RH at the outlet consistently remained lower than at the inlet, with the system achieving rapid RH reduction and stable absolute humidity levels. This indicates the system's capability to deliver dry air effectively, maintaining low humidity levels even under varying initial conditions. The steady enthalpy reduction and absolute humidity control

illustrated the system's ability to perform reliable dehumidification while ensuring continuous cooling.

During humidification, the system allowed processed air to reabsorb moisture at a controlled rate, keeping outlet RH levels close to 95%, independent of the starting air conditions. This balance between dehumidification and controlled humidification demonstrates the system’s adaptability in managing air moisture levels precisely. The humidification capacity could be further adjusted by altering the cold plate temperature or airflow rate, tailoring the system’s performance to specific application needs. In this study, only the maximum dehumidification capacity was evaluated, with the outlet air conditioned until it approached the dew point.

Overall, the system effectively combined high MRR, stable heat transfer, and flexible moisture management, showcasing its potential as a reliable and energy-efficient solution for HVAC applications in environments with variable humidity demands.

## 6.2 General conclusions

The main objectives of this study were to explore the feasibility of separating latent and sensible heat loads using water as an HVAC working fluid, generate cold fog to simulate cloud conditions within the experimental setup, and RH and absolute humidity by forming ice particles. Additionally, this research aimed to quantify the moisture removed from the system as air transitions from saturated vapor to ice. Specific objectives included creating heavy fog within the chamber, producing and directing ice crystals using an ice scrapper system, measuring temperature reduction with a vortex cooling gun and cold plate, and analyzing the system's impact on RH and absolute humidity levels.

This study developed and evaluated an innovative dehumidification system that aims to separate latent and sensible heat loads, create cold fog, and reduce RH and absolute humidity by generating ice particles. Utilizing a vortex cooling gun and cold plate, the system demonstrated effective cooling and moisture control across various conditions, achieving the research objectives and presenting promising implications for advanced HVAC applications. The system's MRR showed a strong correlation with the inlet absolute humidity, which ranged from approximately 2 to 16 g $m^{-3}$. As the inlet absolute humidity increased, MRR rose from around 0.014 g $s^{-1}$ to a peak of approximately 0.03 g $s^{-1}$. Polynomial regression analysis of this relationship yielded an $R^2$ value of 0.9834, validating the system's capability to handle high-humidity environments and maintain reliable dehumidification performance.

In terms of total heat transfer, the system efficiently extracted both sensible and latent heat, with higher heat removal at elevated humidity and temperature levels. The heat removal rate increased with higher inlet RH and inlet temperatures, reaching around 14 kJ $kg^{-1}$ at an inlet temperature of approximately 25°C and inlet RH levels up to 90%. Polynomial regression analysis further supported these findings, with $R^2$ values of 0.81 and 0.94 for the correlation between total heat transfer and inlet RH and temperature, respectively. This strong correlation

underscores the system's effectiveness in achieving enthalpy increase as the air transitions from saturated vapor to ice crystals.

Throughout the dehumidification tests, the system effectively reduced RH, with outlet RH levels consistently maintained below 20% when the inlet RH was as high as 80%. This stable RH reduction was accompanied by a consistent drop in absolute humidity, with outlet absolute humidity reaching approximately 3 g $m^{-3}$ compared to an inlet absolute humidity of over 10 g $m^{-3}$. This substantial decrease demonstrated the system's capacity to provide dry air, even in high-humidity conditions. This adaptability highlights the system's flexibility to meet specific application requirements by adjusting cold plate temperature or airflow rate. During the tests, the maximum dehumidification efficiency observed was approximately 50% at higher inlet humidity levels, indicating the system's effectiveness in managing both dehumidification and cooling processes as needed. Temperature reduction measurements confirmed the cooling performance of the system, with the vortex cooling gun and cold plate achieving temperature drops from an inlet temperature of around 20°C to an outlet temperature below 5°C. This rapid temperature decrease facilitated the formation of ice particles, which played a critical role in the moisture removal process by lowering the air's energy content.

Overall, this study demonstrated that the dehumidification system successfully managed air moisture and temperature with high energy efficiency. It achieved significant reductions in RH and absolute humidity, reaching an MRR of up to 0.03 g $s^{-1}$ and a total heat removal of approximately 14 kJ $kg^{-1}$. These findings contribute to the development of sustainable HVAC systems, providing an innovative and energy-efficient approach to dehumidification suitable for applications requiring precise humidity control. This research advances the field of cooling and dehumidification technologies, offering a practical solution for environments with high humidity demands.

### 6.3 Recommended future studies

This research introduced a novel approach to dehumidification within HVAC systems, providing substantial evidence of its potential for high efficiency and energy savings. However, several areas warrant further exploration to maximize the system's practical applications and improve its design for broader use cases. The following recommendations for future studies aim to deepen the understanding of this dehumidification method, optimize its functionality, and evaluate its feasibility for widespread adoption:

1. Scaling up the prototype system: future studies should explore scaling up this dehumidification system to larger, real-world environments. Testing in industrial or commercial spaces would reveal its ability to handle varying humidity loads on a broader scale, assessing if the same rapid RH reduction and energy efficiency observed in laboratory conditions can be replicated in larger areas.
2. Energy efficiency and sustainability assessments: detailed studies on exergy analysis, sustainability metrics are recommended to quantify the system's environmental impact. By evaluating energy use, carbon footprint, and resource consumption, these assessments will allow for a more comprehensive comparison with traditional HVAC dehumidification methods, validating the system's advantages in sustainable practices.
3. Cost-benefit and payback period analysis: economic feasibility is crucial for the adoption of this novel system. A cost-benefit analysis, including calculations of payback periods under different environmental and usage conditions, would help determine the system's economic viability. Such analyses are essential for understanding the investment value and potential savings over time, making it easier to advocate for its implementation in diverse sectors.

4. Investigating system performance with varying moisture sources: the current study focused on air dehumidification in controlled settings. Future research should investigate how the system handles air with different sources of moisture and contaminants to evaluate its resilience and effectiveness under various environmental conditions. Understanding how factors like outdoor air quality, seasonal humidity changes, and pollutant levels impact performance can guide system adaptations for specific climates or applications.
5. Integration of vegetation and biofiltration: incorporating vegetation or biofiltration layers could enhance both humidity control and indoor air quality. Investigating the effects of a vegetation layer on the system's cooling and dehumidification efficiency would offer insights into natural, bio-inspired modifications. Researching the interactions between plant transpiration, photosynthesis, and humidity control within the system could reveal additional benefits, including thermoregulation and air purification.
6. Reuse of ice crystals and water recycling: a promising area for further research is finding ways to reuse the ice crystals formed during the dehumidification process. Future studies could investigate methods to capture, melt, and recycle the ice, directing the resulting cooled water back into the system as a secondary cooling source. This recycling loop could enhance the system's cooling efficiency while reducing water waste, making the overall design more sustainable and self-sufficient. Developing an automated system for collecting and channelling the cooled water could lead to continuous, low-cost cooling, which is especially advantageous in high-humidity settings.
7. Exploration of automated and smart control systems: to improve adaptability and efficiency, future studies should consider incorporating automation and smart control

systems, such as AI-based algorithms or IoT connectivity. By dynamically adjusting airflow, cooling rates, and target RH levels in response to real-time environmental data, these enhancements could optimize performance and energy usage, especially in high-variability conditions.

These recommended areas for future study would provide a stronger foundation for this novel dehumidification system's broader application, helping bridge the gap between laboratory results and real-world performance. With further development, this system could become a versatile and sustainable solution for advanced humidity management in various industries and climate regions.

## References


Alduchov, O. A., & Eskridge, R. E. (1996). Improved magnus form approximation of saturation vapor pressure. *Journal of Applied Meteorology (1988-2005)*, 601-609.

Allam, S., & Elsaid, A. M. (2020). Parametric study on vehicle fuel economy and optimization criteria of the pleated air filter designs to improve the performance of an IC diesel engine: Experimental and CFD approaches. *Separation and Purification Technology*, *241*, 116680.

Allan, R. P., Barlow, M., Byrne, M. P., Cherchi, A., Douville, H., Fowler, H. J., Gan, T. Y., Pendergrass, A. G., Rosenfeld, D., & Swann, A. L. (2020). Advances in understanding large-scale responses of the water cycle to climate change. *Annals of the New York Academy of Sciences*, *1472*(1), 49-75.

Amer, M., Chen, M.-R., Sajjad, U., Ali, H. M., Abbas, N., Lu, M.-C., & Wang, C.-C. (2019). Experiments for suitability of plastic heat exchangers for dehumidification applications. *Applied Thermal Engineering*, *158*. https://doi.org/10.1016/j.applthermaleng.2019.113827

Amer, O., Boukhanouf, R., & Ibrahim, H. G. (2015). A Review of Evaporative Cooling Technologies. *International Journal of Environmental Science and Development*, *6*(2), 111-117. https://doi.org/10.7763/ijesd.2015.V6.571

Andersen, S. O., Gao, S., Carvalho, S., Ferris, T., Gonzalez, M., Sherman, N. J., Wei, Y., & Zaelke, D. (2021). Narrowing feedstock exemptions under the Montreal Protocol has multiple environmental benefits. *Proceedings of the National Academy of Sciences*, *118*(49), e2022668118.

Ariwibowo, D., & Darmanto, S. (2020). Refrigeration system based-dehumidifier. IOP Conference Series: Materials Science and Engineering,

ASHRAE. (1996). *HVAC systems and equipment* (Vol. 39). chapter.

Bailey, D. W., Bauer, F. C., Slama, C. F., Flack, J., & Barringer, C. (1996). *Investigation of dynamic latent heat storage effects of building construction and furnishings* (0001-2505).

Balaras, C. A., Grossman, G., Henning, H.-M., Ferreira, C. A. I., Podesser, E., Wang, L., & Wiemken, E. (2007). Solar air conditioning in Europe—an overview. *Renewable and Sustainable Energy Reviews*, *11*(2), 299-314.

Bayer-Giraldi, M., Sazaki, G., Nagashima, K., Kipfstuhl, S., Vorontsov, D. A., & Furukawa, Y. (2018). Growth suppression of ice crystal basal face in the presence of a moderate ice-binding protein does not confer hyperactivity. *Proceedings of the National Academy of Sciences*, *115*(29), 7479-7484.

Becker, R., Goldberger, I., & Paciuk, M. (2007). Improving energy performance of school buildings while ensuring indoor air quality ventilation. *Building and Environment*, *42*(9), 3261-3276.

Benedick. (1996). Montreal Protocol on Substances that Deplete the Ozone Layer. *International Negotiation*, *1*(2), 231-246. https://doi.org/https://doi.org/10.1163/15718069620847781

Berardi, U., & Jafarpur, P. (2020). Assessing the impact of climate change on building heating and cooling energy demand in Canada. *Renewable and Sustainable Energy Reviews*, *121*, 109681. https://doi.org/https://doi.org/10.1016/j.rser.2019.109681

Bhatia, A. (2014). Heat rejection options in HVAC systems. *Continuing Education and Development, Inc*.

Bigg, E. (1953). The formation of atmospheric ice crystals by the freezing of droplets. *Quarterly Journal of the Royal Meteorological Society*, *79*(342), 510-519.

Biserni, C., & Garai, M. (2016). Energy balance and second law analysis applied to buildings: an opportunity for Bejan's theory. *International Journal of Heat and Technology*, *34*(S1), S185-S187.

Boutle, I., Price, J., Kudzotsa, I., Kokkola, H., & Romakkaniemi, S. (2018). Aerosol–fog interaction and the transition to well-mixed radiation fog. *Atmospheric Chemistry and Physics*, *18*(11), 7827-7840.

Brandemuehl, M., & Gabel, S. (1994). Development of a toolkit for secondary HVAC system energy calculations. *ASHRAE Transactions*, *100*(1), 21-32.

Braun, J., Klein, S., & Mitchell, J. (1989). Effictiveness models for cooling towers and cooling coils. *ASHRAE Transactions (American Society of Heating, Refrigerating and Air-Conditioning Engineers);(USA)*, *95*(CONF-890609-).

Campen, J., Bot, G., & De Zwart, H. (2003). Dehumidification of greenhouses at northern latitudes. *Biosystems Engineering*, *86*(4), 487-493.

Campen, J. B., & Bot, G. P. A. (2001). SE—Structures and Environment. *Journal of Agricultural Engineering Research*, *78*(1), 65-73. https://doi.org/10.1006/jaer.2000.0633

Cantrell, W., & Heymsfield, A. (2005). Production of ice in tropospheric clouds: A review. *Bulletin of the American Meteorological Society*, *86*(6), 795-808.

Catrini, P., Cellura, M., Guarino, F., Panno, D., & Piacentino, A. (2018). An integrated approach based on Life Cycle Assessment and Thermoeconomics: Application to a water-cooled chiller for an air conditioning plant. *Energy*, *160*, 72-86.

Chang, K., Wang, Y.-Y., & Li, Y.-Z. (2023). A review of water sublimation cooling and water evaporation cooling in complex space environments. *Progress in Aerospace Sciences*, *140*, 100930. https://doi.org/https://doi.org/10.1016/j.paerosci.2023.100930

Chen, J., Dahlin, M. J., Luuppala, L., Bickford, D., Boljka, L., Burns, V., & Johnson, M. S. (2021). Air pollution and climate change: sustainability, restoration, and ethical implications. *Air pollution sources, statistics and health effects*, 279-325.

Chen, X., Riffat, S., Bai, H., Zheng, X., & Reay, D. (2020). Recent progress in liquid desiccant dehumidification and air-conditioning: A review. *Energy and Built Environment*, *1*(1), 106-130. https://doi.org/10.1016/j.enbenv.2019.09.001

Chua, K. J., Chou, S. K., Yang, W. M., & Yan, J. (2013). Achieving better energy-efficient air conditioning – A review of technologies and strategies. *Applied Energy*, *104*, 87–104. https://doi.org/10.1016/j.apenergy.2012.10.037

Chun, L., Gong, G., Peng, P., Wan, Y., Chua, K. J., Fang, X., & Li, W. (2021). Research on thermodynamic performance of a novel building cooling system integrating dew point evaporative cooling, air-carrying energy radiant air conditioning and vacuum membrane-based dehumidification (DAV-cooling system). *Energy Conversion and Management*, *245*, 114551.

CO_GEN, N. G. B. (2007). Bureau of energy efficiency. In: Ministry of Power, Government of India, New Delhi.

Corberan, J. M. (2016). 13 - New trends and developments in ground-source heat pumps. In S. J. Rees (Ed.), *Advances in Ground-Source Heat Pump Systems* (pp. 359-385). Woodhead Publishing. https://doi.org/https://doi.org/10.1016/B978-0-08-100311-4.00013-3

Cui, X., & Wei, X. (2017). Application of phase change heat storage materials in a building. *Journal of Asian urban environment*, 507-510.

Daou, K., Wang, R., & Xia, Z. (2006). Desiccant cooling air conditioning: a review. *Renewable and Sustainable Energy Reviews*, *10*(2), 55-77.

Datta, A. (2007). Porous media approaches to studying simultaneous heat and mass transfer in food processes. I: Problem formulations. *Journal of Food Engineering*, *80*(1), 80-95.
Desideri, U., Proietti, S., & Sdringola, P. (2009). Solar-powered cooling systems: Technical and economic analysis on industrial refrigeration and air-conditioning applications. *Applied Energy*, *86*(9), 1376-1386.
Dharan, S., & Pittet, D. (2002). Environmental controls in operating theatres. *Journal of Hospital Infection*, *51*(2), 79-84.
Ding, Y., Wang, Z., Feng, W., Marnay, C., & Zhou, N. (2015). Influence of occupancy-oriented interior cooling load on building cooling load design. *Applied Thermal Engineering*, *96*. https://doi.org/10.1016/j.applthermaleng.2015.11.096
Ding, Z., Yu, X., Ma, Z., Wu, W., Zhang, L., Denis, Y., & Cheng, D. H. (2022). On-site measurement and simulation investigation on condensation dehumidification and desiccant dehumidification in Hong Kong. *Energy and Buildings*, *254*, 111560.
Donnelly, J., Flynn, J., & Monaghan, P. F. (1994). Integration of energy simulation & ventilation design tools via an object oriented data model. *Renewable Energy*, *5*(5), 1190-1192. https://doi.org/https://doi.org/10.1016/0960-1481(94)90149-X
Drewett, E., & Hartel, R. (2007). Ice crystallization in a scraped surface freezer. *Journal of Food Engineering*, *78*(3), 1060-1066.
Duan, Z., Zhan, C., Zhang, X., Mustafa, M., Zhao, X., Alimohammadisagvand, B., & Hasan, A. (2012). Indirect evaporative cooling: Past, present and future potentials. *Renewable and Sustainable Energy Reviews*, *16*(9), 6823-6850. https://doi.org/10.1016/j.rser.2012.07.007
Dymarska, M., Murray, B. J., Sun, L., Eastwood, M. L., Knopf, D. A., & Bertram, A. K. (2006). Deposition ice nucleation on soot at temperatures relevant for the lower troposphere. *Journal of Geophysical Research: Atmospheres*, *111*(D4).
Ehsan, M. M., Guan, Z., Gurgenci, H., & Klimenko, A. (2020). Feasibility of dry cooling in supercritical CO2 power cycle in concentrated solar power application: Review and a case study. *Renewable and Sustainable Energy Reviews*, *132*, 110055. https://doi.org/https://doi.org/10.1016/j.rser.2020.110055
El-Dessouky, H., Ettouney, H., & Al-Zeefari, A. (2004). Performance analysis of two-stage evaporative coolers. *Chemical Engineering Journal*, *102*(3), 255-266.
Elsaid, A. M., & Ahmed, M. S. (2021). Indoor Air Quality Strategies for Air-Conditioning and Ventilation Systems with the Spread of the Global Coronavirus (COVID-19) Epidemic: Improvements and Recommendations. *Environmental Research*, *199*, 111314. https://doi.org/https://doi.org/10.1016/j.envres.2021.111314
Enteria, N., & Mizutani, K. (2011). The role of the thermally activated desiccant cooling technologies in the issue of energy and environment. *Renewable and Sustainable Energy Reviews*, *15*(4), 2095-2122. https://doi.org/10.1016/j.rser.2011.01.013
Fairbridge, R. W., Askew, A. J., Herschy, R., Herschy, R., Herschy, R., Hordon, R. M., Muller, R. A., Grymes, J. M., Fairbridge, R. W., & Herschy, R. (1998). World Water balance. *Encyclopedia of Hydrology and Water Resources*, 787-790.
Fan, J., Luo, Z., & Li, Y. (2000). Heat and moisture transfer with sorption and condensation in porous clothing assemblies and numerical simulation. *International journal of heat and mass transfer*, *43*(16), 2989-3000.
Fang, X., Winkler, J., & Christensen, D. (2011). Using EnergyPlus to perform dehumidification analysis on Building America homes. *HVAC&R Research*, *17*(3), 268-283.
Fernández-González, S., Wang, P. K., Gascón, E., Valero, F., & Sánchez, J. L. (2016). Latent cooling and microphysics effects in deep convection. *Atmospheric Research*, *180*, 189-199. https://doi.org/https://doi.org/10.1016/j.atmosres.2016.05.022

Fong, K., Chow, T. T., Lee, C. K., Lin, Z., & Chan, L. (2010). Comparative study of different solar cooling systems for buildings in subtropical city. *Solar energy*, *84*(2), 227-244.
Fukuta, N. (1969). Experimental studies on the growth of small ice crystals. *Journal of Atmospheric Sciences*, *26*(3), 522-531.
Gao, P., Zhang, L., & Zhang, H. (2008). Performance analysis of a new type desalination unit of heat pump with humidification and dehumidification. *Desalination*, *220*(1-3), 531-537.
Gao, Z., Guo, H., Brad, R., Waterer, D., & VanDuyvendyke, R. (2011). Energy Efficiency Comparison of Four Greenhouse Dehumidification Methods in Cold Region. 2011 Louisville, Kentucky, August 7-10, 2011,
Geraldini, P., & Spa, S. Numerical Modeling and Performance Optimization Study of a Dehumidification Process in Nuclear Waste Storage.
Geresdi, I., Rasmussen, R., Grabowski, W., & Bernstein, B. (2005). Sensitivity of freezing drizzle formation in stably stratified clouds to ice processes. *Meteorology and Atmospheric Physics*, *88*, 91-105.
Ghoniem, A. F. (2011). Needs, resources and climate change: Clean and efficient conversion technologies. *Progress in energy and combustion science*, *37*(1), 15-51.
Giorgini, S. (2016). *Lecture Notes on Statistical Mechanics - Course for the Master degree in Physics at the University of Trento from 2010 to 2015 (misprints amended and solution to problems added)*.
Girard, E., & Blanchet, J.-P. (2001a). Microphysical parameterization of Arctic diamond dust, ice fog, and thin stratus for climate models. *Journal of the atmospheric sciences*, *58*(10), 1181-1198.
Girard, E., & Blanchet, J.-P. (2001b). Simulation of Arctic diamond dust, ice fog, and thin stratus using an explicit aerosol–cloud–radiation model. *Journal of the atmospheric sciences*, *58*(10), 1199-1221.
Gotaas, Y., & Benson, C. S. (1965). The effect of suspended ice crystals on radiative cooling. *Journal of Applied Meteorology (1962-1982)*, 446-453.
Guan, B., Zhang, T., Jun, L., & Liu, X. (2020). Exergy analysis and performance improvement of liquid-desiccant deep-dehumidification system: An engineering case study. *Energy*, *196*, 117122.
Guieysse, B., Hort, C., Platel, V., Munoz, R., Ondarts, M., & Revah, S. (2008). Biological treatment of indoor air for VOC removal: Potential and challenges. *Biotechnology advances*, *26*(5), 398-410.
Gultepe, I., Heymsfield, A., Field, P., & Axisa, D. (2017). Ice-phase precipitation. *Meteorological Monographs*, *58*, 6.1-6.36.
Gultepe, I., & Heymsfield, A. J. (2016). Introduction ice fog, ice clouds, and remote sensing. *Pure and Applied Geophysics*, *173*, 2977-2982.
Gultepe, I., Heymsfield, A. J., Gallagher, M., Ickes, L., & Baumgardner, D. (2017). Ice fog: The current state of knowledge and future challenges. *Meteorological Monographs*, *58*, 4.1-4.24.
Gultepe, I., Zhou, B., Milbrandt, J., Bott, A., Li, Y., Heymsfield, A. J., Ferrier, B., Ware, R., Pavolonis, M., & Kuhn, T. (2015). A review on ice fog measurements and modeling. *Atmospheric Research*, *151*, 2-19.
Gurubalan, A., & Simonson, C. J. (2021). A comprehensive review of dehumidifiers and regenerators for liquid desiccant air conditioning system. *Energy Conversion and Management*, *240*, 114234.
Habeebullah, B. A. (2010). Performance analysis of a combined heat pump-dehumidifying system. *JKAU Eng Sci*, *21*(1), 97-114.

Hajidavalloo, E., & Eghtedari, H. (2010). Performance improvement of air-cooled refrigeration system by using evaporatively cooled air condenser. *International Journal of Refrigeration*, *33*(5), 982-988. https://doi.org/10.1016/j.ijrefrig.2010.02.001

Han, J., Gao, Z., Guo, H., Brad, R., & Waterer, D. (2015). Comparison of greenhouse dehumidification strategies in cold regions. *Applied Engineering in Agriculture*, *31*(1), 133-142.

Hasani Balyani, H., Sohani, A., Sayyaadi, H., & Karami, R. (2015). Acquiring the best cooling strategy based on thermal comfort and 3E analyses for small scale residential buildings at diverse climatic conditions. *International Journal of Refrigeration*, *57*, 112-137. https://doi.org/10.1016/j.ijrefrig.2015.04.008

Heating, A. S. o., Engineers, A.-C., & Institute, A. N. S. (2001). *Ventilation for acceptable indoor air quality* (Vol. 62). American Society of Heating, Refrigerating and Air-Conditioning Engineers.

Heidarinejad, G., Farmahini Farahani, M., & Delfani, S. (2010). Investigation of a hybrid system of nocturnal radiative cooling and direct evaporative cooling. *Building and Environment*, *45*(6), 1521-1528. https://doi.org/10.1016/j.buildenv.2010.01.003

Henn, S., Richarz, J., Maier, L., Ying, X., Osterhage, T., Mehrfeld, P., & Müller, D. (2022). Influences of usage intensity and weather on optimal building energy system design with multiple storage options. *Energy and Buildings*, *270*, 112222. https://doi.org/https://doi.org/10.1016/j.enbuild.2022.112222

Heymsfield, A. J., Miloshevich, L. M., Schmitt, C., Bansemer, A., Twohy, C., Poellot, M. R., Fridlind, A., & Gerber, H. (2005). Homogeneous ice nucleation in subtropical and tropical convection and its influence on cirrus anvil microphysics. *Journal of the atmospheric sciences*, *62*(1), 41-64.

Heymsfield, A. J., & Sabin, R. M. (1989). Cirrus crystal nucleation by homogeneous freezing of solution droplets. *Journal of the atmospheric sciences*, *46*(14), 2252-2264.

Huh, J.-H., & Brandemuehl, M. J. (2008). Optimization of air-conditioning system operating strategies for hot and humid climates. *Energy and Buildings*, *40*(7), 1202-1213.

J. L. Pérez-Díaz , M. A. Á.-V., J. Sánchez-GarcíaCasarrubios and S. Jiménez-López. (2016). Ice Surface Entropy Induction by Humidity or How Humidity Prompts Freezing. *Multidisciplinary Engineering Science and Technology (JMEST)*.

Jamil, M. A., Imtiaz, N., Ng, K. C., Xu, B. B., Yaqoob, H., Sultan, M., & Shahzad, M. W. (2023). Experimental and parametric sensitivity analysis of a novel indirect evaporative cooler for greener cooling. *Thermal Science and Engineering Progress*, *42*, 101887. https://doi.org/https://doi.org/10.1016/j.tsep.2023.101887

Ji, J., Baltazar, J. C., & Claridge, D. (2008). Study of the outside air enthalpy effects in the screening of metered building energy data.

Jiang-nan, L., Xue-hu, M., Fang-zhou, L., & Jiang-yu, M. (2016). CHARACTERISTICS OF THE LATENT HEAT DUE TO DIFFERENT CLOUD MICROPHYSICAL PROCESSES AND THEIR INFLUENCE ON AN AUTUMN HEAVY RAIN EVENT OVER HAINAN ISLAND. *Journal of Tropical Meteorology*, *22*.

Jin, G.-Y., Cai, W.-J., Lu, L., Lee, E. L., & Chiang, A. (2007). A simplified modeling of mechanical cooling tower for control and optimization of HVAC systems. *Energy Conversion and Management*, *48*(2), 355-365. https://doi.org/10.1016/j.enconman.2006.07.010

Jin, Z., Zheng, Y., Huang, D., Zhang, Y., Lv, S., & Sun, H. (2023). Dehumidification load ratio: influence mechanism on air conditioning and energy saving potential analysis for building cooling. *Sustainable Cities and Society*, *99*. https://doi.org/10.1016/j.scs.2023.104942

Kamal, W. A. (1994). Refrigerants Beyond 1995-An Overview.
Karmacharya, S., Putrus, G., Underwood, C., & Mahkamov, K. (2012). Thermal modelling of the building and its HVAC system using Matlab/Simulink. 2012 2nd International Symposium On Environment Friendly Energies And Applications,
Kasahara, M., Yamazaki, T., Kuzuu, Y., & Hashimoto, Y. (2001). Stability analysis and tuning of PID controller in VAV systems. *ASHRAE Transactions*, *107*, 285.
Khalajzadeh, V., Farmahini-Farahani, M., & Heidarinejad, G. (2012). A novel integrated system of ground heat exchanger and indirect evaporative cooler. *Energy and Buildings*, *49*, 604-610. https://doi.org/10.1016/j.enbuild.2012.03.009
Khalilnejad, A., French, R. H., & Abramson, A. R. (2020). Data-driven evaluation of HVAC operation and savings in commercial buildings. *Applied Energy*, *278*, 115505.
Khattar, M. K. (1997). *Design study of temperature and humidity control in enclosed spaces*. Florida Institute of Technology.
Kiehl, J. T., & Trenberth, K. E. (1997). Earth's annual global mean energy budget. *Bulletin of the American Meteorological Society*, *78*(2), 197-208.
Kikuchi, S., Okuda, S., Igawa, H., Morii, S., Mitsuhashi, M., & Higashimori, H. (2005). Development of air cycle system for refrigeration. *MITSUBISHI JUKO GIHO*, *42*(4), 194.
Kleidon, A., & Renner, M. (2013). Thermodynamic limits of hydrologic cycling within the Earth system: concepts, estimates and implications. *Hydrology and Earth System Sciences*, *17*(7), 2873-2892.
Kloppers, J. C., & Kro¨ ger, D. G. (2005). Cooling tower performance evaluation: Merkel, Poppe, and e-NTU methods of analysis. *J. Eng. Gas Turbines Power*, *127*(1), 1-7.
Korolev, A., & Isaac, G. A. (2006). Relative humidity in liquid, mixed-phase, and ice clouds. *Journal of the atmospheric sciences*, *63*(11), 2865-2880.
Korolev, A. V., & Mazin, I. P. (2003). Supersaturation of water vapor in clouds. *Journal of the atmospheric sciences*, *60*(24), 2957-2974.
Kuhn, T., & Gultepe, I. (2016). Ice fog and light snow measurements using a high-resolution camera system. *Pure and Applied Geophysics*, *173*, 3049-3064.
Kumar, S., Hariharan, G., Fayaz, M., & Kumar, N. (2023). Experimental Investigation on Dehumidification Using a Solid Composite Bio Desiccant Internally Cooled Using Nanofluids for Building Cooling. *Buildings*, *13*(6). https://doi.org/10.3390/buildings13061461
Lamb, D., Hallett, J., & Sax, R. (1981). Mechanistic limitations to the release of latent heat during the natural and artificial glaciation of deep convective clouds. *Quarterly Journal of the Royal Meteorological Society*, *107*(454), 935-954.
Lamb, D., & Verlinde, J. (2011). *Physics and chemistry of clouds*. Cambridge University Press.
Lawal, D., Antar, M., Khalifa, A., Zubair, S., & Al-Sulaiman, F. (2018). Humidification-dehumidification desalination system operated by a heat pump. *Energy Conversion and Management*, *161*, 128-140. https://doi.org/https://doi.org/10.1016/j.enconman.2018.01.067
Lee, T., Hawes, D., Banu, D., & Feldman, D. (2000). Control aspects of latent heat storage and recovery in concrete. *Solar energy materials and solar cells*, *62*(3), 217-237.
Li, B., Lin, Q. Y., & Yan, Y. Y. (2012). Development of solid desiccant dehumidification using electro-osmosis regeneration method for HVAC application. *Building and Environment*, *48*, 128-134. https://doi.org/https://doi.org/10.1016/j.buildenv.2011.09.008
Li, R., Min, Q., Wu, X., & Fu, Y. (2013). Retrieving latent heating vertical structure from cloud and precipitation profiles—Part II: Deep convective and stratiform rain processes.

*Journal of Quantitative Spectroscopy and Radiative Transfer*, *122*, 47-63. https://doi.org/https://doi.org/10.1016/j.jqsrt.2012.11.029
Li, Z., Liu, X.-H., Lun, Z., & Jiang, Y. (2010). Analysis on the ideal energy efficiency of dehumidification process from buildings. *Energy and Buildings*, *42*(11), 2014-2020. https://doi.org/https://doi.org/10.1016/j.enbuild.2010.06.008
Liang, C., Li, X., & Zheng, G. (2022). Optimizing air conditioning systems by considering the grades of sensible and latent heat loads. *Applied Energy*, *322*, 119458.
Liang, J.-D., Huang, B.-H., Chiang, Y.-C., & Chen, S.-L. (2020). Experimental investigation of a liquid desiccant dehumidification system integrated with shallow geothermal energy. *Energy*, *191*. https://doi.org/10.1016/j.energy.2019.116452
Libbrecht, K. G. (2017). Physical dynamics of ice crystal growth. *Annual Review of Materials Research*, *47*, 271-295.
Lin, T., Han, F., Dai, T., & Chen, C. (2023). Numerical investigation of multi-physical field dehumidification control technology for prefabricated chambers. *Journal of Building Engineering*, *80*, 108156. https://doi.org/https://doi.org/10.1016/j.jobe.2023.108156
Liu, X., Xie, Y., Zhang, T., Chen, L., & Cong, L. (2018). Experimental investigation of a counter-flow heat pump driven liquid desiccant dehumidification system. *Energy and Buildings*, *179*, 223-238. https://doi.org/https://doi.org/10.1016/j.enbuild.2018.09.007
Lowenstein, A. (2008). Review of Liquid Desiccant Technology for HVAC Applications. *HVAC&R Research*, *14*(6), 819-839. https://doi.org/10.1080/10789669.2008.10391042
Luo, Y., Shao, S., Xu, H., & Tian, C. (2011). Dehumidification performance of [EMIM] BF4. *Applied Thermal Engineering*, *31*(14-15), 2772-2777.
Ma, Q., Wang, R., Dai, Y., & Zhai, X. (2006). Performance analysis on a hybrid air-conditioning system of a green building. *Energy and Buildings*, *38*(5), 447-453.
Mago, P. J., & Sherif, S. (2005). Frost formation and heat transfer on a cold surface in ice fog. *International Journal of Refrigeration*, *28*(4), 538-546.
Makarieva, A. M., Gorshkov, V. G., Sheil, D., Nobre, A. D., & Li, B.-L. (2013). Where do winds come from? A new theory on how water vapor condensation influences atmospheric pressure and dynamics. *Atmospheric Chemistry and Physics*, *13*(2), 1039-1056.
Masanet, E., Shehabi, A., Lei, N., Smith, S., & Koomey, J. (2020). Recalibrating global data center energy-use estimates. *Science*, *367*(6481), 984-986.
Maykut, G. A. (2018). The ice environment. In *Sea ice biota* (pp. 21-82). CRC press.
Mazoyer, M., Burnet, F., & Denjean, C. (2022). Experimental study on the evolution of droplet size distribution during the fog life cycle. *Atmospheric Chemistry and Physics*, *22*(17), 11305-11321.
Mazoyer, M., Burnet, F., Denjean, C., Roberts, G. C., Haeffelin, M., Dupont, J.-C., & Elias, T. (2019). Experimental study of the aerosol impact on fog microphysics. *Atmospheric Chemistry and Physics*, *19*(7), 4323-4344.
McGouldrick, K., & Barth, E. L. (2023). The Influence of Cloud Condensation Nucleus Coagulation on the Venus Cloud Structure. *The Planetary Science Journal*, *4*(3), 50.
McMurry, P. H. (2000). The history of condensation nucleus counters. *Aerosol Science & Technology*, *33*(4), 297-322.
Mendes, N., Barbosa, R. M., Freire, R. Z., & Oliveira, R. C. (2008). A simulation environment for performance analysis of HVAC systems. Building Simulation,
Merkel, F. (1925). Verdunstungskühlung. *(No Title)*.
Mi, Y., Durant, A., & Shaw, R. (2004). Laboratory measurements of heterogeneous ice nucleation: Contact nucleation inside-out. Proc. 14th Int. Conf. on Clouds and Precipitation,

Moghadam, T. T., Ochoa Morales, C. E., Lopez Zambrano, M. J., Bruton, K., & O'Sullivan, D. T. J. (2023). Energy efficient ventilation and indoor air quality in the context of COVID-19 - A systematic review. *Renewable and Sustainable Energy Reviews*, *182*, 113356. https://doi.org/https://doi.org/10.1016/j.rser.2023.113356

Multiphysics, C. (1998). Introduction to comsol multiphysics®. *COMSOL Multiphysics, Burlington, MA, accessed Feb*, *9*(2018), 32.

Mumtaz, M., Pamintuan, B. C., Fix, A. J., Braun, J. E., & Warsinger, D. M. (2023). Hybrid membrane dehumidification and dewpoint evaporative cooling for sustainable air conditioning. *Energy Conversion and Management*, *294*. https://doi.org/10.1016/j.enconman.2023.117547

Murphy, J. (2002). Dehumidification performance of HVAC systems. *ASHRAE Journal*, *44*(3), 23.

Murray, B., O'sullivan, D., Atkinson, J., & Webb, M. (2012). Ice nucleation by particles immersed in supercooled cloud droplets. *Chemical Society Reviews*, *41*(19), 6519-6554.

Nada, Elattar, H., & Fouda, A. (2015a). Experimental study for hybrid humidification–dehumidification water desalination and air conditioning system. *Desalination*, *363*, 112-125.

Nada, Elattar, H., & Fouda, A. (2015b). Performance analysis of proposed hybrid air conditioning and humidification–dehumidification systems for energy saving and water production in hot and dry climatic regions. *Energy Conversion and Management*, *96*, 208-227.

Nada, S. A., Elattar, H. F., & Fouda, A. (2015). Performance analysis of proposed hybrid air conditioning and humidification–dehumidification systems for energy saving and water production in hot and dry climatic regions. *Energy Conversion and Management*, *96*, 208-227. https://doi.org/10.1016/j.enconman.2015.02.082

Nawaz, K., & Gluesenkamp, K. (2018). Separate sensible and latent cooling systems: A critical review of the state-of-the-art and future prospects.

Ogniewicz, Y., & Tien, C. (1981). Analysis of condensation in porous insulation. *International journal of heat and mass transfer*, *24*(3), 421-429.

Olesen, B. W. (2020). ASHRAE's History With Thermal Comfort. *ASHRAE Journal*, *62*(11), 32-39.

Park, B., & Lee, S. (2020). Investigation on heat and mass transfer characteristics for a zeolite-coated heat exchanger using comparatively low-temperature energy: Heating humidification mode and cooling dehumidification mode. *Indoor and Built Environment*, *30*(9), 1486-1502. https://doi.org/10.1177/1420326X20942291

Pérez-Lombard, L., Ortiz, J., & Pout, C. (2008). A review on buildings energy consumption information. *Energy and Buildings*, *40*(3), 394-398.

Pesaran, A. A., Penney, T. R., & Czanderna, A. W. (1992). *Desiccant cooling: state-of-the-art assessment*.

Pidwirny, M. (2006). Cloud formation processes. In *physicalgeography. net*.

Pillai, J., Desai, R., & Ten, A. (2018). Dehumidification strategies and their applicability based on climate and building typology. 2018 Building Performance Analysis Conference and SimBuild,

Pu, Z., Pardyjak, E. R., Hoch, S. W., Gultepe, I., Hallar, A. G., Perelet, A., Beal, R., Carrillo-Cardenas, G., Li, X., & Garcia, M. (2023). Cold Fog Amongst Complex Terrain. *Bulletin of the American Meteorological Society*, *104*(11), E2030-E2052.

Rabehl, R. J., Mitchell, J. W., & Beckman, W. A. (1999). Parameter Estimation and the Use of Catalog Data in Modeling Heat Exchangers and Coils. *HVAC&R Research*, *5*(1), 3-17. https://doi.org/10.1080/10789669.1999.10391220

Rafique, M. M., Gandhidasan, P., Rehman, S., & Al-Hadhrami, L. M. (2015). A review on desiccant based evaporative cooling systems. *Renewable and Sustainable Energy Reviews*, *45*, 145-159.

Rajaseenivasan, T., & Srithar, K. (2017a). An investigation into a laboratory scale bubble column humidification dehumidification desalination system powered by biomass energy. *Energy Conversion and Management*, *139*, 232-244.

Rajaseenivasan, T., & Srithar, K. (2017b). Potential of a dual purpose solar collector on humidification dehumidification desalination system. *Desalination*, *404*, 35-40.

Ramaswamy, V., Boucher, O., Haigh, J. D., & Hauglustaine, D. (2001). Radiative Forcing of Climate Change. https://www.researchgate.net/publication/271201770_Radiative_Forcing_of_Climate_Chang

Richards, T. W., & Mathews, J. H. (1911). A METHOD FOR DETERMINING HEAT OF EVAPORATION AS APPLIED TO WATER. *Journal of the American Chemical Society*, *33*(6), 863-888.

Rudd, A., Lstiburek, J., & Ueno, K. (2005). Residential Dehumidification Systems Research for Hot-Humid Climates. *Building Science Corporation Research Report*, *505*.

Sanaye, S., & Taheri, M. (2018). Modeling and multi-objective optimization of a modified hybrid liquid desiccant heat pump (LD-HP) system for hot and humid regions. *Applied Thermal Engineering*, *129*, 212-229. https://doi.org/10.1016/j.applthermaleng.2017.09.116

Santamouris, M. (2015). Analyzing the heat island magnitude and characteristics in one hundred Asian and Australian cities and regions. *Science of the Total Environment*, *512*, 582-598.

Sarfraz, O., Bach, C. K., & Bradshaw, C. (2018). A literature review of numerical modeling techniques for vapor compression systems with focus on heat exchanger modeling.

Sasongko, S., Rini, B., Maehiroh, H., Utari, F., & Djaeni, M. (2021). The Effect of Temperature on Vermicelli Drying under Dehumidified Air. IOP Conference Series: Materials Science and Engineering,

Sayegh, M., Hammad, M., & Faraa, Z. (2011). Comparison of two methods of improving dehumidification in air conditioning systems: Hybrid system (refrigeration cycle - Rotary desiccant) and heat exchanger cycle. *Energy Procedia*, *6*, 759-768. https://doi.org/10.1016/j.egypro.2011.05.086

Selamat, H., Haniff, M. F., Sharif, Z. M., Attaran, S. M., Sakri, F. M., & Razak, M. A. H. B. A. (2020). Review on HVAC System Optimization Towards Energy Saving Building Operation. *International Energy Journal*, *20*(3).

Shao, X. (2006). *First Law Energy Balance as a Data Screening Tool* Texas A & M University].

Sharqawy, M. H., Antar, M. A., Zubair, S. M., & Elbashir, A. M. (2014). Optimum thermal design of humidification dehumidification desalination systems. *Desalination*, *349*, 10-21. https://doi.org/10.1016/j.desal.2014.06.016

Sherif, S., Mago, P., Al-Mutawa, N., Theen, R., & Bilen, K. (2001). Psychrometrics in the supersaturated frost zone/Discussion. *ASHRAE Transactions*, *107*, 753.

Sherif, S., Mago, P., & Theen, R. (2002). A study to determine heat loads due to coil defrosting–Phase II. *Final Technical Report No. UFME/SEECL-200201*.

Srithar, K., & Rajaseenivasan, T. (2017). Performance analysis on a solar bubble column humidification dehumidification desalination system. *Process safety and environmental protection*, *105*, 41-50.

Stoecker, W. F. (1975). *Procedures for simulating the performance of components and systems for energy calculations*.

Stolaki, S., Haeffelin, M., Lac, C., Dupont, J.-C., Elias, T., & Masson, V. (2015). Influence of aerosols on the life cycle of a radiation fog event. A numerical and observational study. *Atmospheric Research*, *151*, 146-161.

Storelvmo, T. (2017). Aerosol effects on climate via mixed-phase and ice clouds. *Annual Review of Earth and Planetary Sciences*, *45*, 199-222.

Sugarman, S. C. (2022). *Testing and balancing HVAC air and water systems*. River Publishers.

Szeto, K., & Stewart, R. (1997). Effects of melting on frontogenesis. *Journal of the atmospheric sciences*, *54*(6), 689-702.

Tan, M., Mei, J., & Xie, J. (2021). The Formation and Control of Ice Crystal and Its Impact on the Quality of Frozen Aquatic Products: A Review. *Crystals*, *11*(1). https://doi.org/10.3390/cryst11010068

Tashtoush, B., Molhim, M., & Al-Rousan, M. (2005). Dynamic model of an HVAC system for control analysis. *Energy*, *30*(10), 1729-1745. https://doi.org/10.1016/j.energy.2004.10.004

Teke, A., & Timur, O. (2014). Assessing the energy efficiency improvement potentials of HVAC systems considering economic and environmental aspects at the hospitals. *Renewable and Sustainable Energy Reviews*, *33*, 224-235.

Thornton, G. M., Fleck, B. A., Dandnayak, D., Kroeker, E., Zhong, L., & Hartling, L. (2022). The impact of heating, ventilation and air conditioning (HVAC) design features on the transmission of viruses, including the 2019 novel coronavirus (COVID-19): A systematic review of humidity. *PLoS One*, *17*(10), e0275654.

Vakiloroaya, V., Khatibi, M., Ha, Q. P., & Samali, B. (2011). New integrated hybrid evaporative cooling system for HVAC energy efficiency improvement. In 2011 IEEE/SICE International Symposium on System Integration, SII 2011. https://doi.org/10.1109/SII.2011.6147546

Vakiloroaya, V., Samali, B., Fakhar, A., & Pishghadam, K. (2014). A review of different strategies for HVAC energy saving. *Energy Conversion and Management*, *77*, 738-754. https://doi.org/10.1016/j.enconman.2013.10.023

Velders, G. J., Ravishankara, A. R., Miller, M. K., Molina, M. J., Alcamo, J., Daniel, J. S., Fahey, D. W., Montzka, S. A., & Reimann, S. (2012). Preserving Montreal Protocol climate benefits by limiting HFCs. *Science*, *335*(6071), 922-923.

Vihma, T., Pirazzini, R., Fer, I., Renfrew, I. A., Sedlar, J., Tjernström, M., Lüpkes, C., Nygård, T., Notz, D., & Weiss, J. (2014). Advances in understanding and parameterization of small-scale physical processes in the marine Arctic climate system: a review. *Atmospheric Chemistry and Physics*, *14*(17), 9403-9450.

Vihma, T., Screen, J., Tjernström, M., Newton, B., Zhang, X., Popova, V., Deser, C., Holland, M., & Prowse, T. (2016). The atmospheric role in the Arctic water cycle: A review on processes, past and future changes, and their impacts. *Journal of Geophysical Research: Biogeosciences*, *121*(3), 586-620.

Vivekh, P., Pei, S. D., Pang, W., & Cheng, G. (2023). Air dehumidification performance study of a desiccant wheel by a three-dimensional mathematical model. *International Journal of Refrigeration*, *147*, 163-173. https://doi.org/https://doi.org/10.1016/j.ijrefrig.2022.10.011

Wadnerkar, D., Sun, B., Utikar, R. P., Evans, G., Tade, M. O., Kavanagh, N., Faka, S., & Pareek, V. K. (2018). Numerical study of fog formation around ambient air vaporizers. *Chemical Engineering Science*, *183*, 37-46.

Wærsted, E. G., Haeffelin, M., Steeneveld, G. J., & Dupont, J. C. (2019). Understanding the dissipation of continental fog by analysing the LWP budget using idealized LES and in situ observations. *Quarterly Journal of the Royal Meteorological Society*, *145*(719), 784-804.

Wang, C., Ji, X., Yang, B., Zhang, R., & Yang, D. (2021). Study on heat transfer and dehumidification performance of desiccant coated microchannel heat exchanger. *Applied Thermal Engineering*, *192*, 116913. https://doi.org/https://doi.org/10.1016/j.applthermaleng.2021.116913

Wang, Q., Zhang, Y., Cai, W., & Bi, Q. (1998). Model-based non-linear controller for cooling coil unit. International Conference on Systems, Signals, Controls, Computers, SSCC,

Wang, Y.-W., Cai, W.-J., Soh, Y.-C., Li, S.-J., Lu, L., & Xie, L. (2004). A simplified modeling of cooling coils for control and optimization of HVAC systems. *Energy Conversion and Management*, *45*(18-19), 2915-2930. https://doi.org/10.1016/j.enconman.2003.12.024

Withers, C., & Center, F. S. E. (2018). Optimizing Energy Efficiency and Improved Dehumidification Performance of Variable Capacity Air Conditioning Systems. *ACEEE Summer Study on Energy Efficiency in Buildings; August 2018, American Council for an Energy Efficient Economy*, *1*, 12-13.

Yang, H., & Yang, C. (2021). Analysis of a novel pressurized dehumidification air conditioning system for urban underground space. *Building and Environment*, *206*, 108400. https://doi.org/https://doi.org/10.1016/j.buildenv.2021.108400

Yang, Z., Lin, B., Zhang, K., & Lian, Z. (2015). Experimental study on mass transfer performances of the ultrasonic atomization liquid desiccant dehumidification system. *Energy and Buildings*, *93*, 126-136.

Yao, Y. (2010). Using power ultrasound for the regeneration of dehumidizers in desiccant air-conditioning systems: A review of prospective studies and unexplored issues. *Renewable and Sustainable Energy Reviews*, *14*(7), 1860-1873. https://doi.org/https://doi.org/10.1016/j.rser.2010.03.042

Yao, Y., & Chen, J. (2010). Global optimization of a central air-conditioning system using decomposition–coordination method. *Energy and Buildings*, *42*(5), 570-583.

Yuan, G., Zhang, L., & Zhang, H. (2005). Experimental research of an integrative unit for air-conditioning and desalination. *Desalination*, *182*(1-3), 511-516.

Zhang, L. (2006). Energy performance of independent air dehumidification systems with energy recovery measures. *Energy*, *31*(8-9), 1228-1242.

Zhang, L., Liu, X.-H., & Jiang, Y. (2012). Ideal efficiency analysis and comparison of condensing and liquid desiccant dehumidification. *Energy and Buildings*, *49*, 575-583. https://doi.org/10.1016/j.enbuild.2012.03.012

Zhang, S., Wei, X., & Cheng, Q. (2024). Theoretical and experimental research on heat and mass transfer process of positive pressure condensation dehumidification for humid air. *International Journal of Refrigeration*, *159*, 74-87. https://doi.org/https://doi.org/10.1016/j.ijrefrig.2023.12.034

Zhang, Y., Wright, J. A., & Hanby, V. I. (2006). Energy Aspects of HVAC System Configurations—Problem Definition and Test Cases. *HVAC&R Research*, *12*(sup3), 871-888. https://doi.org/10.1080/10789669.2006.10391214

Zhou, X., & Braun, J. E. (2007). A simplified dynamic model for chilled-water cooling and dehumidifying coils—Part 1: Development (RP-1194). *HVAC&R Research*, *13*(5), 785-804.

Zubair, M. I., Al-Sulaiman, F. A., Antar, M., Al-Dini, S. A., & Ibrahim, N. I. (2017). Performance and cost assessment of solar driven humidification dehumidification desalination system. *Energy Conversion and Management*, *132*, 28-39.